Smart Manufacturing in Machining Process Using Industrial Edge Device

by

Mohammadreza Chehrehzad

A Dissertation Submitted to the
Graduate School of Sciences and Engineering
in Partial Fulfillment of the Requirements for
the Degree of

Doctor of Philosophy

in

Mechanical Engineering

KOÇ ÜNİVERSİTESİ

August, 2025

Smart Manufacturing in Machining Process Using Industrial Edge Device

Koç University

Graduate School of Sciences and Engineering

This is to certify that I have examined this copy of a doctoral dissertation by

Mohammadreza Chehrehzad

and have found that it is complete and satisfactory in all respects,

and that any and all revisions required by the final

examining committee have been made.

Committee Members:

Prof. Ismail Lazoglu (Advisor)

Assist. Prof. Levent Beker

Prof. Demircan Canadinc

Assoc. Prof. Umut Karagüzel

Prof. Mustafa Bakkal

Date:

This dissertation is dedicated to my father and mother for their unwavering support and sacrifices, and to my sisters for their constant encouragement and support throughout my academic journey.

ABSTRACT

Smart Manufacturing in Machining Process Using Industrial Edge Device
Mohammadreza Chehrehzad
Doctor of Philosophy in Mechanical Engineering
August, 2025

In modern manufacturing, smart machining solutions leverage advanced data analytics, real-time monitoring, and adaptive control strategies to optimize production efficiency, minimize costs, and ensure the quality of the product with remarkable precision and reliability. This thesis, titled ”Smart Manufacturing in Machining Process Using Industrial Edge Device,” explores innovative approaches for integrating industrial Edge devices into machining operations, enabling real-time monitoring, predictive maintenance, and cost-effective process optimization. The research is structured into four main items, each addressing a critical aspect of smart manufacturing in machining processes, specifically focusing on tool wear prediction, sensorless cutting forces and torque measurement, tool chipping detection, and runout monitoring.

First, an AI-assisted digital shadow was developed to predict tool flank wear using data acquired from an industrial Edge device in a drilling operation. The study combines high-frequency data acquisition from an industrial Edge device and a rotary dynamometer, followed by extensive feature engineering. A recurrent neural network (RNN) model utilizing bidirectional long short-term memory (Bi-LSTM) and bidirectional gated recurrent unit (Bi-GRU) architectures is employed to analyze tool wear regions. The developed digital shadow enhances cost efficiency by reducing the dependency on expensive multi-sensor systems and mitigating unnecessary tool replacements, aligning with the principles of smart manufacturing.

Second, a novel sensorless method is introduced for real-time measurement of cutting forces and torque in the milling process. Accurate measurement of cutting forces and torque is critical for process monitoring, tool condition assessment, and optimization in machining operations. However, conventional dynamometers, while precise, are costly and introduce complexities in experimental setups. This study

leverages an industrial Edge device to extract spindle current and torque data in real time. Experimental validation during the milling of Titanium alloy Ti6Al4V demonstrates strong correlations between dynamometer and Edge device cutting data, achieving mean errors of less than 12%. This sensorless approach significantly reduces setup time and cost while ensuring precise force monitoring, making it a viable alternative to traditional measurement techniques in smart machining environments.

Third, tool condition monitoring was investigated with a focus on detecting cutting-edge chipping in the milling of titanium alloys. As a critical factor, tool chipping significantly impacts machining efficiency and tool life. The study analyzes spindle current and torque signals obtained from an industrial Edge device operating at a high-frequency sampling rate of 500 Hz in the time and frequency domains. Fast Fourier Transform (FFT) analysis reveals significant spectral differences in Edge device signals before and after tool chipping occurrences. These findings establish industrial Edge computing as a reliable tool for tool condition monitoring, minimizing the need for expensive multi-sensor systems and enabling early detection of chipping events to prevent catastrophic tool failure.

Finally, an innovative sensorless approach for in-process runout detection was proposed. Runout, a key factor influencing machining accuracy, surface finish, and tool wear, is traditionally assessed using contact-based sensors. This study demonstrates that spindle current and torque signals, captured through an industrial Edge device, are highly correlated with dynamometer measurements, enabling real-time frequency-domain analysis for runout detection. The proposed method is experimentally validated during milling of Ti6Al4V, presenting a cost-effective and efficient approach to improve machining precision and stability in smart manufacturing environments.

In summary, this thesis contributes to the advancement of smart manufacturing in machining processes by harnessing the potential of industrial Edge devices for real-time monitoring, predictive maintenance, and sensorless process optimization. The proposed methodologies reduce reliance on expensive sensors, improve machining efficiency, and enhance cost-effectiveness, thereby paving the way for the next generation of intelligent and autonomous manufacturing systems.

ÖZETÇE

Doktora Tez Başlığı
Mohammadreza Chehrehzad
Mechanical Mühendisliği, Doktora
Ağustos 2025

Günümüz modern üretiminde, akıllı işleme çözümleri, gelişmiş veri analitiği, gerçek zamanlı izleme ve uyarlanabilir kontrol stratejilerinden yararlanarak üretim verimliliğini optimize eder, maliyetleri minimize eder ve üstün ürün kalitesini olağanüstü hassasiyet ve güvenilirlikle sağlar. ”Endüstriyel Edge Cihazı Kullanarak İşleme Sürecinde Akıllı Üretim” başlıklı bu tez, endüstriyel Edge cihazlarının işleme operasyonlarına entegrasyonuna yönelik yenilikçi yaklaşımları araştırmaktadır. Bu entegrasyon, gerçek zamanlı izleme, kestirimci bakım ve maliyet etkin süreç optimizasyonunu mümkün kılmaktadır. Araştırma, akıllı üretimin işleme süreçlerindeki dört kritik yönünü ele alan dört ana bölümden oluşmaktadır: takım aşınmasının tahmini, sensörsüz kesme kuvveti ölçümü, takım çentiklenmesi tespiti ve eksantriklik izleme.

İlk olarak, bir yapay zeka destekli dijital gölge modeli geliştirilerek endüstriyel Edge cihazı kullanılarak matkap takımlarının sırt aşınması tahmin edilmiştir. Çalışmada, yüksek frekansta veri toplama işlemi endüstriyel Edge cihazı ve döner dinamometre kullanılarak gerçekleştirilmiş, ardından geniş kapsamlı özellik mühendisliği uygulanmıştır. Takım aşınması tahmininde çift yönlü uzun-kısa süreli bellek (Bi-LSTM) ve çift yönlü kapılı tekrar eden birim (Bi-GRU) mimarilerine sahip bir tekrarlayan sinir ağı (RNN) modeli kullanılmıştır. Geliştirilen dijital gölge modeli, pahalı çoklu sensör sistemlerine olan bağımlılığı azaltarak maliyet etkinliğini artırmakta ve gereksiz takım değişimlerini önleyerek akıllı üretim prensiplerine uygunluk sağlamaktadır.

İkinci olarak, işleme sürecinde kesme kuvvetlerinin ve torkun gerçek zamanlı ölçümü için yenilikçi, sensörsüz bir yöntem önerilmiştir. Kesme kuvveti ve torkun doğru ölçülmesi, süreç izleme, takım durumu değerlendirme ve optimizasyon açısından kritik öneme sahiptir. Ancak geleneksel dinamometreler, yüksek hassasiyet sağlasa da, pahalıdır ve deneysel kurulumlarda zorluklar yaratmaktadır. Bu çalışmada, endüstriyel Edge cihazı kullanılarak iş mili akımı ve tork verileri gerçek zamanlı

olarak çıkarılmıştır. Ti6Al4V titanyum alaşımının işlenmesi sırasında yapılan deneysel doğrulama, dinamometre ile Edge cihazı verileri arasında güçlü bir korelasyon olduğunu göstermiş, ortalama hata oranı %12'nin altında bulunmuştur. Bu sensörsüz yaklaşım, geleneksel ölçüm tekniklerine kıyasla kurulum süresini ve maliyeti önemli ölçüde azaltırken, hassas kuvvet izleme sağlayarak akıllı işleme ortamları için uygun bir alternatif sunmaktadır.

Üçüncü olarak, titanyum alaşımlarının işlenmesi sırasında takım çentiklenmesini tespit etmeye odaklanan bir takım durumu izleme çalışması gerçekleştirilmiştir. Takım çentiklenmesi, işleme verimliliği ve takım ömrü üzerinde önemli bir etkiye sahiptir. Bu çalışmada, 500 Hz yüksek frekanslı örnekleme oranına sahip endüstriyel Edge cihazından elde edilen iş mili akımı ve tork sinyalleri analiz edilmiştir. Hızlı Fourier Dönüşümü (FFT) analizi, takım çentiklenmesi oluşmadan önce ve sonra Edge cihazı sinyallerinde önemli spektral farklılıklar olduğunu ortaya koymuştur. Bu bulgular, endüstriyel Edge bilişimin, takım durumu izleme için güvenilir bir araç olarak kullanılabileceğini göstermektedir. Böylece, pahalı çoklu sensör sistemlerine duyulan ihtiyaç azaltılarak takım çentiklenmelerinin erken tespit edilmesi ve ciddi takım hasarlarının önlenmesi sağlanmıştır.

Son olarak, işleme sırasında eksantriklik tespiti için yenilikçi bir sensörsüz yaklaşım önerilmiştir. Eksantriklik, işleme hassasiyetini, yüzey kalitesini ve takım aşınmasını doğrudan etkileyen kritik bir faktördür ve geleneksel olarak temaslı sensörler ile ölçülmektedir. Bu çalışmada, iş mili akımı ve tork sinyallerinin, endüstriyel Edge cihazı aracılığıyla kaydedilen verilerle dinamometre ölçümleriyle güçlü bir korelasyon gösterdiği kanıtlanmıştır. Gerçek zamanlı frekans alanı analizi ile eksantriklik tespit edilerek, sensörsüz ve müdahale gerektirmeyen bir yöntem sunulmuştur. Ti6Al4V titanyum alaşımının işlenmesi sırasında yapılan deneyler, bu yöntemin doğruluğunu kanıtlamış ve akıllı üretim sistemlerinde işleme hassasiyetini ve stabilitesini artırmada maliyet etkin ve verimli bir çözüm sunduğunu göstermiştir.

Sonuç olarak, Bu tez, endüstriyel Edge cihazlarının gerçek zamanlı izleme, kestirimci bakım ve sensörsüz süreç optimizasyonu için kullanımına odaklanarak akıllı üretim alanına önemli katkılarda bulunmaktadır. Önerilen yöntemler, pahalı sensörlere olan bağımlılığı azaltırken, işleme verimliliğini artırmakta ve maliyet etkinliğini iyileştirmektedir. Bu araştırma, geleceğin akıllı ve otonom üretim sistemlerine geçişi hızlandırarak yeni nesil üretim teknolojilerine katkı sağlamaktadır.

ACKNOWLEDGMENTS

First and foremost, I am deeply grateful to God for granting me the opportunity, strength, patience, and perseverance to complete this work.

I would like to express my sincere gratitude to Prof. Ismail Lazoglu, for his invaluable guidance, support, and for providing me with the opportunity to conduct research at the Manufacturing and Automation Research Center (MARC). His mentorship has been instrumental in shaping my academic journey and my research perspective.

I am also grateful to my jury committee members, Prof. Demircan Canadinc, Prof. Levent Beker, Prof. Umut Karagüzel, and Prof. Mustafa Bakkal, for dedicating their time to reviewing my thesis and for their insightful comments and suggestions, which have greatly contributed to improving the quality of this work.

I sincerely appreciate the Ford Otosan company for providing the necessary hardware, software, and materials that enabled my work on the AITOC: Artificial Intelligence-Supported Tool Chain in Manufacturing Engineering project. I would also like to extend my thanks to my colleagues Dr. Uğur Üresin, Gamze Keçibaş, Cemile Başirova, Deniz Bilgili, and Toprak Pehlivan from Ford Otosan for their teamwork and collaboration throughout this project.

My heartfelt thanks also go to my colleagues Hanife Unal Helvacioglu, Mumin Irican, Kağan Uçak, Onur, and Tugce Tepe from Siemens for their support in providing essential resources and for their contributions to establishing the Siemens IoT Edge Research Lab at the Manufacturing and Automation Research Center (MARC) at Koç University. This research lab has been instrumental in facilitating the necessary testing and measurement activities for my research.

I also extend my sincere gratitude to the Scientific and Technological Research Institution of Turkey (TÜBİTAK) for providing financial support through their scholarship program, which has significantly contributed to my research journey.

Special thanks go to my friends at KOC University and at the MARC lab, with whom I have shared a journey of learning, collaboration, and mutual support, especially Dr. Ehsan Layegh, Muzaffer Butun, Dr. Aamir Shahzad, Dr. Hammad Ur Rahman, Dr. Pouya Pashak, Dr. Vahideh Hayyolalam, Farouk Abdulhamid, Hassan Akbar. Their encouragement and assistance have made the research process both rewarding and enjoyable.

Last but not least, I would like to express my deepest appreciation to my family, who raised me, supported me, and supported me throughout every moment of my life. Their unwavering patience, encouragement, and belief in me have been my greatest source of strength throughout my graduate studies abroad and this long PhD journey. I wholeheartedly dedicate this work to them.

TABLE OF CONTENTS

LIST OF TABLES

LIST OF FIGURES

ABBREVIATIONS

a_p	Axial depth of cut
A_{xo}	Fourier series coefficient
α	Helix angle
C_E	Spindle current of Edge device
CWD	Chip width density of the cutter
D	Tool diameter
r	Tool radius
f	machining feedrate
fpt	machining feed per tooth
K	Normalized spindle frequency
K_r	Specific radial constant
K_t	Specific tangential constant
N	Number of flutes
ω_s	Spindle frequency
P_{1o}	Fourier series coefficient
P_{2o}	Fourier series coefficient
ρ	Tool runout
R_s	Static measured tool runout
S	Spindle speed
θ_{ex}	Exit angle of tool engagement
θ_{st}	Entry angle of tool engagement
T_E	Spindle torque of Edge device
T_D	Spindle torque of dynamometer
V	Cutting velocity

Chapter 1

INTRODUCTION

1.1 Overview

Smart manufacturing is an advanced approach to production that integrates data analytics, real-time monitoring, and intelligent control strategies. With the advent of Industry 4.0, manufacturing systems have evolved toward automation, connectivity, and adaptability, leading to greater productivity, cost efficiency, and precision. In machining operations, process optimization, predictive maintenance, and tool condition monitoring play a vital role in ensuring high-quality production while minimizing downtime.

Industrial Edge devices have emerged as powerful tools in smart manufacturing, enabling real-time data acquisition, processing, and AI-driven decision-making during the machining process. Unlike conventional monitoring systems that rely on expensive multi-sensor setups, Edge devices facilitate sensorless monitoring techniques, reducing costs while maintaining accuracy and efficiency. By leveraging high-frequency data processing and AI-driven analytics, Edge computing enhances the overall reliability and sustainability of machining processes. Moreover, Edge devices facilitate this by processing the machining data locally at the manufacturing site before selectively transmitting it to the cloud or a data center. This approach reduces latency, improves security, and enhances overall operational efficiency in the future.

This thesis, titled "Smart Manufacturing in Machining Process Using Industrial Edge Device," focuses on the integration of industrial Edge devices into machining operations to enable sensorless monitoring of the machining process to reduce costs and enhance efficiency. The research is structured into four key areas: tool wear prediction, sensorless cutting force measurement, tool chipping detection, and in-process runout monitoring. this study demonstrates the feasibility of cost-effective and smart manufacturing solutions, contributing to the next generation of autonomous machining systems through experimental validation.

1.2 Research Objectives

The primary objective of this research is to develop innovative methodologies for enhancing machining process monitoring and optimization using industrial Edge devices. The specific research objectives include:

1. Developing an AI-Assisted Digital Shadow for Tool Wear Prediction:
   - Implement a predictive model for drilling tool flank wear using a combination of high-frequency Edge device data and dynamometer signals.
   - Utilize recurrent neural network (RNN) architectures, including Bi-LSTM and Bi-GRU, for accurate tool wear estimation.
   - Reduce dependence on expensive sensor systems while maintaining high predictive accuracy.
2. Implementing a Sensorless Approach for Cutting Force and Torque Measurement:
   - Establish a novel method for real-time cutting force and torque measurement using Edge device-extracted spindle current and torque data.
   - Validate the correlation between Edge device data and dynamometer measurements to ensure reliability.
   - Minimize the cost and complexity associated with traditional force and torque measurement techniques.
3. Investigating Tool Chipping Detection in Milling Operations:

- Analyze spindle current and torque signals from an industrial Edge device for real-time detection of tool chipping events.
- Apply Fast Fourier Transform (FFT) analysis to identify frequency-domain characteristics associated with chipping occurrences.
- Improve tool condition monitoring and reduce the risk of premature tool failure.

4. Developing a Sensorless Method for In-Process Runout Detection:

   - Utilize frequency-domain analysis of spindle current and torque signals to detect machining runout.
   - Validate the feasibility of real-time runout detection through experimental investigations.
   - Improve machining accuracy, surface finish, and tool life while reducing reliance on conventional runout measurement systems.

Through the achievement of these objectives, this thesis contributes to the advancement of smart manufacturing in machining processes by utilizing an industrial Edge device. The proposed methodologies provide cost-effective, efficient, and scalable solutions for real-time process monitoring, predictive maintenance, and adaptive machining control, paving the way for fully autonomous and intelligent manufacturing environments in the future.

Chapter 2

LITERATURE REVIEW

2.1 Overview

This thesis aims to investigate novel approaches for integrating industrial Edge devices into machining operations, enabling real-time monitoring, predictive maintenance, and cost-effective process optimization during machining in smart manufacturing systems. The research is structured around four main areas, each addressing a specific aspect of smart manufacturing in machining processes: tool flank wear prediction, sensorless measurement of cutting forces and torque, tool chipping detection, and tool runout monitoring. This chapter provides a comprehensive review of previous research conducted in each of these areas.

2.2 Tool wear prediction through AI-assisted digital shadow using Industrial Edge device

Drilling is a fundamental machining operation, accounting for approximately 40% of all machining activities in the manufacturing industry [1]. Despite its widespread use, accurately assessing tool wear, predicting tool failure, and ensuring hole quality remain challenging tasks. Studies indicate that tool failures contribute to nearly 20% of production downtime, negatively impacting both productivity and energy efficiency [2], [3]. Among various tool wear mechanisms, flank wear is the most prevalent, primarily caused by friction between the tool's flank face and the surface of the workpiece. This wear mechanism is strongly influenced by cutting forces and the temperature generated in the tool–workpiece contact area. As tool wear progresses, it results in degraded surface finish, dimensional inaccuracies, and increased energy usage [4–8]. Moreover, inefficient tool replacement strategies such as premature or delayed tool changes can lead to reduced product quality and lower operational efficiency [9]. Consequently, accurately predicting flank wear is crucial for optimizing machining performance.

In recent years, digital twins have emerged as a key component of smart manufacturing systems, enabling real-time monitoring and control of production operations. The extent of integration between the physical system and its digital representation is typically categorized into three levels: digital model, digital shadow, and digital twin. A digital model provides a detailed virtual representation of the physical system; however, it lacks real-time data interaction with the physical counterpart. In contrast, a digital shadow includes one-way real-time data flow from the physical environment to the digital system [10], serving as a real-time data repository, especially valuable when handling complex data [11–13]. Digital twins, the most advanced of the three, are interactive virtual models that replicate and interconnect with the physical manufacturing environment to simulate, optimize, and manage system behavior [14]. These models enable two-way data exchange and real-time control between the physical and virtual systems through technologies such as sensors, big data analytics, and the Internet of Things [15, 16].

Although digital twins still face limitations, including simulation accuracy, responding promptly to real-time AI-driven decisions, and adapting to dynamic systems, they are considered a key enabler for real-time, AI-supported decision-making in manufacturing [17]. For example, Liu et al. [8] developed a digital twin-driven framework for surface roughness prediction and adaptive process parameter optimization in milling, using the Improved Particle Swarm Optimization-Generalized Regression Neural Networks (IPSO-GRNN) model. Rossi et al. [17] applied dynamic recurrent neural networks based on NARX models to construct a digital twin for the extrusion process in fused filament fabrication. Similarly, Zhang et al. [18] implemented an online Gaussian process-based prediction model for seam tracking and control of the welding head in a coaxial vision-assisted laser welding setup. Ward et al. [19] introduced a digital twin for real-time simulation-based control in milling to manage residual stress, chatter, and feed rate. In another study, Phua et al. [20]

proposed a digital twin architecture incorporating Bayesian optimization to control powder separation in metal additive manufacturing. Chen et al. [21] presented a real-time digital twin approach for estimating 3D temperature fields in friction stir welding using a cyber-physical fusion algorithm.

Numerous researchers have explored various techniques and sensor-based approaches to monitor tool wear during machining. Broadly, tool flank wear monitoring techniques can be divided into direct and indirect signal acquisition methods [22]. Direct or offline methods often involve optical measurement systems or tool imaging to assess wear [23, 24]. These techniques provide high precision but suffer from limitations such as interference from cutting fluids, inconsistent lighting conditions, and a lack of real-time adaptability. Conversely, indirect techniques estimate tool wear based on measurements of machining parameters like cutting forces, temperature, vibrations, acoustic emissions, or surface quality, often followed by calibration processes. Though indirect monitoring is not as accurate as the direct techniques, it allows in-process monitoring. However, it frequently requires significant computational activity. For example, Kaya et al. [25] developed an online indirect monitoring scheme based on spindle speed variations as inputs to a mathematical model during turning processes. Drouillet et al. [26] applied root mean square (RMS) values of spindle power in the time domain to determine the condition of the tool and the remaining useful life. Wang et al. [27] introduced a real-time model correlating flank wear evolution with milling forces and including crucial temperature thresholds corresponding to various wear mechanisms during machining Inconel 182. Pal et al. [28] created a neural network-based wear monitoring model based on strain gauge signals from the tool holder and motor current signals during turning. Uekita et al. [29] integrated short-time Fourier transform (STFT) and spectral kurtosis (SK) analysis of vibration signals from accelerometers to identify the occurrence of tool wear and chatter during drilling. Jaini et al. [30] introduced the use of a neural network-based monitoring method based on gap sensor signals, with an explicit relationship between signal intensity and the severity of the tool wear. Li et al. [31] proposed a new method of monitoring tool wear based on audio signal analysis. Their system utilized ensemble deep learning networks with audio sensors, fast Fourier transform (FFT), and band-pass filters to capture features related to wear under cutting operations. The performance revealed consistent wear predictions under different cutting conditions.

Furthermore, several researchers have explored artificial intelligence (AI)-based strategies to forecast tool wear during machining operations. These predictive models typically incorporate physical modeling, signal processing, machine learning, and deep learning techniques. Liu et al. [32] introduced a two-phase approach to estimate the remaining useful life (RUL) of cutting tools, utilizing bidirectional long short-term memory (Bi-LSTM) networks trained on time-domain current signals from the machine. The most relevant features were selected based on monotonicity rankings. Xu et al. [33] developed a deep learning technique that employs parallel convolutional neural networks (CNNs) to perform multi-scale feature fusion for tool wear estimation. Gao et al. [34] proposed an innovative method combining hybrid domain fusion and gated recurrent units (GRUs) for multi-sensor signal integration in tool wear prediction. Javed et al. [35] presented a data-driven model that uses an ensemble of summation wavelet-extreme learning machines with an incremental learning algorithm, allowing real-time updates of model parameters using cutting force signals. Martinez et al. [8] applied CNNs in combination with the Gramian angular summation field (GASF) encoding technique to analyze cutting forces, vibrations, and acoustic emissions, achieving an 85% accuracy rate in predicting tool wear. Yang et al. [9] proposed a model that combines trajectory similarity-based prediction (TSBP) with differential evolution support vector regression (DE-SVR) to estimate both tool wear and remaining life from cutting force data processed through time, frequency, and wavelet domain analysis. Yan et al. [36] implemented a real-time monitoring system using CNNs trained on acceleration and cutting force signals, with cutting time also included as an input to improve predictive accuracy. Marani et al. [37] designed an LSTM-based model that evaluates tool condition using spindle motor current signals gathered during milling operations. Kong et al. [38] introduced a hybrid framework combining relevance vector machines (RVM) and kernel principal component analysis enhanced by improved radial basis functions (KPCA-IRBF). The RVM component predicts tool wear along with confidence intervals, while KPCA-IRBF minimizes noise and redundancy by increasing the dimensionality of feature data. Wang et al. [39] developed a GRU-based recurrent neural network that uses the time and frequency domain features to forecast tool wear in dry milling with high accuracy by compressing the raw time-series signals. Cheng et al. [40] proposed a hybrid kernel extreme learning machine (KELM) for surface roughness prediction, integrating Gaussian and arc-cosine kernels and optimized with a whale optimization algorithm. The model also incorporates a tool wear monitoring component that leverages an attention mechanism alongside deep learning techniques. Mohanraj et al. [41] extracted wavelet coefficients, Holder's exponent (HE), and statistical features from vibration signals and tested multiple machine learning algorithms—including SVM, KNN, kernel Bayes, multilayer perceptron, and decision trees (DT). Their findings indicated that HE outperformed traditional statistical features, with DT and SVM delivering the most accurate results. Hou et al. [42] proposed a domain-adaptive tool wear prediction method using a SE-DAAMSCLSTM network, which integrates multiscale convolution, channel attention, and domain adversarial training to extract domain-invariant spatiotemporal features. Their model showed strong performance on milling datasets. Finally, Liu et al. [43] developed a GRU-DenseNet hybrid model for flank wear prediction using force, vibration, and acoustic emission signals, reporting an average prediction error of less than 8%.

While the integration of predictive AI algorithms and multi-sensor systems within digital twin-enabled smart manufacturing shows strong potential for industrial use, deploying numerous high-cost sensors during machining remains impractical due to budgetary and operational constraints. Additionally, applying multiple AI models across different subsets of data allows for the selection of the most effective model for each segment, thereby enhancing overall prediction accuracy. In this study, an AI-assisted digital shadow was developed to enable real-time prediction of flank wear in drilling tools. Cutting forces in three axes and torque signals were acquired via a rotary dynamometer, while spindle motor current, torque, encoder position, and Z-axis contour deviation data were captured using an edge computing device. Comprehensive feature engineering was performed for the first time on drilling signals acquired concurrently from both the edge device and the dynamometer. This analysis, performed in both time and frequency domains, identified the features most strongly correlated with flank wear in drilling tools. Furthermore, a comparative evaluation of recurrent neural network architectures, Bi-LSTM and Bi-GRU, was conducted on segmented datasets categorized by tool wear stages. This allowed identification of the optimal AI model based on prediction accuracy and computational efficiency. The proposed AI-enhanced digital shadow delivers fast and precise flank wear predictions using real-time data, without relying on extensive sensor arrays. It offers a cost-effective solution to reduce machine downtime and prevent premature or excessive tool usage, making it a compelling option for integration into digital twin frameworks in advanced manufacturing environments.

2.3 Sensorless measurement of cutting forces and Torque via Industrial Edge device

Consistent online measurement of cutting forces and torques is vital for maintaining product quality, enabling effective condition monitoring, and optimizing energy usage in machining operations. These measurements are essential to enhance the productivity and reliability of modern manufacturing systems. However, obtaining accurate and real-time values for these parameters continues to be a significant challenge, as they are directly linked to process efficiency, cost reduction, and operational stability in complex machining environments. Among the most widely used tools for this purpose are dynamometers, which provide precise and direct measurements of cutting torques and forces during real-time machining [44–50]. Despite their proven accuracy, dynamometers have notable limitations, including high cost, limited frequency bandwidth, complex setup procedures, and spatial constraints that can complicate installation and pose collision risks between the sensor and tool. These issues restrict their widespread adoption, especially in industrial settings beyond laboratory research. To overcome such limitations, alternative direct measurement systems have been explored. Boujnah et al. [51] introduced a spindle-mounted system using strain sensors to measure cutting forces directly. Rezvani et al. [52] developed a hybrid vise-based sensing system that utilizes strain gauges and custom-built piezoelectric sensors to capture both cutting and clamping forces during milling operations. Similarly, Mohring et al. [53] implemented a sensory machine tool equipped with strain gauges to directly measure machining forces. Additionally, Rizal et al. [54] proposed a wireless, integrated multi-sensor approach combining strain gauges and accelerometers to monitor cutting torque and forces during machining.

Indirect approaches to measuring cutting forces, torque, and current can be divided into sensor-based and sensorless methods. Although direct measurement techniques generally offer higher accuracy, indirect methods are often more suitable for real-time industrial applications due to their reduced complexity and improved adaptability [55]. Mostaghimi et al. [56] developed an indirect estimation technique that first uses acceleration data from the spindle housing and subsequently employs spindle current signals to estimate cutting forces during milling. Yamada et al. [57] introduced a method to estimate cutting forces by analyzing multi-encoder signals, isolating rigid-body motion, and utilizing relative displacement, velocity, and acceleration between the motor and table in vibration mode. In the same study, Yamada et al. also proposed a sensorless technique for high-frequency force estimation in fully closed-loop ball-screw systems using a multi-encoder disturbance observer (MEDOB), targeting force components that exceed the bandwidth limitations of conventional current control loops. Jeong et al. [58] employed feed motor current sensing with a bandwidth of 130 Hz, achieving force estimation accuracy within 20%. Albrecht et al. [59] introduced a method based on capacitance displacement sensing embedded in the spindle to detect gap variations between the sensor head and the rotating spindle shaft under load. Bleicher et al. [60] proposed a dynamic force monitoring system using MEMS accelerometers. Yoon et al. [61] focused on analyzing power consumption in machine tool feed drives, using a PAC3200 power meter

(Siemens) operating at a 5 Hz sampling rate to measure input power at the supply board. Huang et al. [62] presented a real-time force measurement system using Fiber Bragg Grating (FBG) optical sensors, which allows for simultaneous multi-axis force detection over long distances, even in demanding machining environments. Subasi et al. [63] designed a triaxial dynamometer incorporating photo-interrupter sensors to measure cutting forces. Gupta et al. [64] implemented a real-time power consumption monitoring setup using a KAEL-manufactured analyzer installed at the CNC machine's power input. Vogl et al. [65] proposed a cutting force estimation framework combining accelerometer data, a physics-informed data-driven algorithm, and a magnet-equipped tool holder, enabling force estimation under any spindle speed, tool type, or cutting condition. Finally, Postel et al. [66] demonstrated an estimation method using spindle-mounted accelerometers along with Kalman filtering to correct signal distortion, achieving high-bandwidth force measurements up to 1600 Hz. [67] demonstrated that spindle and feed motor internal current signals in high-speed milling could effectively track tool wear progression, with their findings validated using force measurements from a dynamometer. This sensorless monitoring method enabled continuous observation during dry machining of aerospace-grade aluminum alloys. Similarly, [68] leveraged torque and power data from machine servomotors to estimate broaching tool wear. By applying machine learning models such as random forest and support vector regression, they achieved high predictive accuracy using only CNC and PLC system data—showcasing the practicality of sensorless monitoring in rigorous industrial settings. [69] provided a comprehensive review of recent advances in intelligent tool wear monitoring, emphasizing the importance of multisource data fusion, feature engineering, and pattern recognition. They noted the increasing shift toward indirect monitoring via internal signals, which reduces reliance on external sensors and supports real-time AI-based decision-making. Additionally, [70] analyzed industrial communication protocols including OPC-UA, Modbus, and Ethernet/IP, comparing their effectiveness and software integration challenges in real-time data collection. Their results underscore the importance of reliable communication systems for enabling edge-computing-based, sensorless monitoring technologies.

Although multiple external sensors provide precise measurements of cutting forces and torque, their use entails several drawbacks, such as increased maintenance requirements, potential accumulation of measurement errors, and decreased system robustness. As an alternative, sensorless techniques that leverage internal data from machine tools offer a more cost-effective and sustainable solution. However, achieving accurate and broadband sensorless measurements is challenging due to the complexity of structural dynamics and nonlinear effects, such as friction, which can obscure the true values of cutting parameters. These challenges often require the implementation of advanced signal processing and modeling approaches to achieve reliable estimation. In this study, an online method is proposed for measuring cutting torque, tangential force, and current during milling of a titanium alloy workpiece. Cutting force and torque data were collected using a rotary dynamometer, while spindle current and torque signals were simultaneously acquired through an industrial edge computing device operating at a high sampling rate (approximately 500 Hz). Analysis of the data from both sources revealed strong correlations between the recorded signals. Validation experiments confirmed that the method achieved satisfactory accuracy, with mean errors under 12% for both repeatability and cross-validation across different feed rates. These results highlight the potential of using industrial edge devices for sensorless, real-time monitoring of torque and force in machining applications. This approach can reduce dependence on costly external sensors, simplify setup procedures, and enhance overall process efficiency.

2.4 Tool chipping detection using an Industrial Edge device

Tool failure can be any undesired defect in the fresh cutting tool that disturbs the cutting ability of the tool and decreases the machining quality. These defects can be caused by wear mechanisms or tool breakage. Tool chipping is the slight loss of particles from the cutting edge that leads to tool breakage if not detected in time [71]. It was reported that 20% of downtime in plants is accounted for by tool failure, which adversely affects productivity, production quality, and energy efficiency in manufacturing systems [2, 6, 7, 72]. Therefore, timely tool failure detection during machining has been a crucial topic among researchers.

The methods of signal acquisition for tool wear and failure detection can be categorized into direct and indirect types [22]. The direct detection type is based on the use of the tool image and optical measurement for tool wear monitoring [23, 24, 73]. Qu et al. [74] proposed a vision method for on-machine measurement of the milling tool damage in the face milling process using an industrial camera, lens, and LED ring lighting mounted on the camera support. Although this method is not online and has limitations when used with the presence of cutting fluid and illumination, it has high accuracy. The indirect detection type consists of measuring machining parameters using various sensors, processing the data, and correlating data with the tool failure. The collected data can be cutting force, torque, vibration, temperature, sound, and surface roughness. While this type provides real-time detection, it also needs high computational effort. Kang et al. [75] presented a tool chipping detection method using the peak period of spindle vibration during the milling of the Inconel 718. Also, in their research, the spindle current data are unsuitable for tool chipping detection because of their noise-free form. Recently, some research has used Artificial intelligence (AI) techniques on the machining data to predict tool wear. Bleicher et al. [60] proposed a process monitoring and tool chipping prediction method using a machine learning algorithm on the vibration data of an instrumented tool holder in the milling process. Gao et al. [34] demonstrated a novel tool wear prediction method based on multi-sensor hybrid domain information fusion by the gated recurrent units that combine feature layer information fusion and a deep neural network. Chehrehzad et al. [76] reported a tool wear prediction AI-based method based on a recurrent neural n network using the milling data from a dynamometer and Industrial Edge device. Yan et al. [36] demonstrated a tool condition monitoring method based on the convolutional neural network using acceleration and cutting force signals during machining. Jiang et al. [77] presented a tool-chipping monitoring method based on cutting vibration polar coordinate images and a residual neural network (ResNet) model in the milling process.

This study proposed a method for real-time tool chipping detection during the milling process on the titanium alloy workpiece utilizing the industrial Edge device. The milling cutting data were collected simultaneously using a rotary dynamometer and an industrial Edge device. On the other hand, the tool chipping measurements were conducted using the stereomicroscope. After processing and analyzing the milling data from both the dynamometer and industrial Edge devices in the time and frequency domains, it was observed that there are significant differences in the FFT (Fast Fourier Transform) results of the spindle current and torque of Edge device data of the fresh tool and chipped tool during the milling process, which enables the tool chipping detection. This approach offers a novel alternative for online tool chipping detection, potentially reducing the need for expensive multi-sensors in a smart manufacturing system.

2.5 Runout detection using Industrial Edge device

Runout is a critical phenomenon in milling operations, as it significantly influences cutting force patterns, tool wear progression, and machining precision. This issue is particularly problematic in high-precision industries such as aerospace and precision component manufacturing, where stringent dimensional tolerances must be maintained. Runout occurs when there is misalignment or eccentricity between the spindle's rotational axis and the tool's geometric center, leading to uneven chip thickness, fluctuating cutting forces, and degraded surface finish. Its presence not only accelerates tool degradation but also disrupts chip load distribution, thereby reducing machining efficiency, shortening tool life, and compromising part accuracy. Due to its critical impact, extensive studies have been conducted to detect, model, and compensate for runout in machining processes. Multiple researchers have developed models to capture the influence of runout on cutting force behavior. Kline et al. [78] introduced a milling force model that accounted for geometric deviations and variations in chip thickness caused by cutter runout. Liang et al. [79] proposed a convolution-based analytical method for runout identification, enhancing prior work by incorporating frequency-domain analysis and Fourier series to detect the runout signature. Their findings showed that runout contributes additional frequency components to the cutting force signal, making spindle frequency a key indicator. Building on this, Hekman et al. [80] presented a real-time runout estimation technique using recursive Fourier transforms of the force signal, allowing the method to adapt dynamically to changes in cutting conditions. Wang et al. [81] introduced a model for cutter offset detection that avoids the need for predefined cutting coefficients by using constant plowing and shearing terms within a convolution and Fourier framework. More recently, Lee et al. [82] developed a frequency-domain-based monitoring approach to simultaneously estimate runout and axial/radial depth of cut during milling in real time. On the other hand, precise real-time measurement of cutting forces and torque is crucial for maintaining part quality, implementing effective condition monitoring, and optimizing energy consumption in machining. For many years, rotary and table-type dynamometers have been the benchmark instruments for directly capturing force and torque data [44,47,55]. While they offer high accuracy, dynamometers come with notable limitations, such as high cost, lengthy setup times, and spatial constraints that can complicate integration with machine tools and pose risks of collision with cutting tools. To overcome these drawbacks, researchers have proposed a range of alternative force and torque estimation techniques. These include methods based on integrated strain gauges and accelerometers [51,52], capacitance-based displacement sensors [59], fiber Bragg grating (FBG) optical sensors [83], feed motor current analysis [58], and encoder-based disturbance observer systems [57].

This study presents a novel approach for detecting tool runout during milling operations through the use of an industrial edge device, eliminating reliance on conventional sensors such as dynamometers, laser systems, or accelerometers. Spindle torque and current signals were simultaneously acquired using a high-frequency industrial edge device, while force and torque data were also recorded using a rotary dynamometer for validation purposes. A strong linear correlation was identified between the spindle current and torque signals from the edge device and the torque measurements obtained from the dynamometer. Runout estimation was performed using convolution-based analytical models, which incorporated the force modeling approach from [79] and the torque-based runout identification method from [82]. The resulting runout values derived from both datasets showed high agreement, validating the effectiveness of the proposed sensorless method for real-time monitoring. These results highlight the feasibility of using industrial edge devices for in-process runout estimation, offering a cost-effective and efficient alternative to sensor-based systems. The approach contributes to advancing smart manufacturing by improving machining accuracy and enabling real-time process control without additional hardware.

Chapter 3

TOOL WEAR PREDICTION THROUGH AI-ASSISTED DIGITAL SHADOW USING INDUSTRIAL EDGE DEVICE

3.1 Overview

Flank wear in drilling tools is a key factor that impacts both product quality and overall manufacturing productivity. This study proposes an AI-assisted digital shadow for real-time prediction of drilling tool flank wear. Drilling data were simultaneously gathered from both an industrial edge device and a rotary dynamometer. Comprehensive feature engineering was applied to the acquired signals in both time and frequency domains. A recurrent neural network (RNN) framework, incorporating bidirectional long short-term memory (Bi-LSTM) and bidirectional gated recurrent unit (Bi-GRU) architectures, was employed on datasets segmented by tool wear regions. The digital shadow was developed by combining the edge-collected data with the trained AI model, aiming to reduce reliance on costly multi-sensor setups, minimize production interruptions, and avoid premature or delayed tool replacement in smart manufacturing environments. The resulting system delivers accurate and computationally efficient predictions, making it suitable for seamless integration into digital twin platforms.

3.2 Experimental method

3.2.1 Experimental procedure and data acquisition

The drilling tests were conducted on a Spinner U1530 five-axis CNC machine equipped with a Siemens SINUMERIK 840D sl controller. The workpieces consisted of AISI

1045 carbon steel blocks measuring 400 × 325 × 25 mm. A TiAlN-coated carbide twist drill with a diameter of 8.5 mm and a 140° tip angle was used. The tests were designed to produce a dataset for training an AI-based tool flank wear prediction model, utilizing measurements from a dynamometer and an Edge device.

Cutting forces and torque during drilling were measured via a Kistler rotary dynamometer mounted to the machine spindle, and the drill tool was fixed in it. The analog signals captured by the dynamometer were amplified via a Kistler Type 5223 charge amplifier and digitized using a NI USB-6259 data acquisition system by National Instruments [84]. Each channel of the dynamometer had a cut-off frequency of 1 kHz, and data were sampled at a rate of 7.8 kHz per channel. Although rotary dynamometers offer the advantage of high-frequency data acquisition for drilling force and torque signals, their high cost and incompatibility with coolant-based machining remain key limitations.

Additionally, spindle motor current, torque, encoder position, and Z-axis motor contour deviation signals were captured via the Siemens SINUMERIK 840D sl controller using a SIMATIC IPC227E industrial edge device, enabled through Siemens' Internet of Things (IoT) Edge Application. The edge device provided a sampling frequency of 500 Hz. Although SINUMERIK controllers support OPC UA and MTConnect protocols, these typically only offer data throughput up to 50 Hz. However, by integrating the Sinumerik adapter with the HF probe, sampling rates can be extended to 500 Hz with significantly larger data bandwidths. The industrial edge device connects directly to the CNC controller via a communication cable and leverages an internal communication bus for high-speed data transfer. This high-frequency data acquisition enables detailed analysis of tool–workpiece interactions over short durations during drilling. These signals reveal critical characteristics across time and frequency domains, facilitating advanced diagnostics in machining processes. While the industrial edge device captures comprehensive data on spindle and feed drive dynamics, its primary limitation lies in its maximum sampling frequency, capped at 500 Hz. The experimental setup used in this study is illustrated in Figure 3.1.

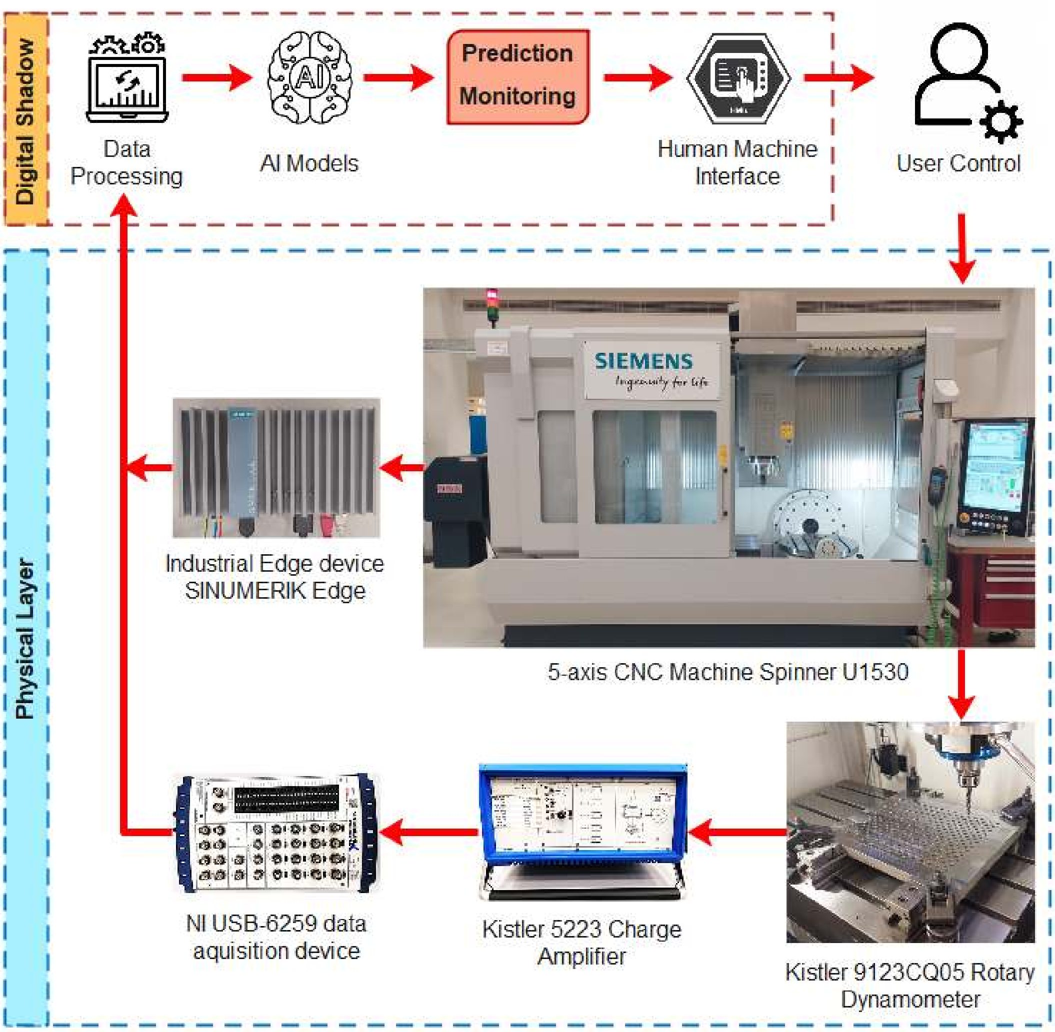

Figure 3.1: The experimental process.

A total of 2676 holes were drilled using the specified twist drill in this study. As the drilling was performed under dry-cutting conditions, a thermal management strategy was implemented to prevent excessive heat buildup on the tool. Specifically, drilling was carried out in batches of six consecutive holes, followed by a two-minute cooling interval before proceeding with the next set. The data corresponding to each set of six drilled holes, recorded from both the rotary dynamometer and the industrial edge device, are illustrated in Figure 3.2 and Figure 3.3. For all experiments, the spindle speed and feedrate were set at 2400 revolutions per minute (rpm) and 400 mm/min, respectively.

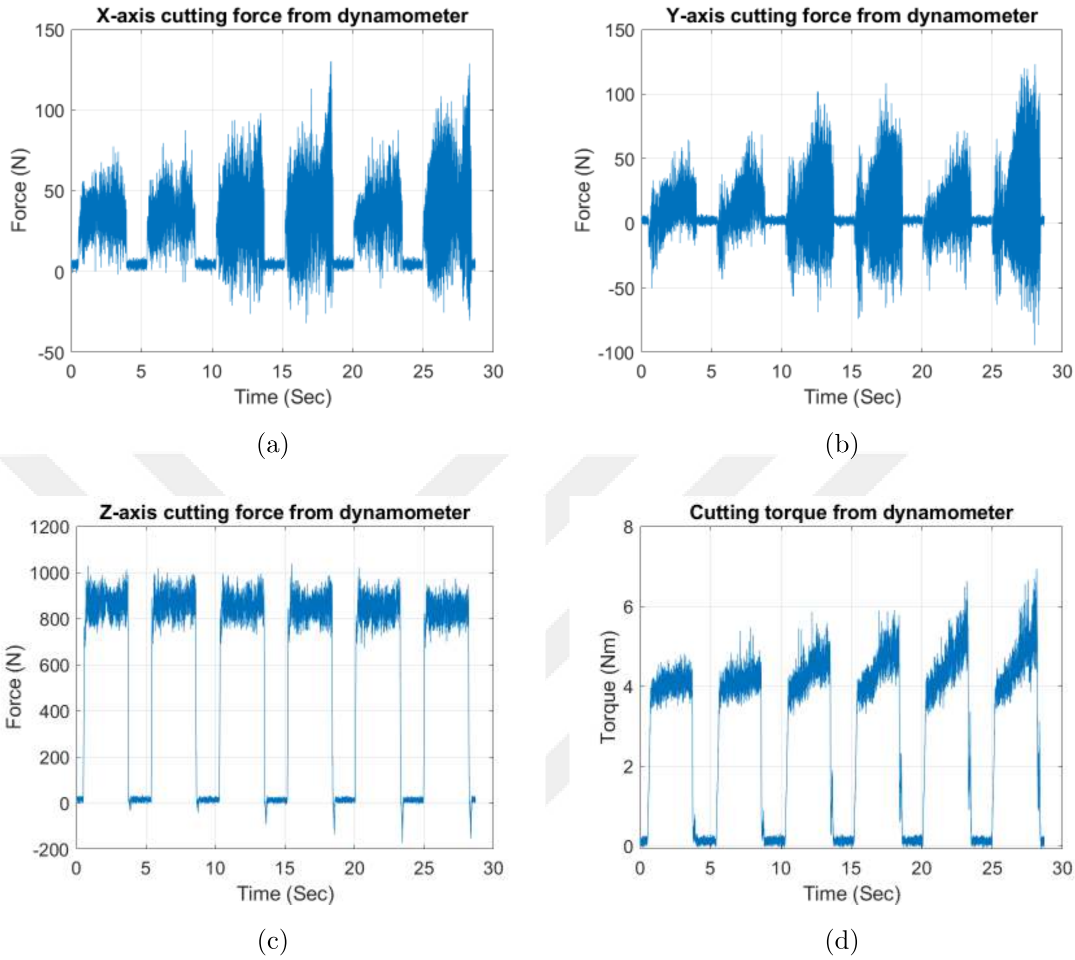

Figure 3.2: The three-axis cutting force and torque data of the dynamometer corresponding to a representative set of six successive drilling holes.

To measure flank wear, the tool was removed from the dynamometer after every 48 drilled holes and examined using a stereomicroscope. The mean values of cutting torque and three-axis cutting forces obtained from the dynamometer, along with the mean spindle motor current, torque, encoder position, and Z-axis motor contour deviation data collected by the edge device for all drilled holes, are presented in Figure 3.4 and Figure 3.5.

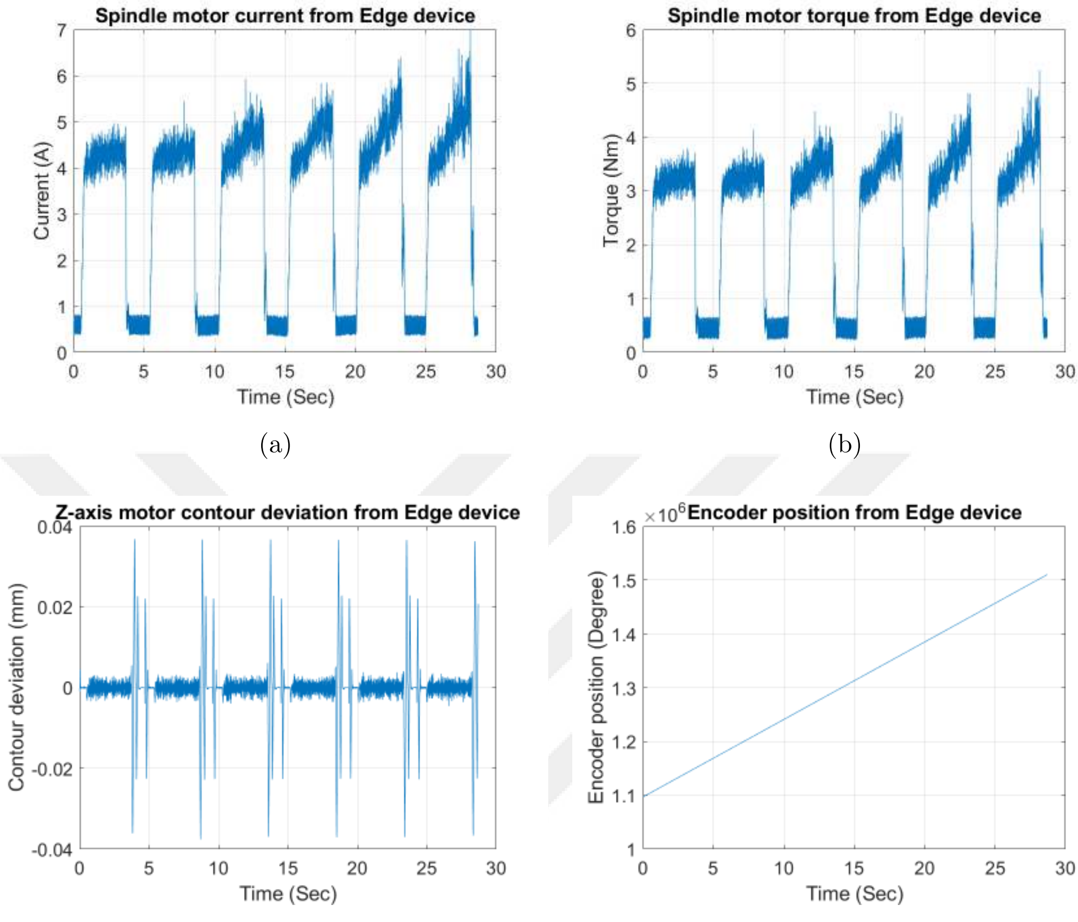

(a) (b) (c) (d)

Figure 3.3: The spindle motor current, torque, encoder position, and Z-axis motor contour deviation data via the edge device corresponding to a representative set of six sequential drilling holes.

3.2.2 Tool flank wear measurement

Tool flank wear was assessed on both flank faces of the twist drill using a Leica S9 I Stereomicroscope following each drilling cycle, consisting of 48 holes. To ensure precise measurement, the tool's flank face was positioned perpendicular to the stereomicroscope's objective lens. For this purpose, a custom stand was designed to match the geometry of the twist drill. Maximum flank wear was measured on both flank faces of the tool. The recorded wear values for selected measurement intervals are illustrated in Figure 3.6. These measurements served as reference data

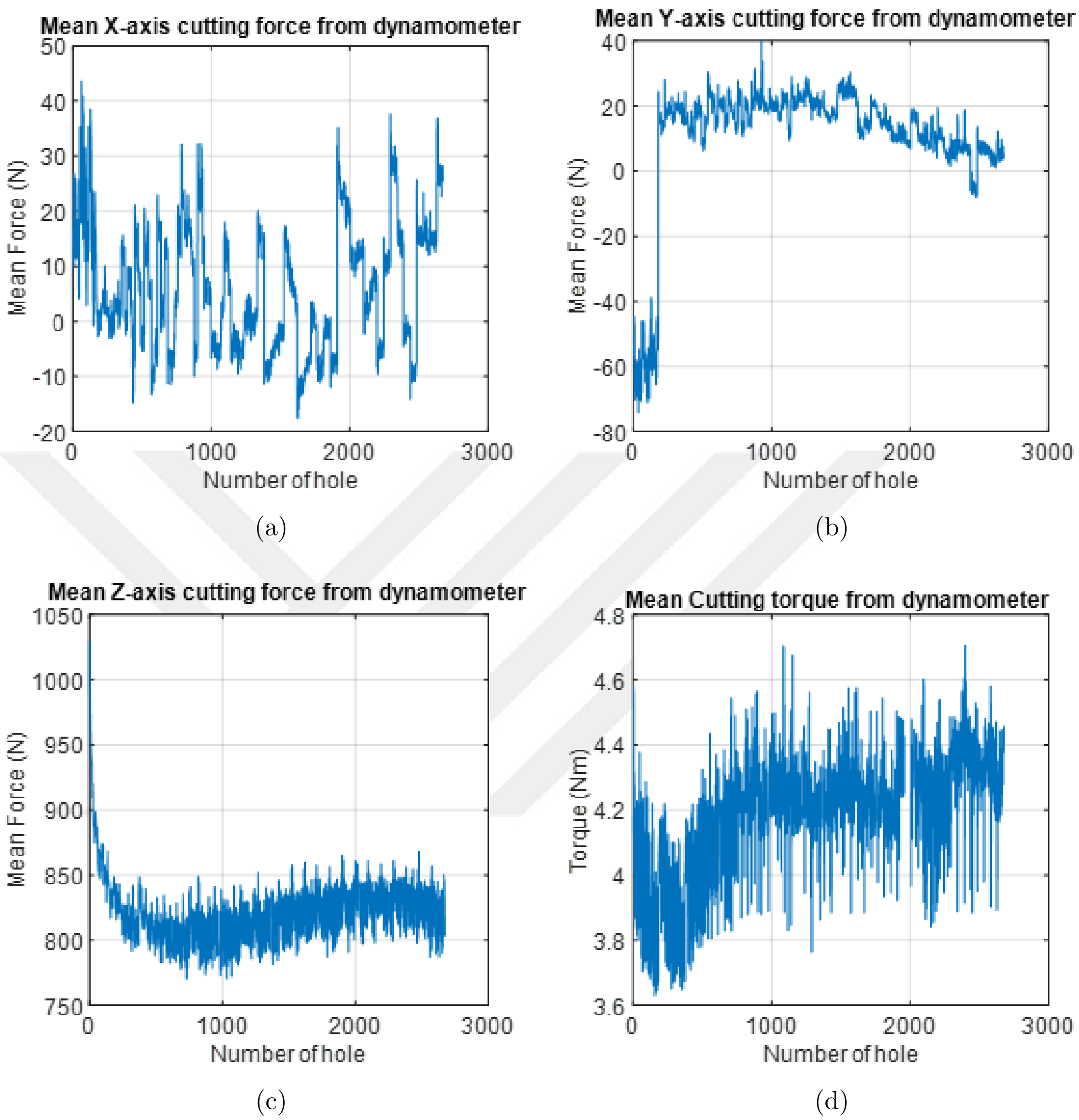

Figure 3.4: The mean cutting force components in all three directions and torque measurements collected by the dynamometer across all drilled holes.

for validating the predictive models of tool flank wear.

3.3 Proposed method for flank wear prediction

3.3.1 Data-driven prediction of tool flank wear

The development framework is informed by three key studies: Marani et al. [37], which focused on predicting flank wear during high-speed turning of steel alloys; H.

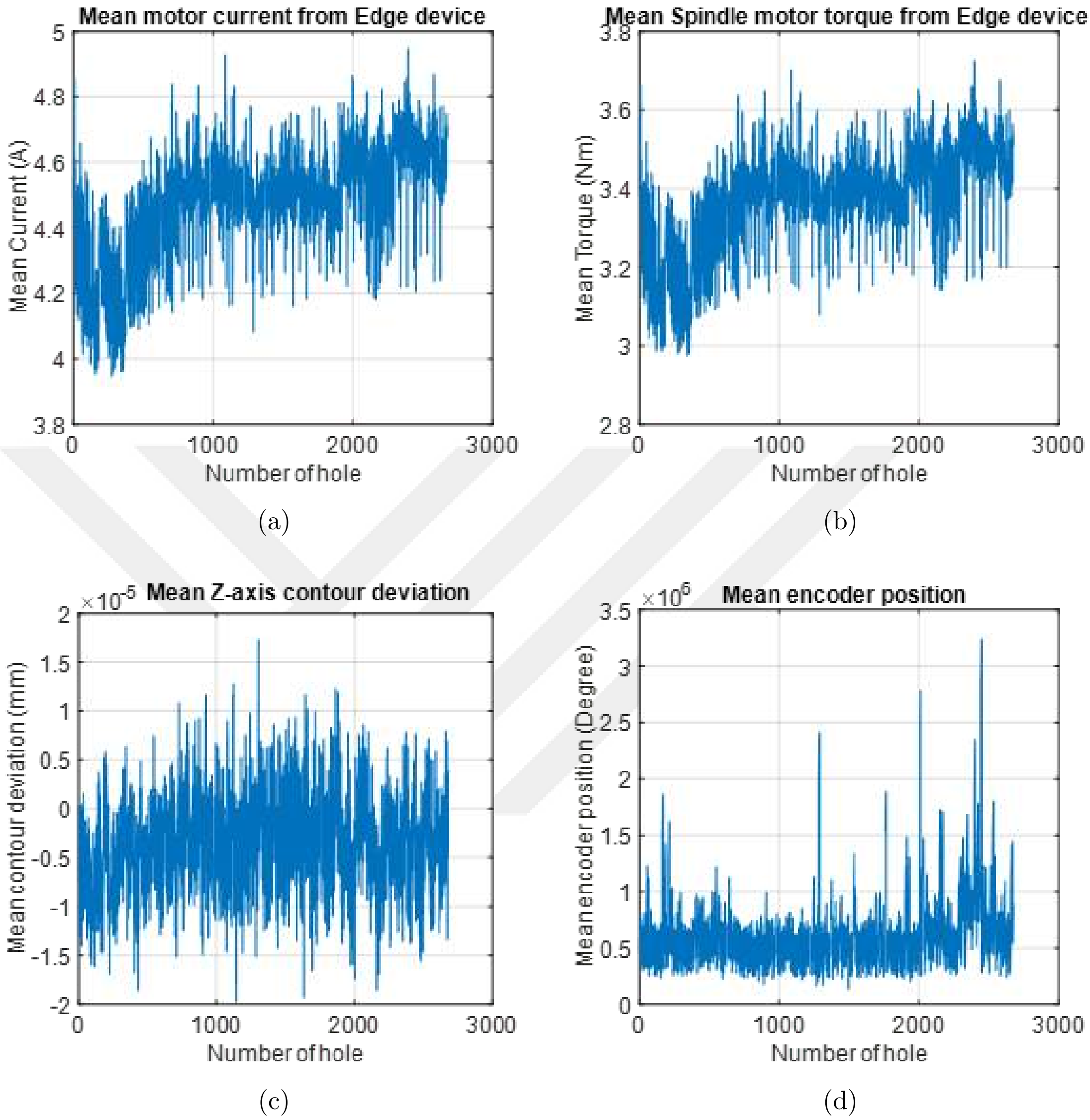

Figure 3.5: The mean values of spindle motor current, torque, encoder position, and Z-axis motor contour deviation collected by the edge device for all drilling holes.

Sun et al. [85], who investigated tool flank wear prediction in milling operations; and Wang et al. [86], who applied an LSTM model for monitoring milling tool conditions. Building on these foundations, the current study is structured into three main stages aimed at enhancing the accuracy of AI-based flank wear prediction in drilling operations using a coated tool.

1. Data pre-processing to clean data and determine the workable region.

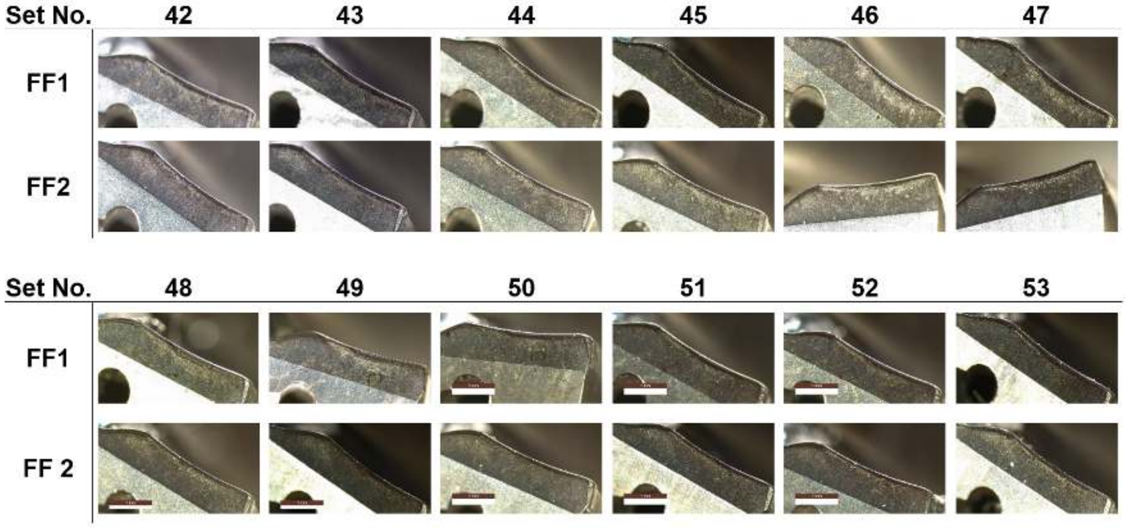

Figure 3.6: Tool flank wear for selected measurement sets, where FF1 and FF2 denote Flank Face 1 and Flank Face 2, respectively.

The signals collected from both the edge device and the rotary dynamometer during the drilling of 2676 holes encompassed data from both air-cutting and full engagement phases of the tool–workpiece interaction. Only the full engagement portions were extracted for statistical feature generation used in model training. Features most strongly correlated with tool flank wear were selected for training the predictive models. After data cleaning, a total of 2559 valid hole entries remained for AI model development. To prevent misleading patterns in the model caused by noise or irregular fluctuations, the increasing trend in wear progression across sequential holes was smoothed. This was done to avoid the distortion of essential data that could negatively impact model learning. Flank wear values were quantized while maintaining the relative progression between measurement points. This quantization step ensured that each hole could be effectively utilized in training data-driven models while preserving the inherent relationship among wear measurements across the dataset.

2. Feature engineering to obtain related input parameters.

As the AI models rely on real-time data from the digital shadow as input, the efficiency of training and inference times becomes increasingly important. To address this, feature engineering was applied to clean the dataset and reduce feature dimensionality, thereby optimizing the computational load and time required for deep learning model development. Accordingly, features were extracted from both the time and frequency domains based on the refined dataset.

3. Data-driven AI models training, validation, and testing.

   The selection of the AI model architecture was guided by iterative experimentation, ranging from multilayer perceptrons (MLPs) to recurrent neural networks (RNNs). Among the tested configurations, the Bi-LSTM and Bi-GRU architectures yielded the most accurate predictions while maintaining a balance between training time and testing performance.

3.3.2 Bidirectional long-short term memory

The unidirectional long short-term memory (LSTM) architecture is designed to retain long-term dependencies through its gating mechanism. In contrast, the key advantage of the bidirectional LSTM (Bi-LSTM) lies in its ability to capture contextual relationships across past, present, and future time steps within a single layer [87]. Achieving this functionality requires two separate unidirectional LSTM layers, which can increase computational demand due to the added model complexity. The architectures of both unidirectional LSTM and Bi-LSTM models are illustrated in Figure 3.7.

3.3.3 Bidirectional gate recurrent unit

The gated recurrent unit (GRU), introduced by Cho et al. in 2014 [88], was developed to simplify the long short-term memory (LSTM) architecture by reducing the number of trainable parameters. Unlike LSTM cells, GRUs do not maintain a separate memory component and instead merge the forget and update gates into a

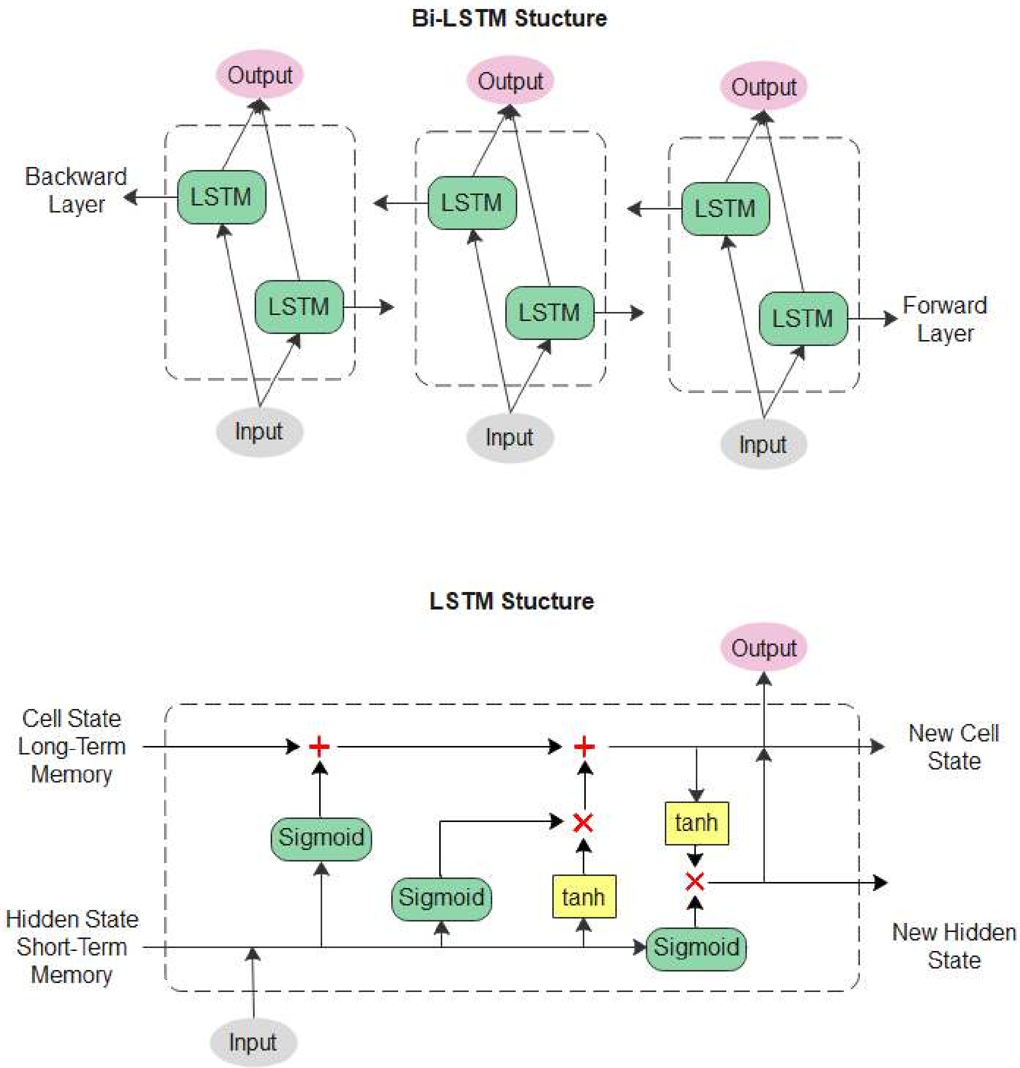

Figure 3.7: The LSTM and Bidirectional LSTM architectures.

single mechanism. This streamlined structure allows GRUs to train more efficiently, often requiring less computational time than LSTMs. However, this simplification can sometimes result in slightly lower predictive accuracy due to the reduced representational capacity.

Bi-LSTM and Bi-GRU are both advanced forms of recurrent neural networks designed to process sequential data, such as time-series signals or ordered events.

These architectures are particularly effective at learning temporal patterns, as they analyze input sequences in both forward and backward directions. By leveraging information from both past and future contexts, they enhance the model's ability to make accurate predictions—such as estimating tool wear progression during drilling—based on dynamic behavior over time.

The implementation and training of the AI models in this study were carried out on a Dell Precision 5820 workstation equipped with an Intel Xeon W-2223 CPU (3.6 GHz) and an NVIDIA RTX6000 GPU, providing the necessary computational performance for deep learning tasks.

3.4 Results and Discussion

The development process of the proposed approach followed the steps previously outlined. After quantizing the measured tool flank wear values, the total number of wear values was aligned with the number of drilled holes. This was achieved by applying linear interpolation between successive wear measurements, while a random noise component was introduced to simulate variations in operational conditions, such as chip adhesion. The resulting quantized maximum flank wear values for both flank faces are presented in Figure 3.8. Based on the observed trend in maximum wear progression, the data were segmented into three distinct regions, which are hypothesized to reflect the characteristic wear behavior of the tool's coated layer.

Feature engineering was performed, followed by correlation analysis to evaluate the relationship between tool flank wear and various statistical and spectral attributes of the collected signals. These attributes included the maximum, minimum, mean, variance, and the three dominant frequency components extracted via FFT in both the time and frequency domains. For time-domain analysis, selected input signals for the data-driven models included the Z-axis cutting force from the dynamometer, as well as spindle motor torque, current, encoder position, and Z-axis motor contour deviation from the industrial edge device. Features that exhibited weak correlation with flank wear were excluded from the model input set. Specifically, the cutting forces in the X and Y directions from the dynamometer and other

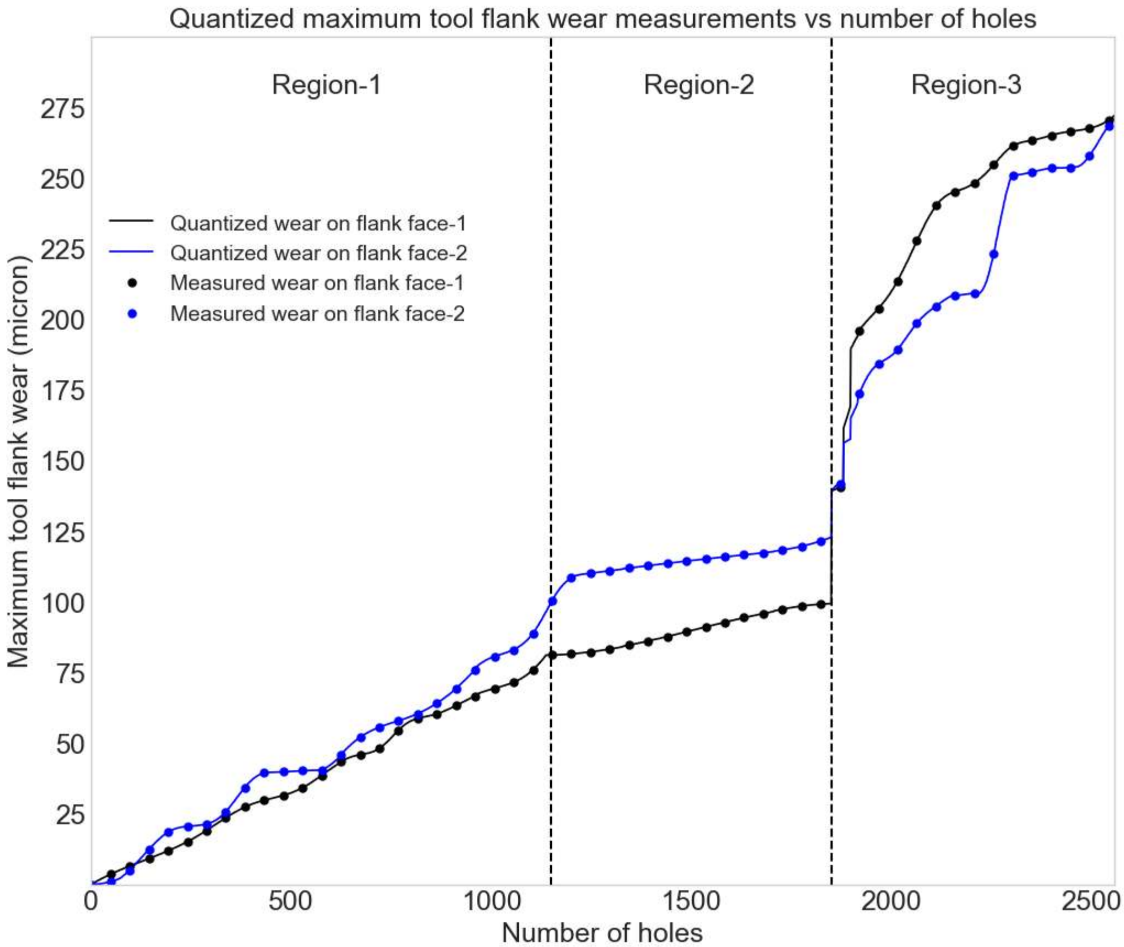

Figure 3.8: Quantized Maximum Tool Flank Wear on Both Flank Faces.

less relevant signals from the edge device were omitted. The final dataset was normalized using a min-max scaling approach to ensure uniform feature distribution. The correlations between the engineered features and flank wear measurements on both flank faces are illustrated in Figure 3.9.

Following data processing and feature engineering, a total of 35 features were extracted from the combined datasets of the industrial edge device and the dynamometer. The use of feature extraction and data standardization played a critical role in reducing computational load and training time. In industrial settings, this also contributes to mitigating data storage constraints. As a result, the processed dataset primarily consisted of clean and relevant drilling data associated with tool

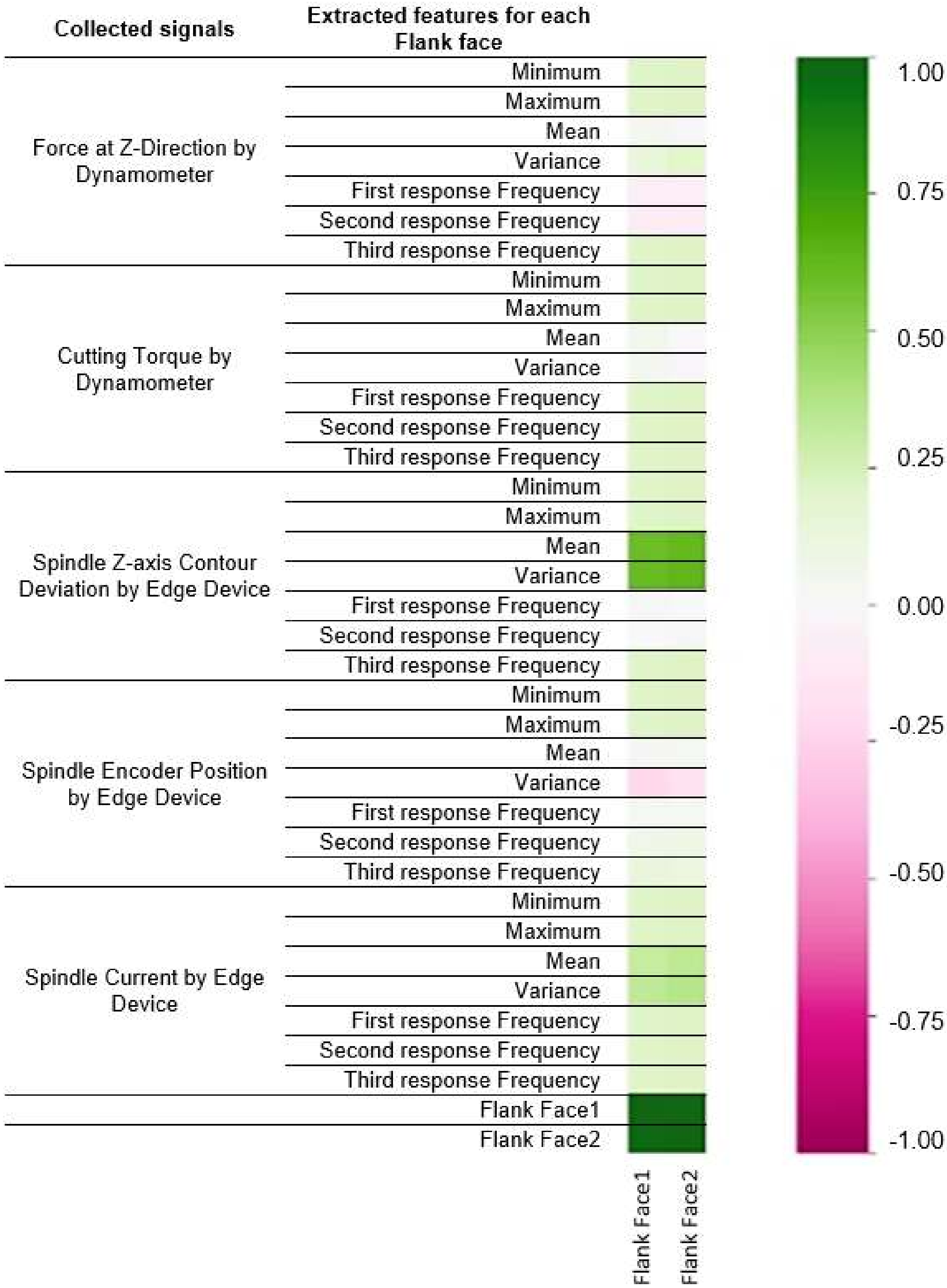

Figure 3.9: The generated features correlations with both flank faces.

Table 3.1: Sample numbers for each region in training, validation, and testing datasets.

	Train samples	**Test samples**	**Validation samples**
Region 1 (R1)	920	173	57
Region 2 (R2)	560	105	35
Region 3 (R3)	568	106	35

flank wear progression.

After completing the drilling experiments and feature engineering, the dataset was partitioned into two stages: first to define tool life stages, and then to separate training and testing sets. Tool life stages were categorized based on the progression of flank wear observed on each cutting edge of the drill, as illustrated in Figure 3.9. These stages were segmented according to the wear progression trends. Subsequently, the dataset was divided using a conventional 80/20 ratio for training and testing, respectively. Additionally, the test set was further split into validation and final test subsets using a 15/5 ratio. The distribution of training, validation, and testing samples across each tool wear stage is summarized in Table 3.1.

These data subsets were used for training and evaluating the AI models. The model architecture was implemented using the TensorFlow Keras framework, and hyperparameter optimization was carried out using Keras Tuner. The optimized hyperparameters are detailed in Table 3.2.

The Keras Tuner library employed Bayesian optimization to guide the development of AI models. This optimization technique iteratively identifies optimal hyperparameter combinations by leveraging the outcomes of previous trials, allowing models to reach near-optimal performance with fewer iterations. As a result, the time and computational resources required to minimize the loss function are significantly reduced. To further accelerate convergence, an early stopping mechanism was implemented during training, substantially decreasing the total training time. The effectiveness of deep learning models, particularly those trained on indirect signals, depends on the sufficiency and quality of the input data [33]. The

Table 3.2: Fine-tuned parameters of the AI model.

Hyperparameters in tuner	**Range**
Number of layers	1,2,3,4,5,6,7,8,9
Number of units in a layer	16, 32, 48, 64, ..., 256
Regularizer (L1, L2 and ElasticNet)	0, 0.001, 0.005, 0.01, 0.05
Activation functions	ReLU, tanh, eLU, GeLU
Dropout rates (forward & recurrent)	0.1, 0.2, 0.3, 0.4, 0.5
Learning rate	0.00001, 0.0001, 0.001, 0.01, 0.1
Optimizer	RMSprop
Loss function	Mean absolute error (MAE)

models developed in this study demonstrated high predictive performance without signs of overfitting, indicating that the training data was appropriately captured and generalized by the models. Among the evaluated architectures, bidirectional models outperformed their unidirectional counterparts. Unlike unidirectional RNNs, bidirectional structures can incorporate both past and future information, enabling real-time prediction of tool wear without the need for extensive data storage or delayed processing (approximately 10 seconds). Across all wear regions, bidirectional models showed a prediction accuracy improvement exceeding 10 microns compared to unidirectional RNNs and standard deep neural networks. In this context, the Bi-LSTM architecture proved more effective than its unidirectional counterpart for tool wear prediction. To address the three tool wear stages identified in Figure 3.8, separate Bi-LSTM models were trained for each region. While Bi-LSTMs generally offer improved accuracy due to their more complex gating mechanisms—including input, output, and forget gates—Bi-GRU architectures may offer faster training and greater computational efficiency due to their simpler structure with only update and reset gates. Depending on the specific task, either architecture may offer performance advantages. Each model was optimized over ten tuning iterations and trained for 500 epochs per iteration. The final Bi-LSTM model architectures are presented in

Figure 3.10. a–c. For the first wear region, the tuner converged after 65 minutes, resulting in a model with 6,850 trainable parameters and a training duration of 269 seconds. As shown in Figure 3.10. b, the second wear region model converged in 86 minutes, featuring 2,886,274 trainable parameters and a total training time of 2,555 seconds, as shown in 3.10. c.

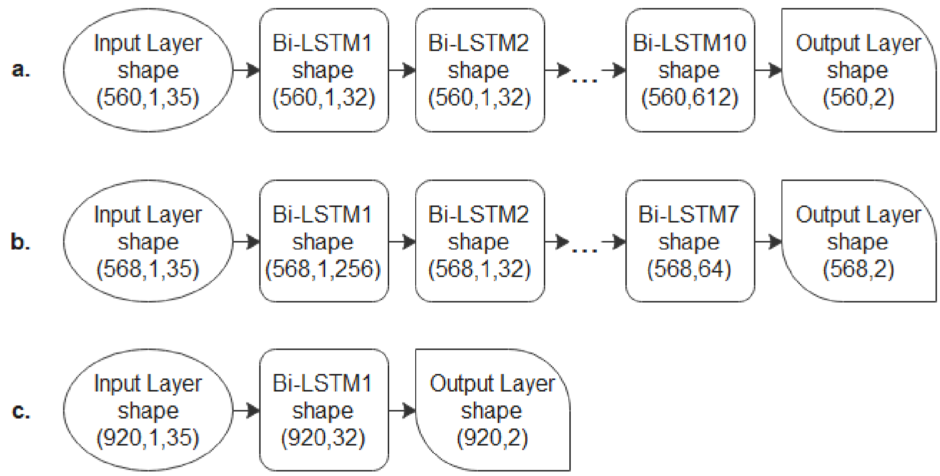

Figure 3.10: Structure of the Bi-LSTM model used for predicting three tool wear regions.

For the final tool wear region, the tuner completed convergence of the model in 159 minutes. This model comprised 424,834 trainable parameters and required 1,888 seconds for training. In this study, GRU-based models were also implemented using a bidirectional architecture. The performance outcomes and corresponding model structures are depicted in Figure 3.11.a–c. For the first tool wear region, the tuner converged after 85 minutes, producing a model with 307,842 trainable parameters and a training time of 460 seconds, as illustrated in Figure 3.11.a. In the second region, the tuner finalized the model within 72 minutes, yielding 5,310,978 trainable parameters and a total training duration of 2,259 seconds, as shown in Figure 3.11. b. Finally, for the third tool wear region, convergence was achieved after 91 minutes. The resulting model consisted of 1,165,304 trainable parameters and required 1,542 seconds for training, as presented in Figure 3.11. c.

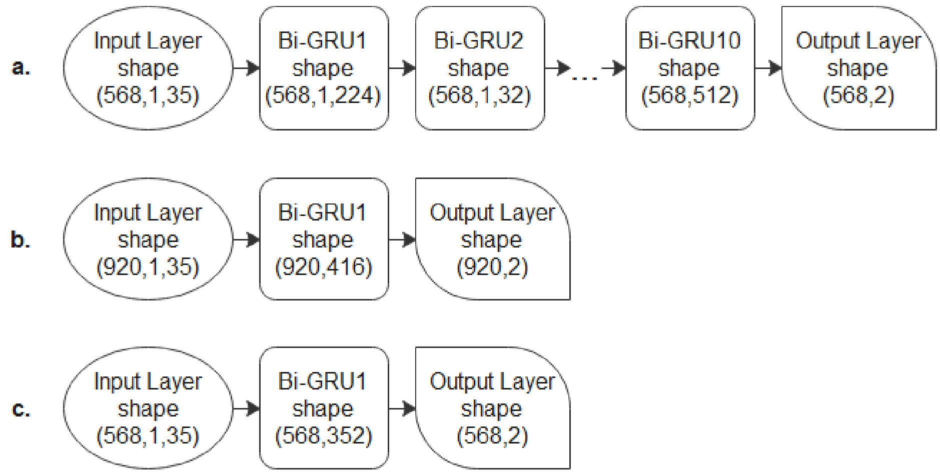

Figure 3.11: Structure of the Bi-GRU model used for predicting three tool wear regions.

For the final region of tool wear, the tuner completed model convergence in 62 minutes. The resulting model comprised 226,690 trainable parameters and required 308 seconds for training. All developed models are capable of generating predictions in under one minute for a single-hole drilling operation. The predictive results of both Bi-LSTM and Bi-GRU models across the flank faces for each wear region are illustrated in Figure 3.12 and Figure 3.13.

Both models demonstrated high accuracy and efficiency in terms of computational time during both training and inference. A comparison of the training and prediction times for the Bi-LSTM and Bi-GRU models across all tool wear regions is presented in Figure 3.14 and Figure 3.15.

Based on the computational time results for the three distinct tool wear regions, the Bi-LSTM model exhibited the shortest test time in Region 1, whereas the Bi-GRU model achieved the lowest test computational times in the remaining regions. A comparison of the validation loss and test accuracy for both Bi-LSTM and Bi-GRU models across all wear regions is provided in Figure 3.16 and Figure 3.17.

According to the accuracy results across the three distinct tool wear regions, the Bi-GRU model achieved the highest test accuracy in Region 1 and Region 3, while

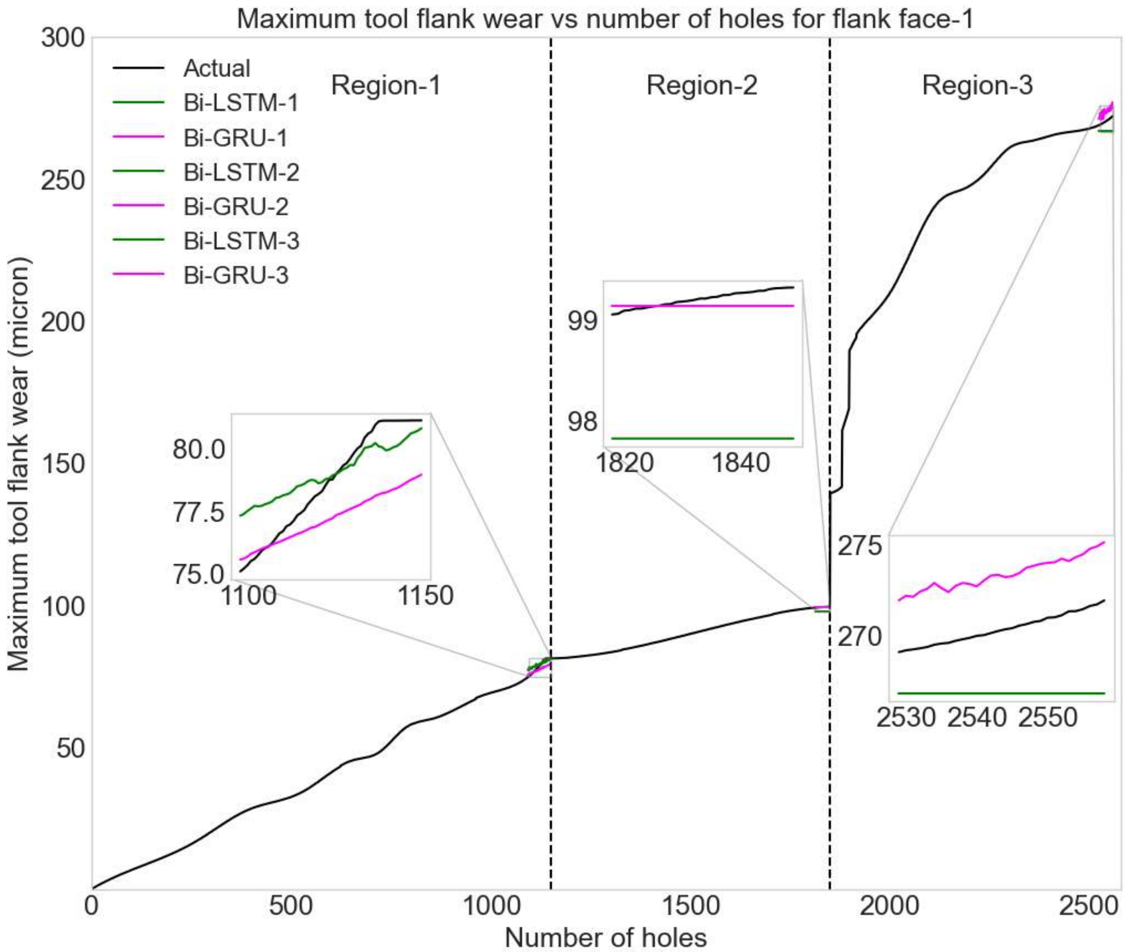

Figure 3.12: Bi-LSTM and Bi-GRU prediction models for tool flank face-1 across all wear regions.

the Bi-LSTM model demonstrated superior performance in Region 2.

Ultimately, once machine learning models are trained on the Edge device for specific tools and machining conditions, their generalizability to other tools or workpieces may vary. Key factors such as tool geometry, material properties, and operational parameters significantly influence tool wear behavior. In cases where tools or workpieces share similar characteristics, the models may be transferable with minimal adjustments. However, substantial differences in properties may require either full retraining or model fine-tuning with new data. Implementing a continuous learning framework, where the model is incrementally updated using real-time data, can significantly enhance its adaptability and prediction accuracy over time.

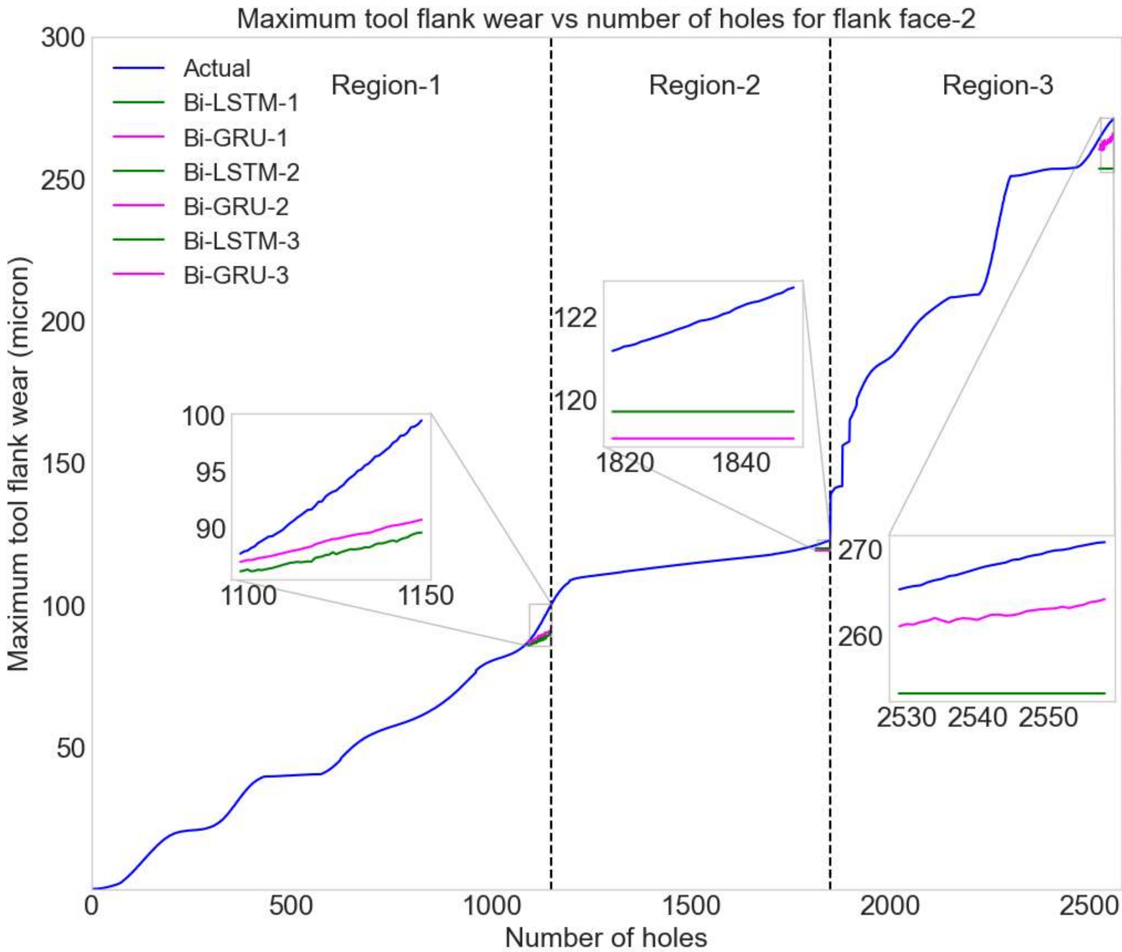

Figure 3.13: Bi-LSTM and Bi-GRU prediction models for tool flank face-2 across all wear regions.

3.5 Summary

An AI-assisted digital shadow was developed to enable real-time prediction of flank wear during the drilling process. Drilling data were simultaneously acquired from an industrial edge device and a rotary dynamometer. For the first time, feature engineering was applied to this combined dataset in both the time and frequency domains, allowing the identification of features most strongly correlated with drilling tool flank wear. The most relevant indicators included the Z-axis cutting force and torque from the dynamometer, as well as the spindle motor current, encoder position, and Z-axis motor contour deviation obtained from the industrial edge device.

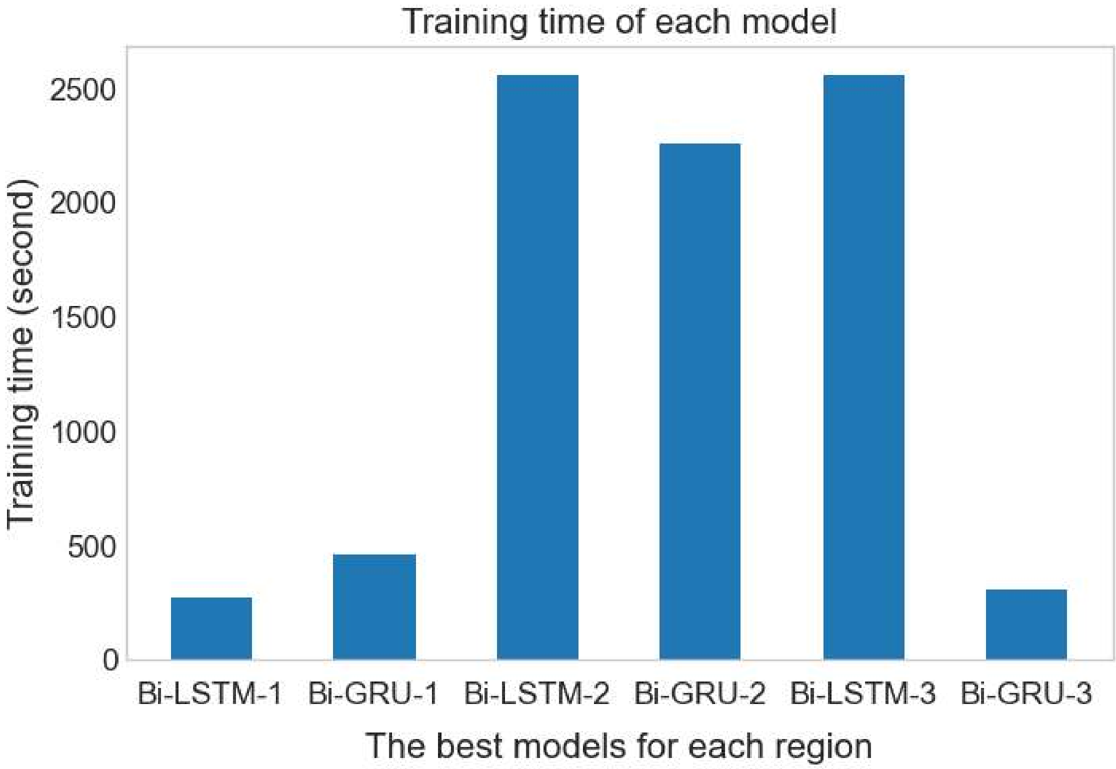

Figure 3.14: Training time comparison of Bi-LSTM and Bi-GRU prediction models across all wear regions.

Recurrent neural networks utilizing Bi-LSTM and Bi-GRU architectures were implemented for each defined wear region in the dataset. This study marks the first application of these architectures to such data, with the most accurate and computationally efficient model identified for each wear region subset. The resulting digital shadow, constructed from edge device data and the trained AI model, offers a cost-effective solution by reducing reliance on expensive multi-sensor systems, minimizing downtime, and preventing tool underuse or overuse in smart manufacturing environments. Furthermore, this approach is well-suited for integration into digital twin systems. Future work will focus on enhancing the digital shadow by incorporating it into a real-time control and feedback mechanism within the physical layer of a digital twin framework.

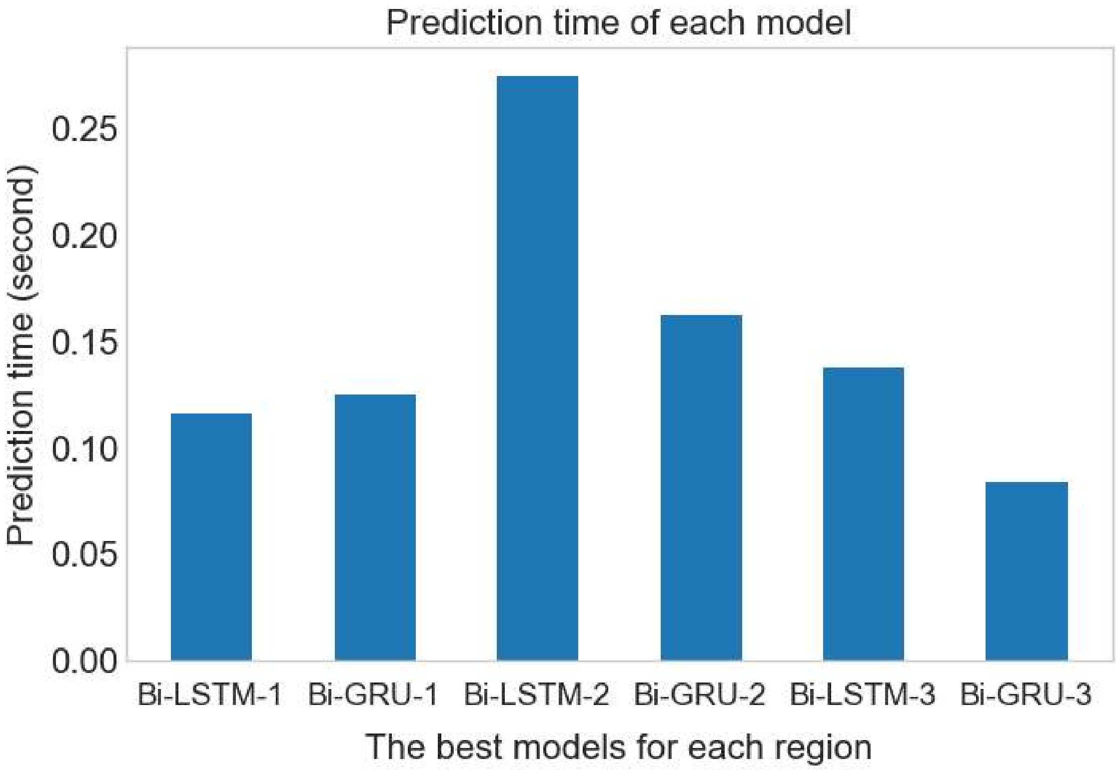

Figure 3.15: Prediction time comparison of Bi-LSTM and Bi-GRU models across all wear regions.

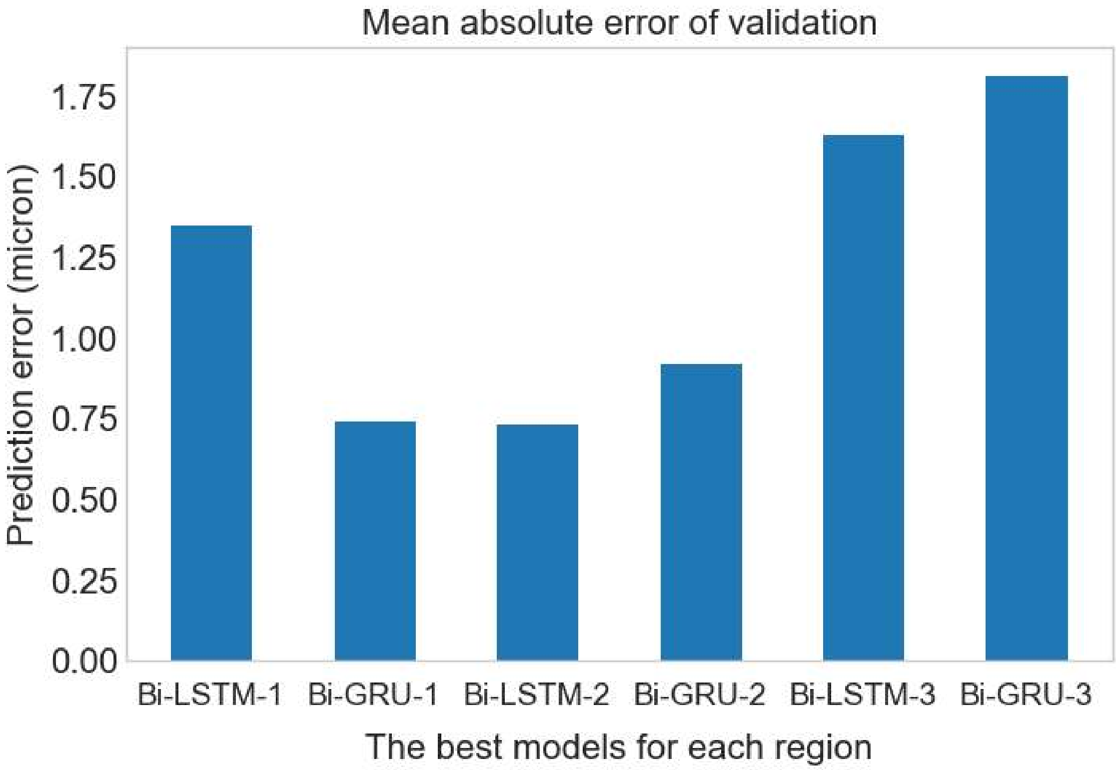

Figure 3.16: Prediction error comparison of Bi-LSTM and Bi-GRU models across all wear regions.

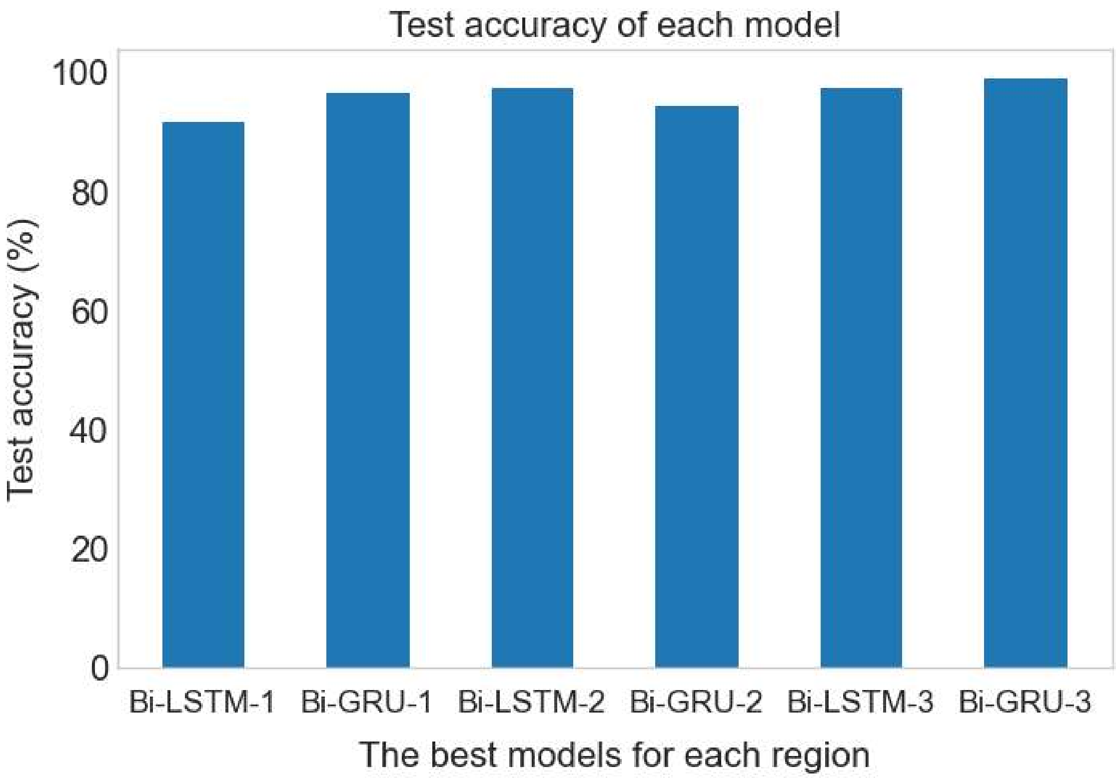

Figure 3.17: Test accuracy comparison of Bi-LSTM and Bi-GRU models across all wear regions.

Chapter 4

SENSORLESS MEASUREMENT OF CUTTING FORCES AND TORQUE VIA INDUSTRIAL EDGE DEVICE

4.1 Overview

Accurate measurement of cutting forces and torque during machining traditionally relies on high-cost sensors such as dynamometers. This study presents a novel sensorless method for real-time monitoring of cutting forces, torque, tangential forces, and spindle current during milling operations. In the proposed approach, cutting forces and torque were acquired via a rotary dynamometer, while spindle torque and current data were simultaneously collected via a high-frequency industrial edge device during the milling operation of Ti6Al4V titanium alloy. Data analysis revealed strong correlations between the dynamometer outputs and the edge device measurements. Validation results indicated that the method achieves mean errors below 12%. This sensorless technique provides a compelling alternative for in-process monitoring, offering potential benefits such as reduced reliance on expensive sensors, shorter setup times, and improved machining efficiency.

4.2 Experimental method and data acquisition

The milling experiments were conducted on a Spinner U1530 five-axis CNC machining center equipped with a Siemens Sinumerik 840D sl controller. A Titanium alloy (Ti-6Al-4V) workpiece with dimensions of 300 × 225 × 25 mm was used. Slot milling was performed using a 12 mm diameter, 5-flute fresh AlCrN-coated tool. Cutting force and torque data were collected using two types of dynamometers: a Kistler 9257B table-type dynamometer fixed beneath the workpiece on the CNC machine table, and a Kistler 9123C rotary dynamometer mounted on the spindle. The signals from both dynamometers were amplified using Kistler Type 5019 and 5223 charge amplifiers, respectively, and converted into digital form via a NI USB-6259 data acquisition system from National Instruments. Additionally, spindle motor current and torque data were simultaneously recorded through the Siemens Sinumerik 840D sl controller using a Simatic IPC227E industrial edge device running Siemens' IoT Edge Application, with a sampling frequency of 500 Hz. The experimental procedure is illustrated in Figure 4.1.

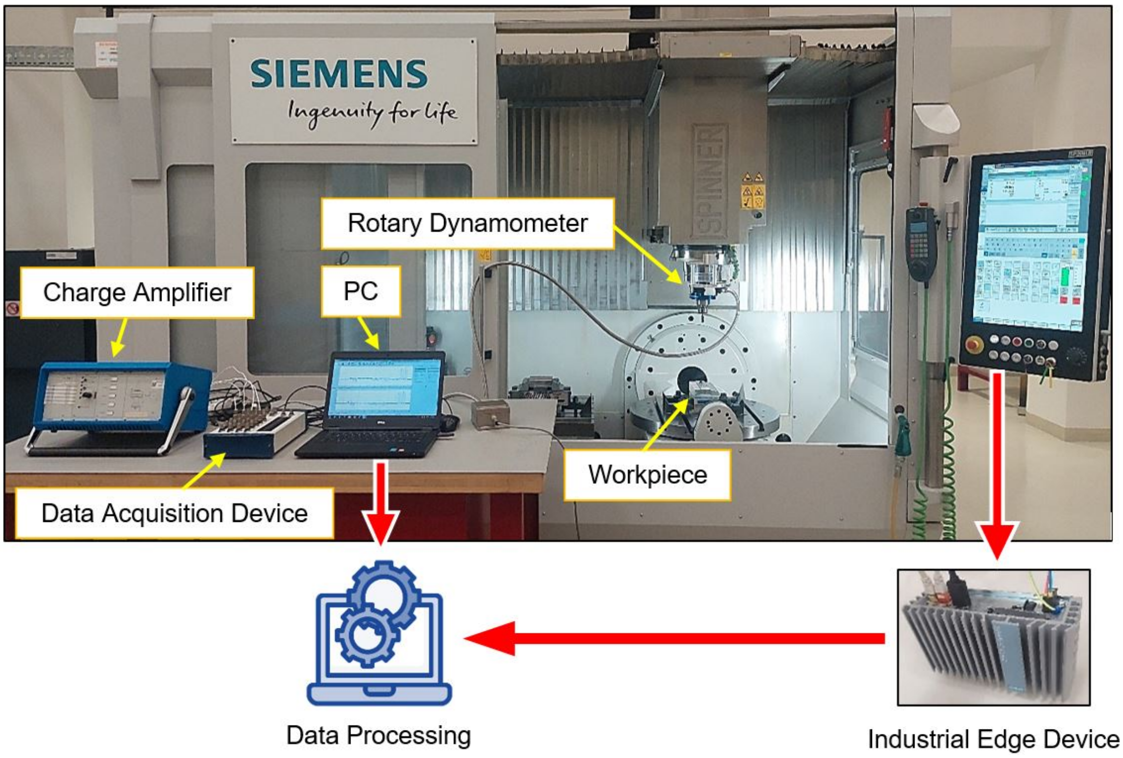

Figure 4.1: The experimental process.

To ensure reliable and consistent correlation results between the data obtained from the dynamometer and the edge device, a series of slot milling experiments were carried out on a Titanium alloy workpiece. These experiments were conducted under varying cutting speed and feedrate values, while maintaining a constant axial depth of cut of 3 mm. Two types of validation tests were conducted for repeatability and validation of different feedrate values approaches [89]. The experimental design for the repeatability tests, consisting of three trials (two for testing and one for vali-

Table 4.1: Experimental design for repeatability validation.

Exp. No.	f (mm/min)	S (rpm)	fpt (mm/tooth)	V (m/min)
1	53	1060	0.01	40
2	106	1060	0.02	40
3	159	1060	0.03	40
4	79	1590	0.01	60
5	159	1590	0.02	60
6	238	1590	0.03	60
7	106	2122	0.01	80
8	212	2122	0.02	80
9	318	2122	0.03	80

dation), is detailed in Table 4.1. Meanwhile, the experimental setup for validating various feedrate values is provided in Table 4.2.

The directions of cutting forces and torque are determined by the fixed orientation of the cutter edges and the workpiece within the rotary-type dynamometer setup. An example of the raw tangential force and torque data recorded by the rotary dynamometer is presented in Figure 4.2.

A sample of the raw spindle torque and current data acquired from the edge device is illustrated in Figure 4.3.

4.3 Results and discussion

After acquiring raw signals from both the edge device and the rotary dynamometer, the slot milling signals of the steady-state cutting interval were carefully processed and analyzed. This included compensating for any temporal misalignment between the signals and aligning them precisely within the actual cutting intervals for accurate comparison. The process of estimating cutting torque, tangential force, and current via the edge device was carried out in three key steps:

Table 4.2: Experimental design for validation across different feedrate values.

Exp. No.	f (mm/min)	S (rpm)	fpt (mm)	V (m/min)
1	27	1060	0.005	40
2	80	1060	0.015	40
3	133	1060	0.025	40
4	40	1590	0.005	60
5	120	1590	0.015	60
6	199	1590	0.025	60
7	53	2122	0.005	80
8	160	2122	0.015	80
9	299	2122	0.025	80

4.3.1 Cutting torque correlation

In the first step, the correlation between cutting torque values obtained from the dynamometer and spindle torque data recorded by the edge device was examined across multiple milling tests. The analysis revealed strong linear correlations between the two data sources under various cutting velocities and feedrate conditions, indicating the feasibility of estimating cutting torque using only the edge device. The raw spindle torque data obtained from the edge device, along with the corresponding torque measurements recorded by the dynamometer for Trial 1, are depicted in Figures 4.4, 4.5, and 4.6.

The findings demonstrate a consistent and reliable correlation between the torque measurements obtained from the dynamometer and those recorded by the industrial edge device across different milling trials. The results of the repeatability validation experiments indicate mean errors ranging from as low as 3.4% to a maximum of 11.9%, representing the best and worst cases, respectively, as illustrated in Figures 4.7, 4.8, and 4.9.

Figure 4.10 presents representative correlation results between the raw torque data obtained from the dynamometer and the Edge device across different feedrate

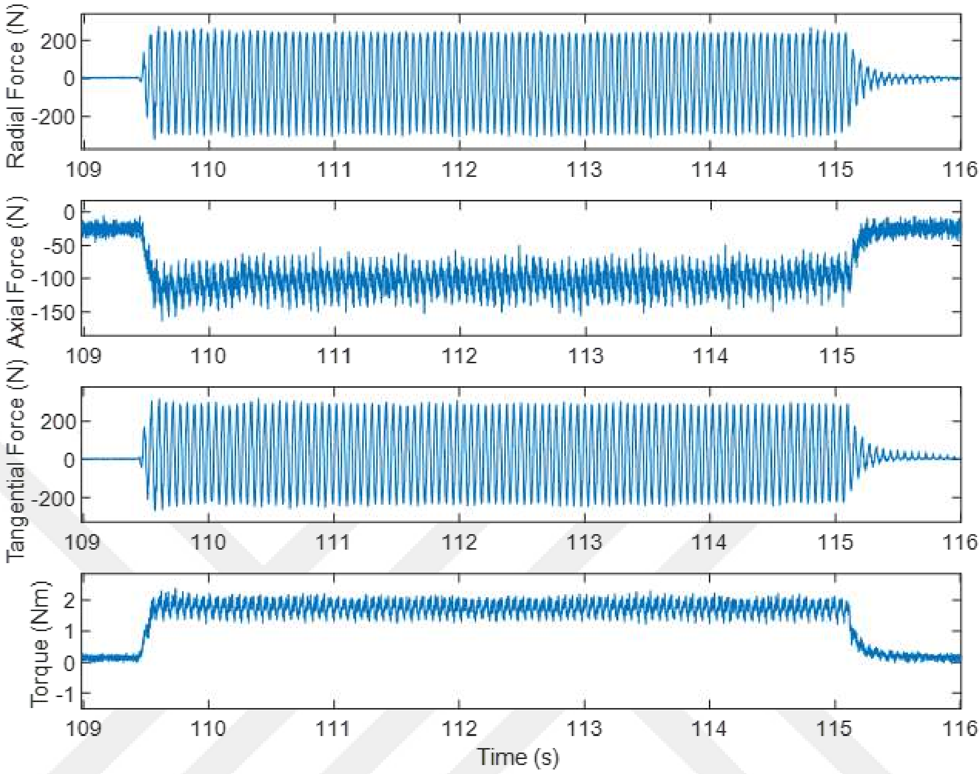

Figure 4.2: Sample raw milling data collected by the dynamometer in Experiment 3.

values at a cutting speed of 40 m/min.

The correlation between the spindle torque data obtained from the Edge device and the torque data from the dynamometer at various feedrate values for cutting velocities of 40 m/min, 60 m/min, and 80 m/min is expressed in Equations 4.1, 4.2, and 4.3, respectively. In these equations, T_E denotes the raw spindle torque data from the Edge device [Nm], and T_D represents the corresponding torque data from the dynamometer [Nm]. The coefficients of determination (R^2) for Equations (1), (2), and (3) are 92%, 90%, and 88%, respectively.

$$T_E = 0.64 \times T_D + 0.39 \tag{4.1}$$

$$T_E = 0.44 \times T_D + 0.9 \tag{4.2}$$

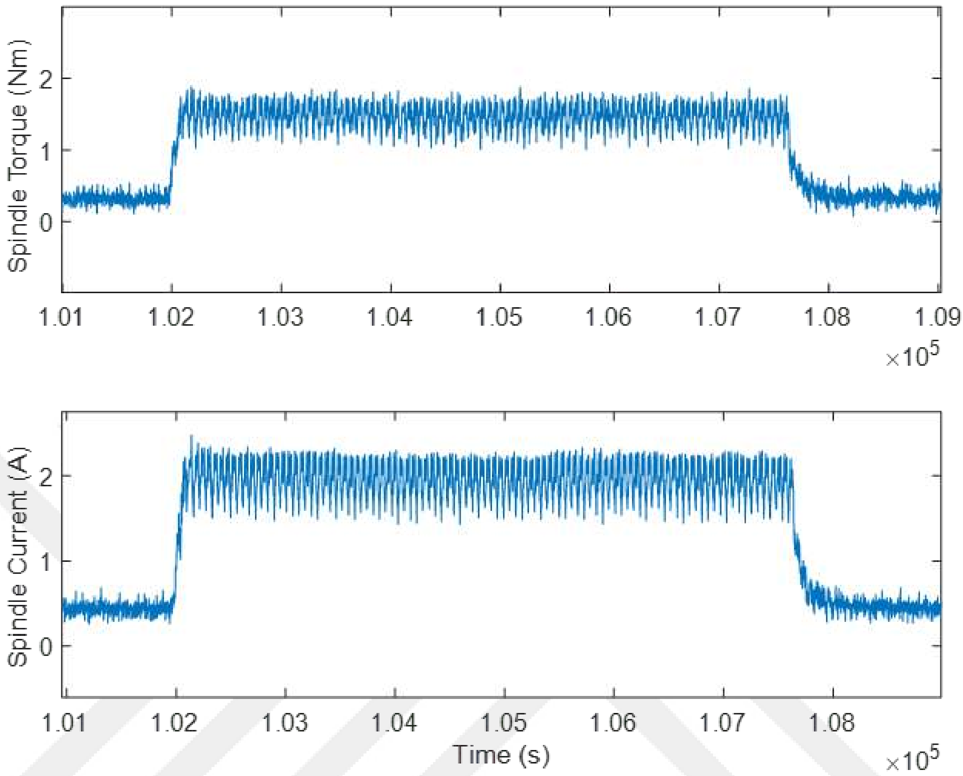

Figure 4.3: Sample raw data collected by the Edge device in Experiment 3.

$$T_E = 0.34 \times T_D + 1.12 \tag{4.3}$$

The validation outcomes demonstrate satisfactory prediction accuracy between the torque raw data obtained from both the Edge device and the dynamometer across different feedrate and cutting velocity conditions. The mean percentage error ranged from as low as 3.4% to a maximum of 11.86%, as illustrated in Figures 4.11, 4.12, and 4.13.

4.3.2 Tangential force correlation

In the second phase, the correlation between the tangential cutting force data obtained from the dynamometer and the spindle torque data recorded by the industrial edge device was analyzed. The results revealed a strong relationship between these datasets across various milling experiments, as depicted in Figures 4.14, 4.15, and

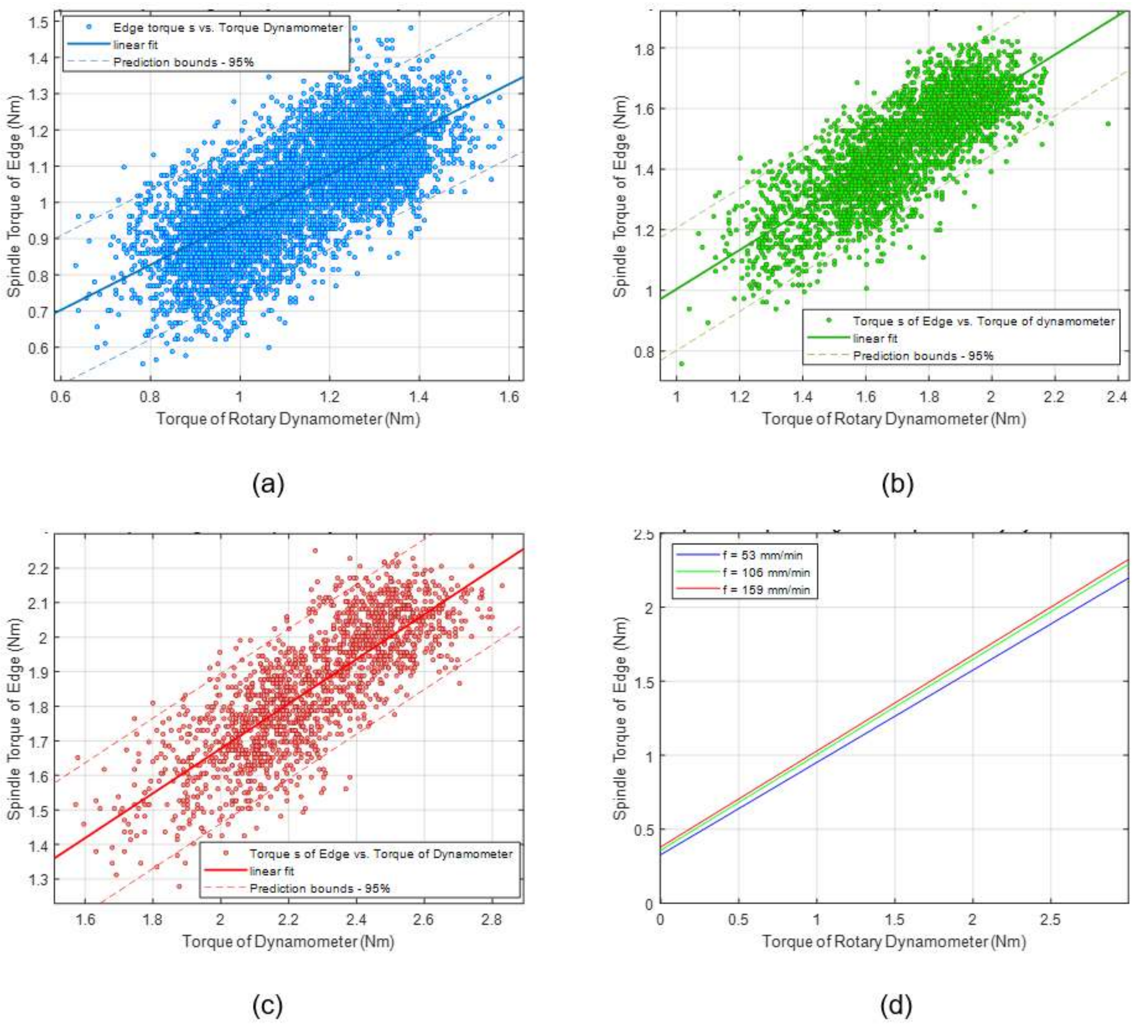

Figure 4.4: Spindle torque measured by the Edge device vs. torque collected by the dynamometer at a cutting speed of 40 m/min and feedrate values of (a) 53 mm/min, (b) 106 mm/min, (c) 159 mm/min, and (d) all values for Trial 1.

4.16.

The results demonstrate a consistent correlation between the tangential force measurements from the dynamometer and the spindle torque data acquired from the industrial edge device across different milling experiments. In the repeatability validation tests, the mean error ranged from as low as 1.2% to a maximum of 10.7%, as illustrated in Figures 4.17, 4.18, and 4.19.

Figure 4.20 illustrates sample correlation results between the raw tangential force data obtained from the dynamometer and the spindle torque data recorded by the

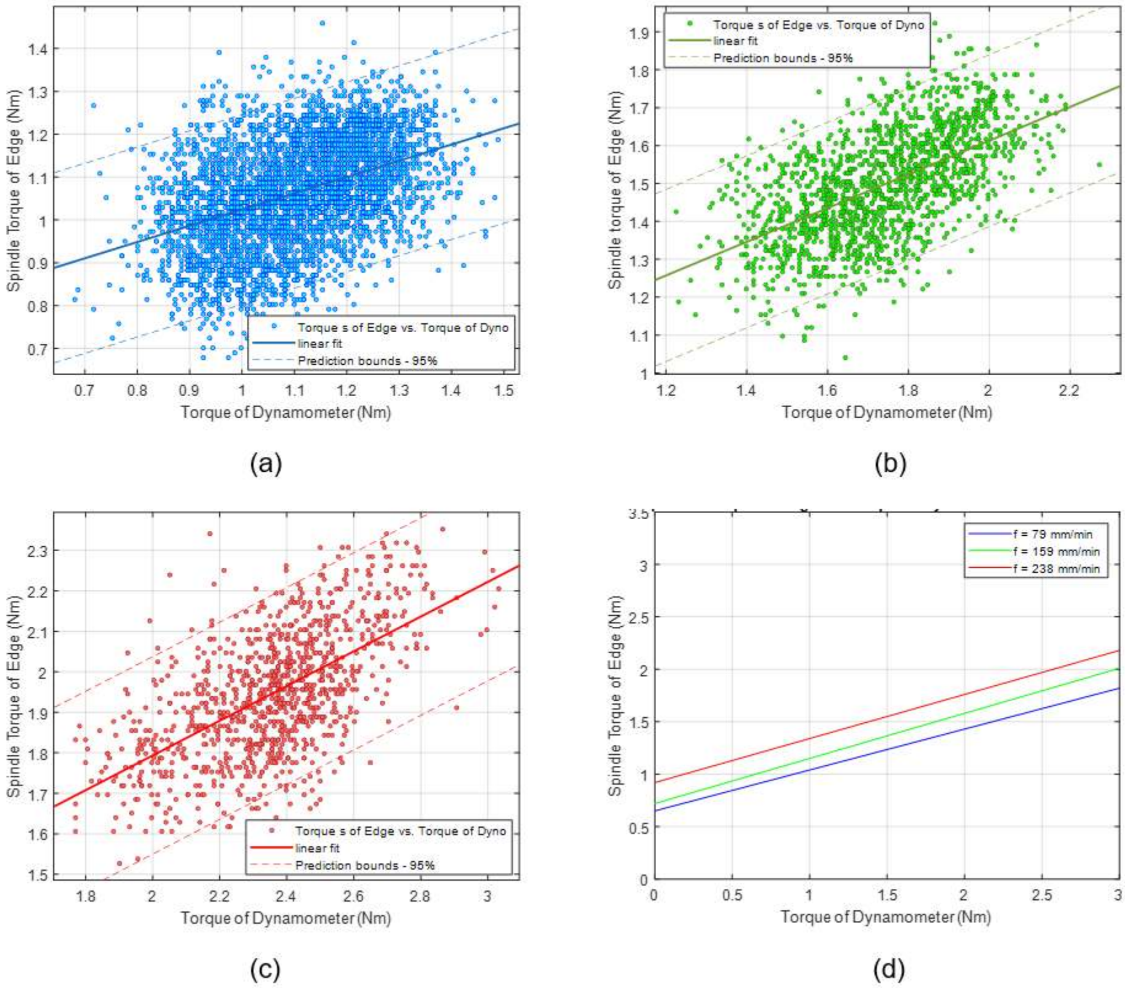

Figure 4.5: spindle torque measured by the Edge device vs torque collected by the dynamometer at a cutting speed of 60 m/min and feedrate values of (a) 79 mm/min, (b) 159 mm/min, (c) 238 mm/min, and (d) all values for Trial 1.

industrial edge device across various feedrate values at a cutting speed of 40 m/min.

The correlation equations between the tangential force data from the dynamometer and the spindle torque data from the industrial edge device, obtained under varying feedrate conditions at cutting speeds of 40 m/min, 60 m/min, and 80 m/min, are presented in Equations 4.4, 4.5, and 4.6. In these equations, T_E denotes the spindle torque data from the edge device [Nm], F_{tD} represents the tangential force measured by the dynamometer [N], and f stands for the feedrate.

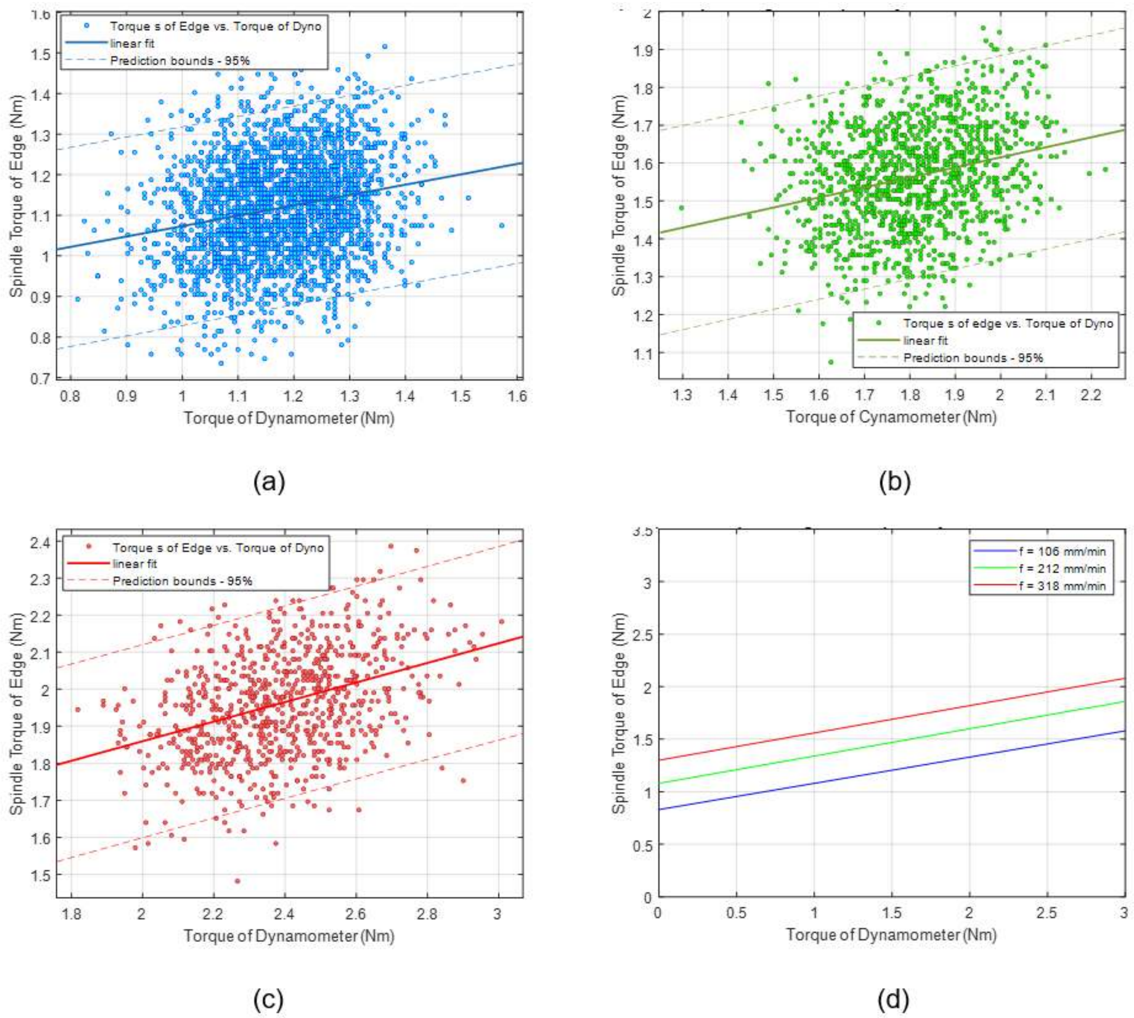

Figure 4.6: spindle torque measured by the Edge device vs. torque collected by the dynamometer at a cutting speed of 80 m/min and feedrate values of (a) 106 mm/min, (b) 212 mm/min, (c) 318 mm/min, and (d) all values for Trial 1.

$$T_E = 0.0056 \times F_{tD} + 0.191 \times f^{-0.56} \tag{4.4}$$

$$T_E = 0.0005 \times F_{tD} + 0.151 \times f^{-0.542} \tag{4.5}$$

$$T_E = 0.00042 \times F_{tD} + 0.147 \times f^{-0.559} \tag{4.6}$$

The validation results demonstrate reliable prediction accuracy between the raw tangential force measurements from the dynamometer and the spindle torque data from the industrial edge device across various feedrate and cutting speed conditions.

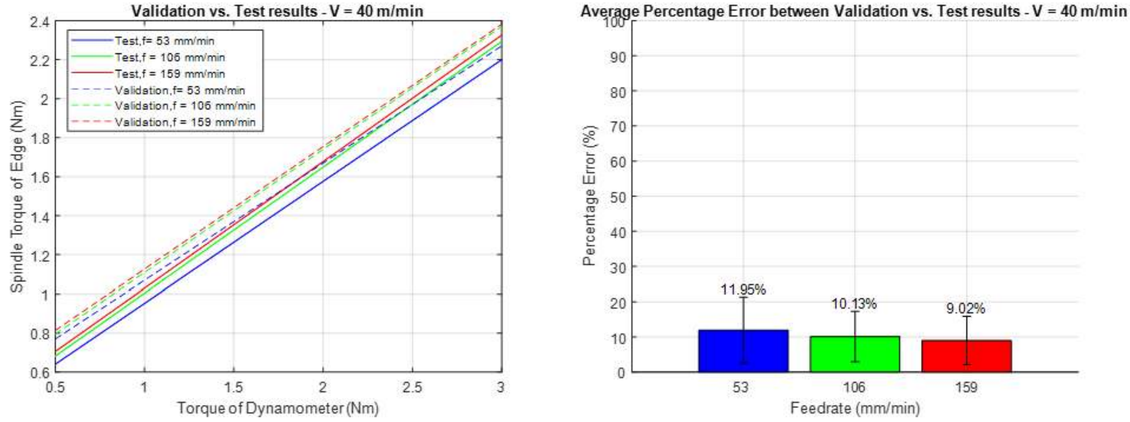

Figure 4.7: Validation of repeatability of edge device spindle torque vs. dynamometer torque measurements at the cutting speed of 40 m/min.

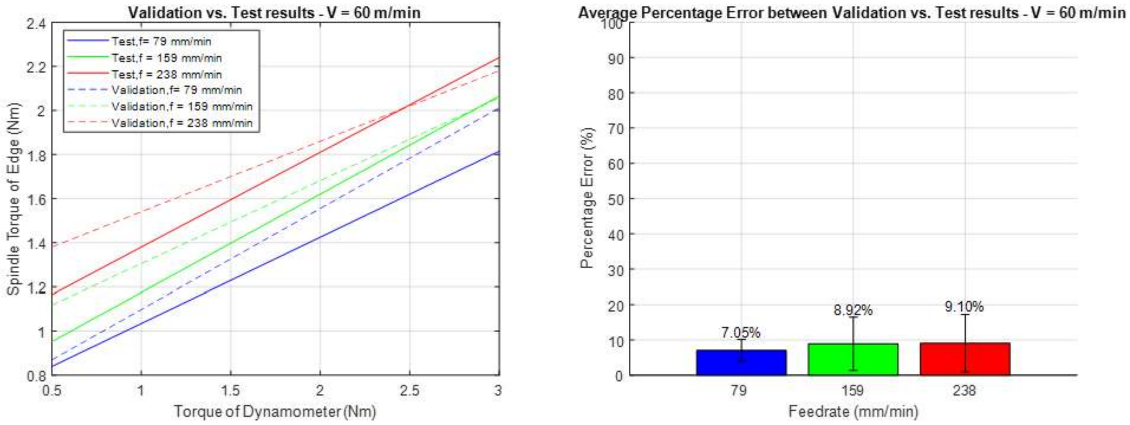

Figure 4.8: Validation of repeatability of edge device spindle torque vs. dynamometer torque measurements at the cutting speed of 60 m/min.

The mean prediction errors ranged from as low as 0.61% to a maximum of 7.82%, as illustrated in Figures 4.21, 4.22, and 4.23.

4.3.3 Cutting current correlation

In the third stage, the correlation between the spindle current obtained from the industrial edge device and the torque measured by the rotary dynamometer was examined to enable the estimation of cutting current. The analysis revealed a strong relationship between these parameters, as presented in Figures 4.24, 4.25, and 4.26.

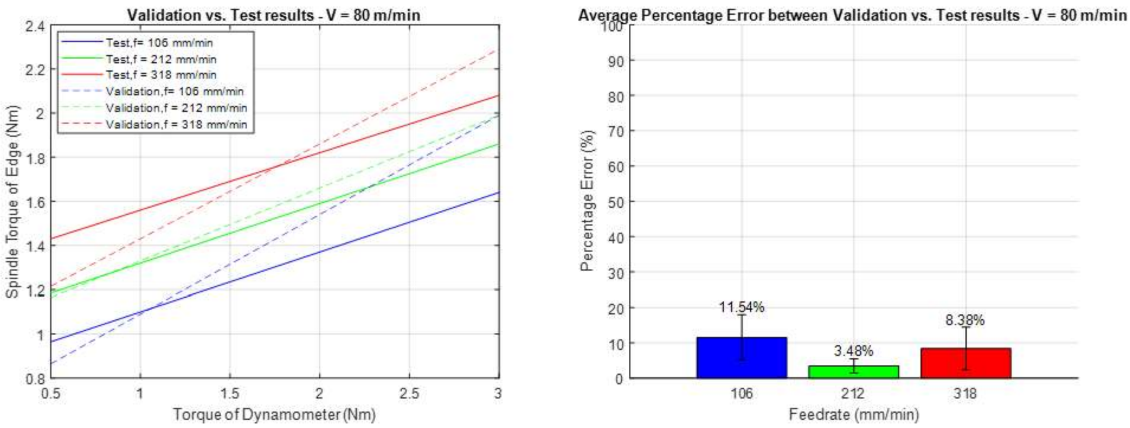

Figure 4.9: Validation of repeatability of edge device spindle torque vs. dynamometer torque measurements at the cutting speed of 80 m/min.

The results indicate a strong correlation between the torque data obtained from the dynamometer and the industrial Edge device across various milling experiments. The repeatability validation tests yielded mean error rates ranging from 7.47% (best case) to 12.66% (worst case), as illustrated in Figures 4.27, 4.28, and 4.29.

Figure 4.30 presents sample correlation results between the raw torque measurements from the dynamometer and the spindle current data captured by the industrial edge device at various feedrate values, conducted at a cutting speed of 40 m/min.

The correlation equations between the dynamometer's torque data and the raw spindle current data from the industrial edge device at feedrate variations for cutting velocities of 40 m/min, 60 m/min, and 80 m/min are presented in Equations 4.7, 4.8, and 4.9, where C_E denotes the spindle current [A] from the edge device, and T_D represents the torque measured by the dynamometer [Nm].

$$C_E = 0.77 \times T_D + 0.64 \tag{4.7}$$

$$C_E = 0.5 \times T_D + 1 \tag{4.8}$$

$$C_E = 0.38 \times T_D + 1.2 \tag{4.9}$$

The validation outcomes demonstrate reliable prediction performance between the raw torque data from the dynamometer and the spindle current data from the

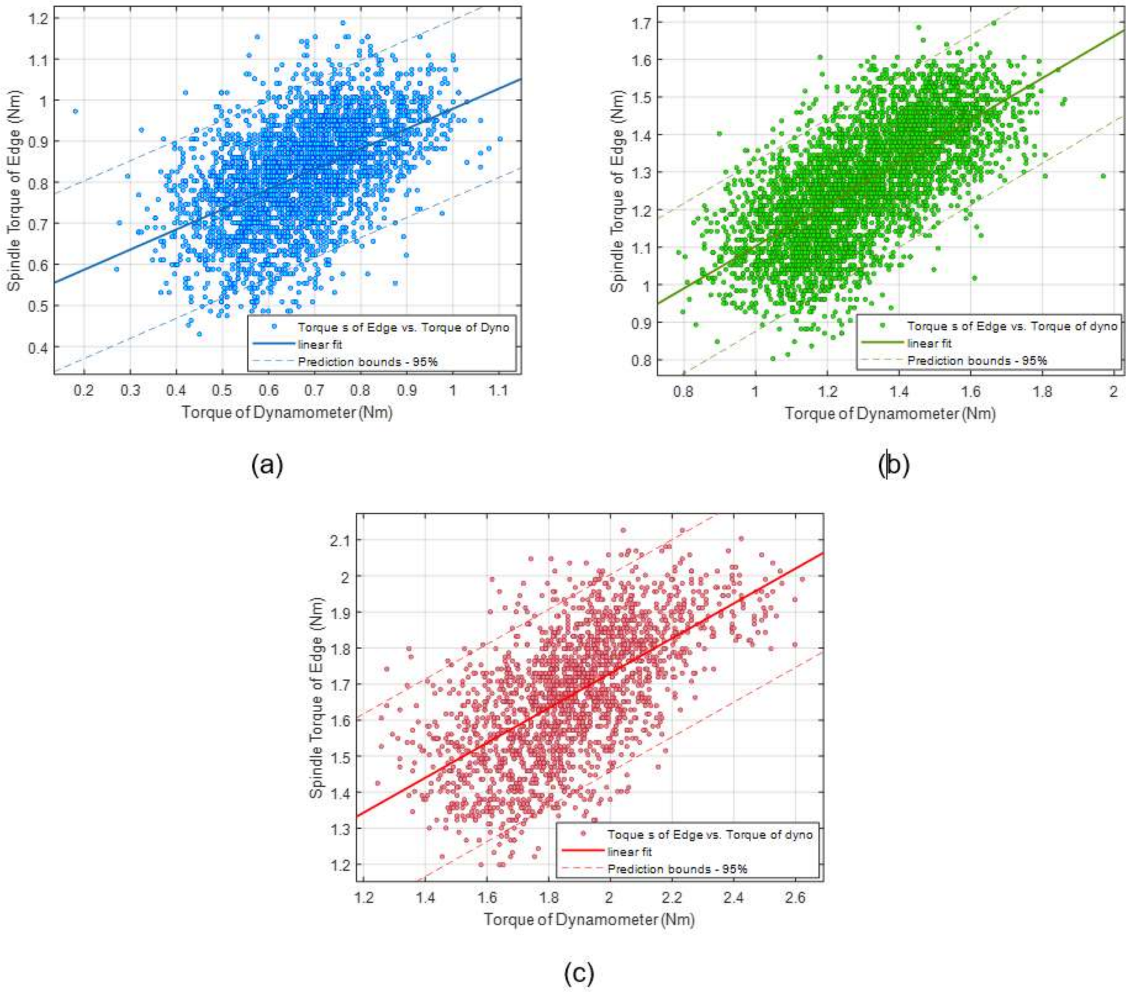

Figure 4.10: Correlation results between spindle torque measured by the Edge device and torque recorded by the dynamometer at a cutting speed of 40 m/min, with feedrate values of (a) 27 mm/min, (b) 80 mm/min, and (c) 133 mm/min.

industrial edge device across various feedrates and cutting speeds. The mean error ranged from 1.99% (best case) to 11.55% (worst case), as illustrated in Figures 4.31, 4.32, and 4.33.

4.4 Summary

This study involved conducting a series of milling tests on titanium alloy workpieces under varying cutting speeds and feedrate conditions. During these trials, cutting forces and torque were simultaneously recorded using a rotary-type dynamometer,

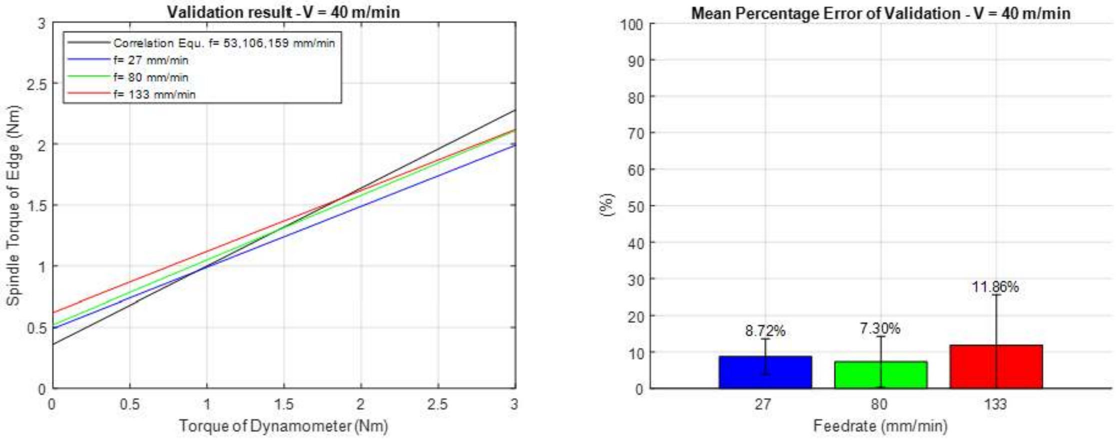

Figure 4.11: Validation results of the spindle torque data from Edge vs. torque measurements from dynamometer at various feedrate values, with a cutting speed of 40 m/min.

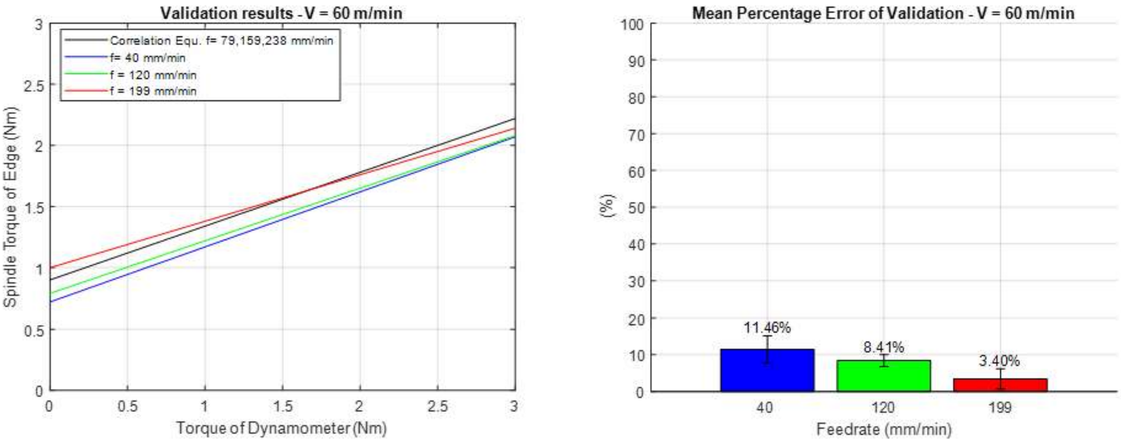

Figure 4.12: Validation results of the spindle torque data from Edge vs. torque measurements from dynamometer at various feedrate values, with a cutting speed of 60 m/min.

while spindle current and torque data were captured through an industrial edge device. Subsequent data analysis revealed strong correlations between the measurements obtained from the dynamometer and those recorded by the edge device. Three key relationships were investigated across different cutting parameters: (1) spindle torque from the edge device versus torque from the dynamometer, (2) spindle torque from the edge device versus tangential force from the dynamometer, and (3) spindle

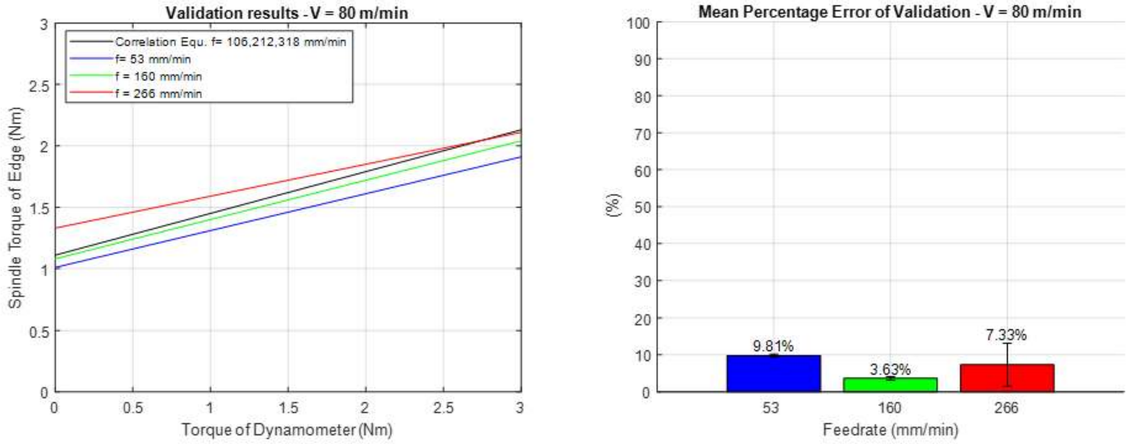

Figure 4.13: Validation results of the spindle torque data from Edge vs. torque measurements from dynamometer at various feedrate values, with a cutting speed of 80 m/min.

current from the edge device versus torque from the dynamometer.

The correlation analysis yielded the following repeatability validation results:

- Cutting torque estimation using edge device spindle torque: Mean errors ranged from less than 3.4% (best case) to 11.9% (worst case).
- Tangential force estimation using edge device spindle torque: Mean errors ranged from less than 1.2% to 10.7%.
- Cutting torque estimation using edge device spindle current: Mean errors ranged between less than 7.47% and 12.66%.

Similarly, validation across different feedrates showed:

- Cutting torque estimation via spindle torque data: Mean errors ranged from less than 3.4% to 11.46%.
- Tangential force estimation via spindle torque data: Mean errors ranged from less than 0.61% to 7.82%.

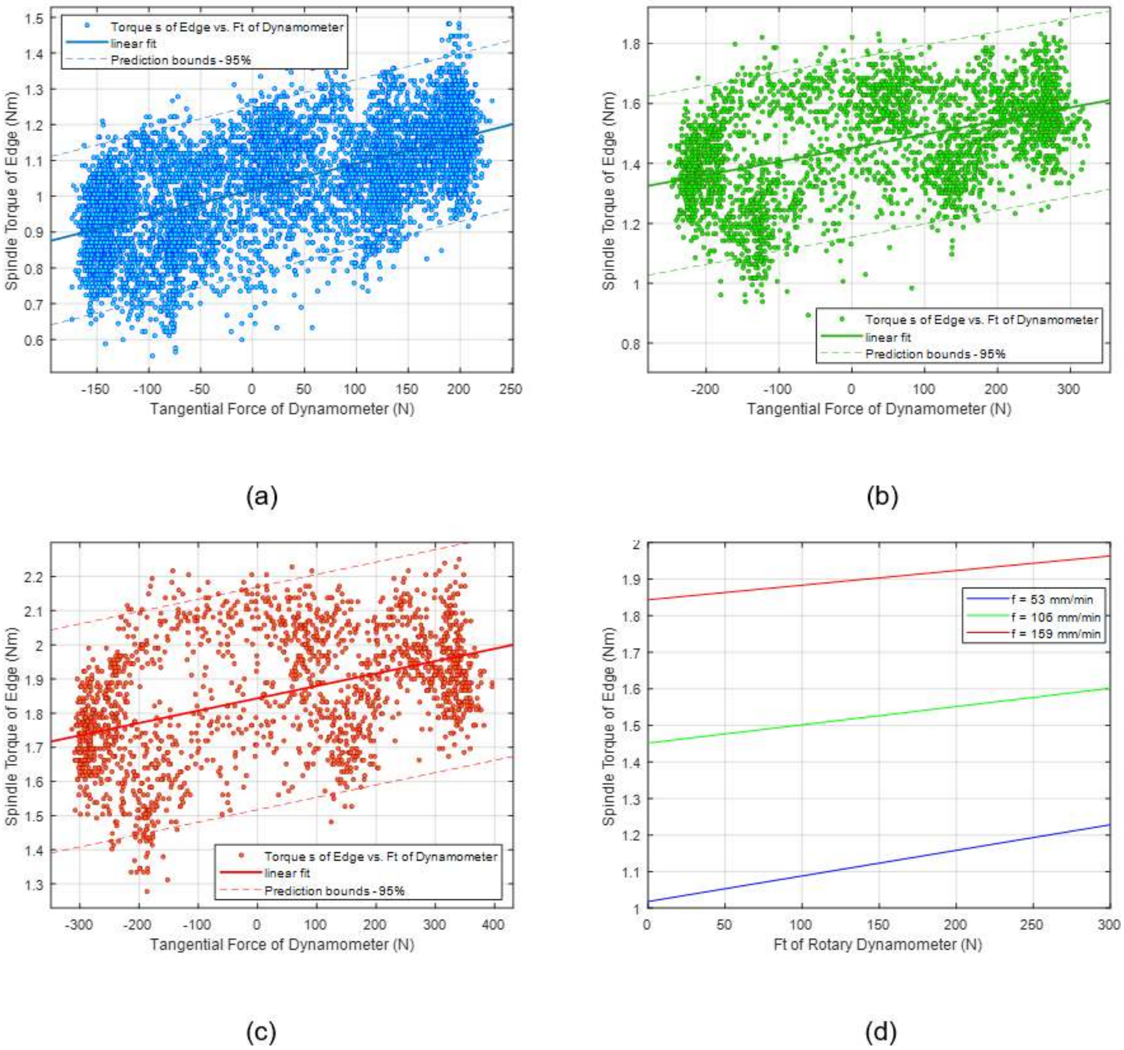

Figure 4.14: Spindle torque measured by the Edge device vs. tangential force collected by the dynamometer at a cutting speed of 40 m/min and feedrate values of (a) 53 mm/min, (b) 106 mm/min, (c) 159 mm/min, and (d) all values for Trial 1.

- Cutting torque estimation via spindle current data: Mean errors ranged from less than 1.99% to 11.55%.

These results demonstrate the feasibility of using industrial edge devices for real-time, sensorless estimation of cutting torque, tangential force, and spindle current in machining operations. The proposed method offers a cost-effective alternative to traditional sensor systems by reducing hardware dependency and setup time, ultimately contributing to more efficient and smarter manufacturing environments.

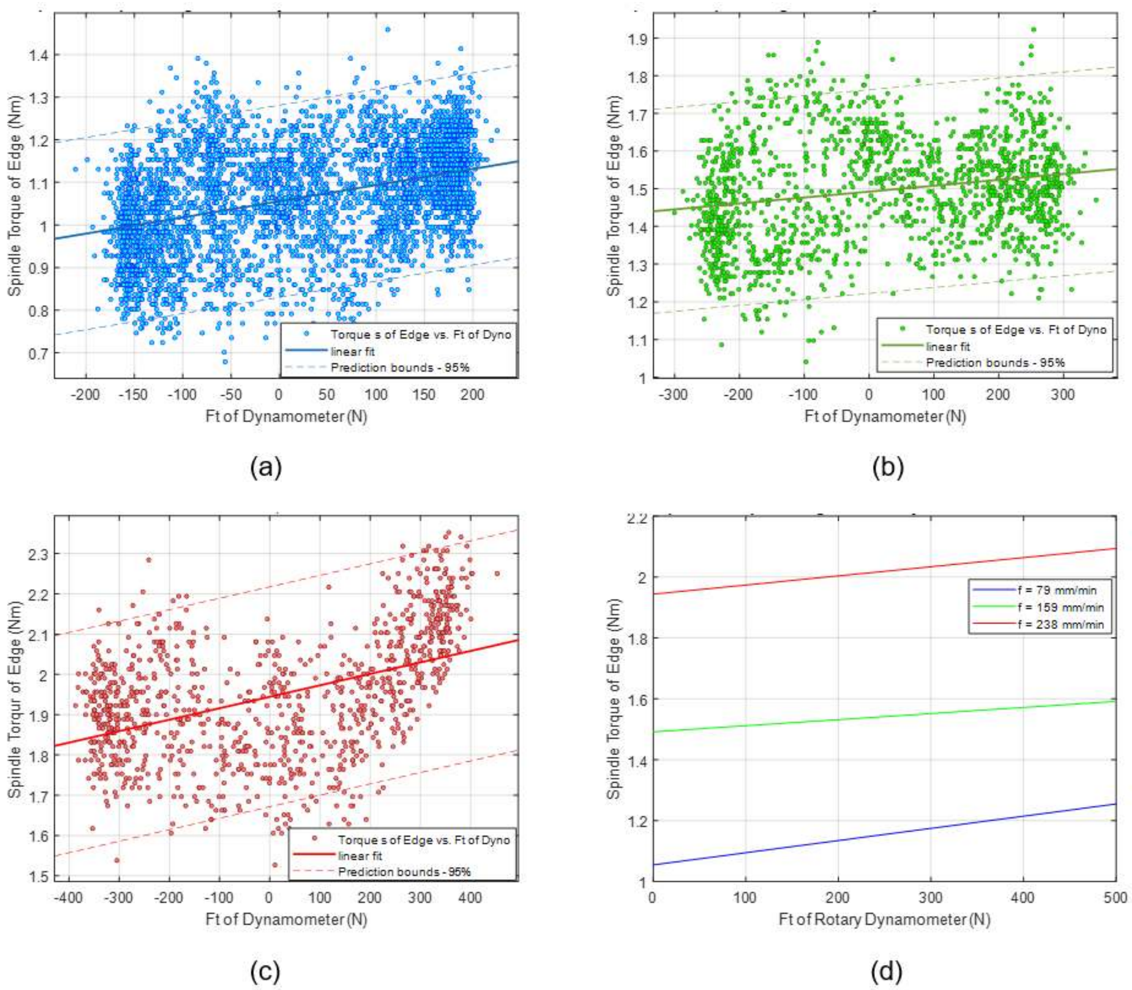

Figure 4.15: Spindle torque measured by the Edge device and tangential force collected by the dynamometer at a cutting speed of 60 m/min and feedrate values of (a) 79 mm/min, (b) 159 mm/min, (c) 238 mm/min, and (d) all values for Trial 1.

Future research could explore the use of more sophisticated machine learning algorithms to improve prediction accuracy and capture complex nonlinear patterns within the data. Furthermore, testing the proposed method across a wider variety of workpiece materials, cutting tools, machining operations, cutting conditions, and spindle setups will be essential to evaluate its robustness and applicability in diverse industrial scenarios.

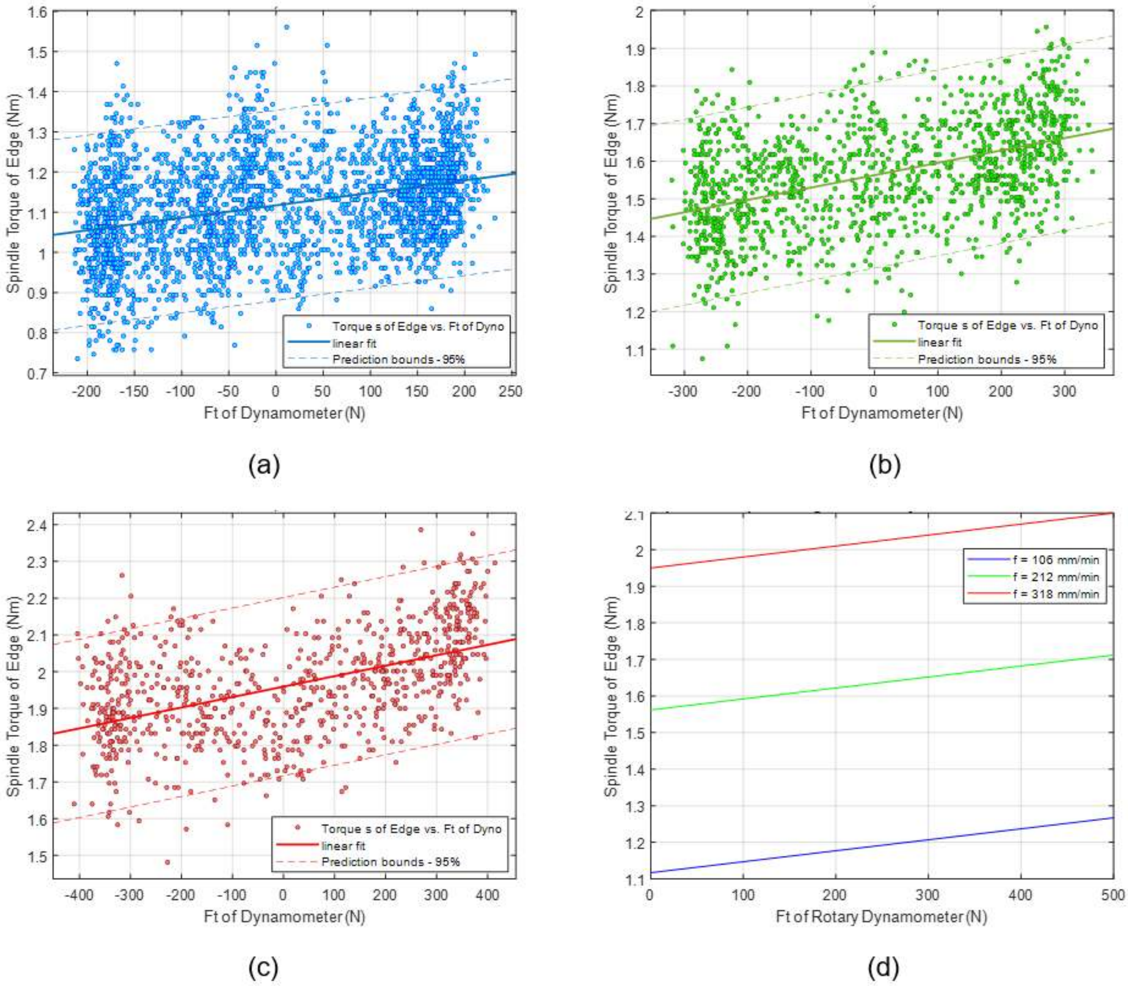

Figure 4.16: Spindle torque measured by the Edge device vs. tangential force collected by the dynamometer at a cutting speed of 80 m/min and feedrate values of (a) 106 mm/min, (b) 212 mm/min, (c) 318 mm/min, and (d) all values for Trial 1.

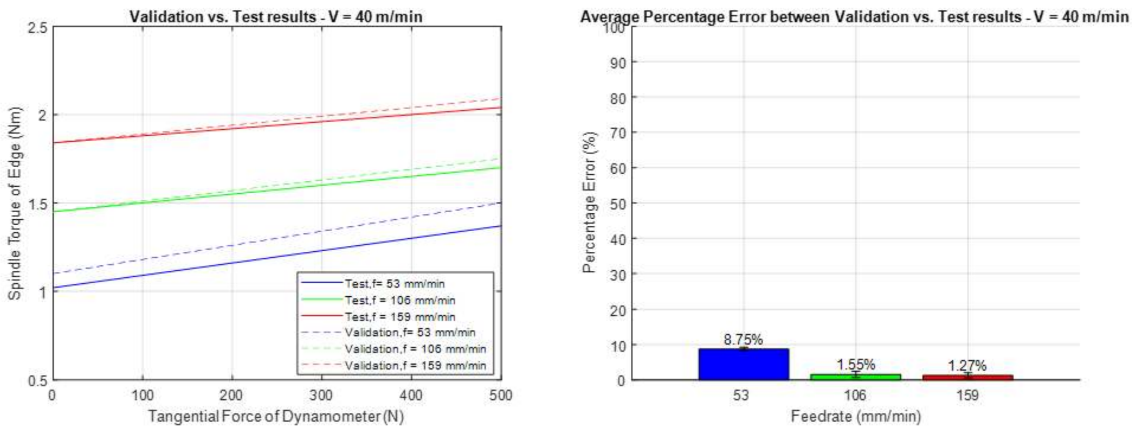

Figure 4.17: Repeatability validation of the spindle torque data via Edge device compared to the tangential force measurements from the dynamometer at a cutting speed of 40 m/min.

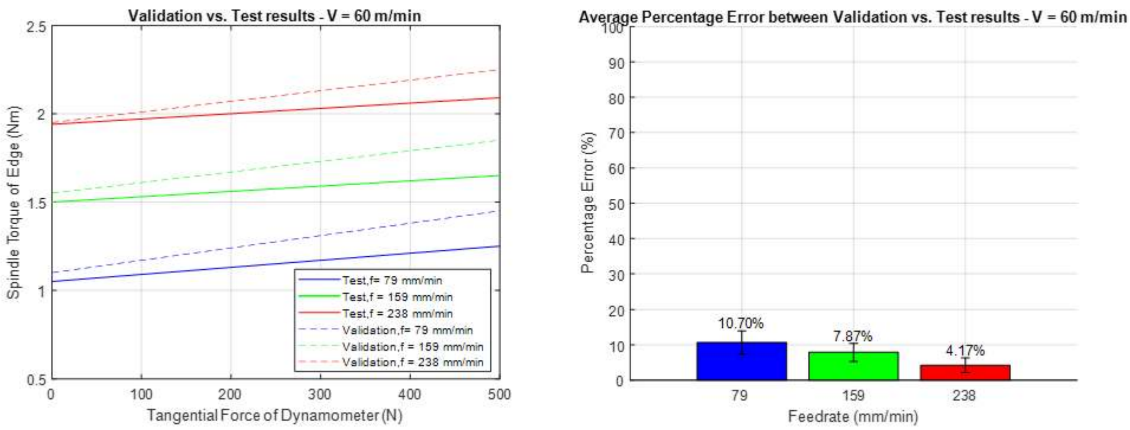

Figure 4.18: Repeatability validation of the spindle torque data via Edge device compared to the tangential force measurements from the dynamometer at a cutting speed of 60 m/min.

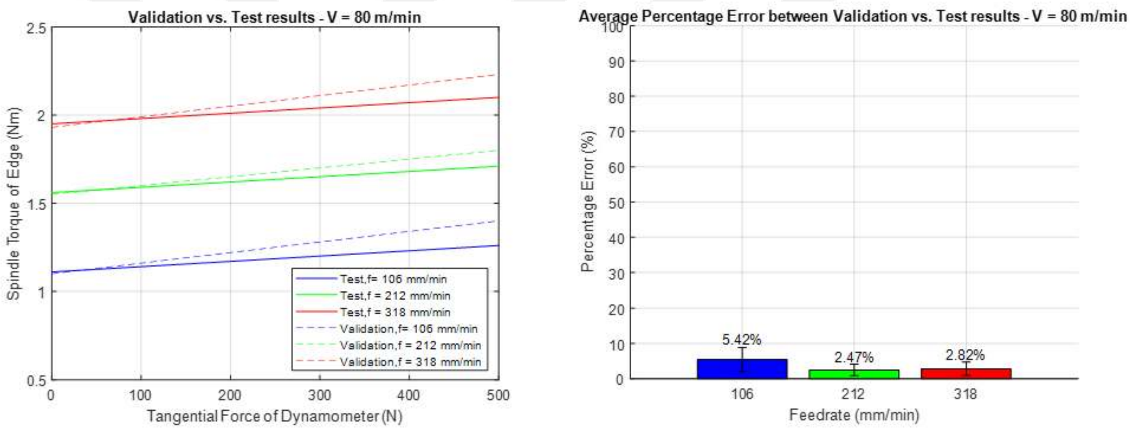

Figure 4.19: Repeatability validation of the spindle torque data via Edge device compared to the tangential force measurements from the dynamometer at a cutting speed of V= 80 m/min.

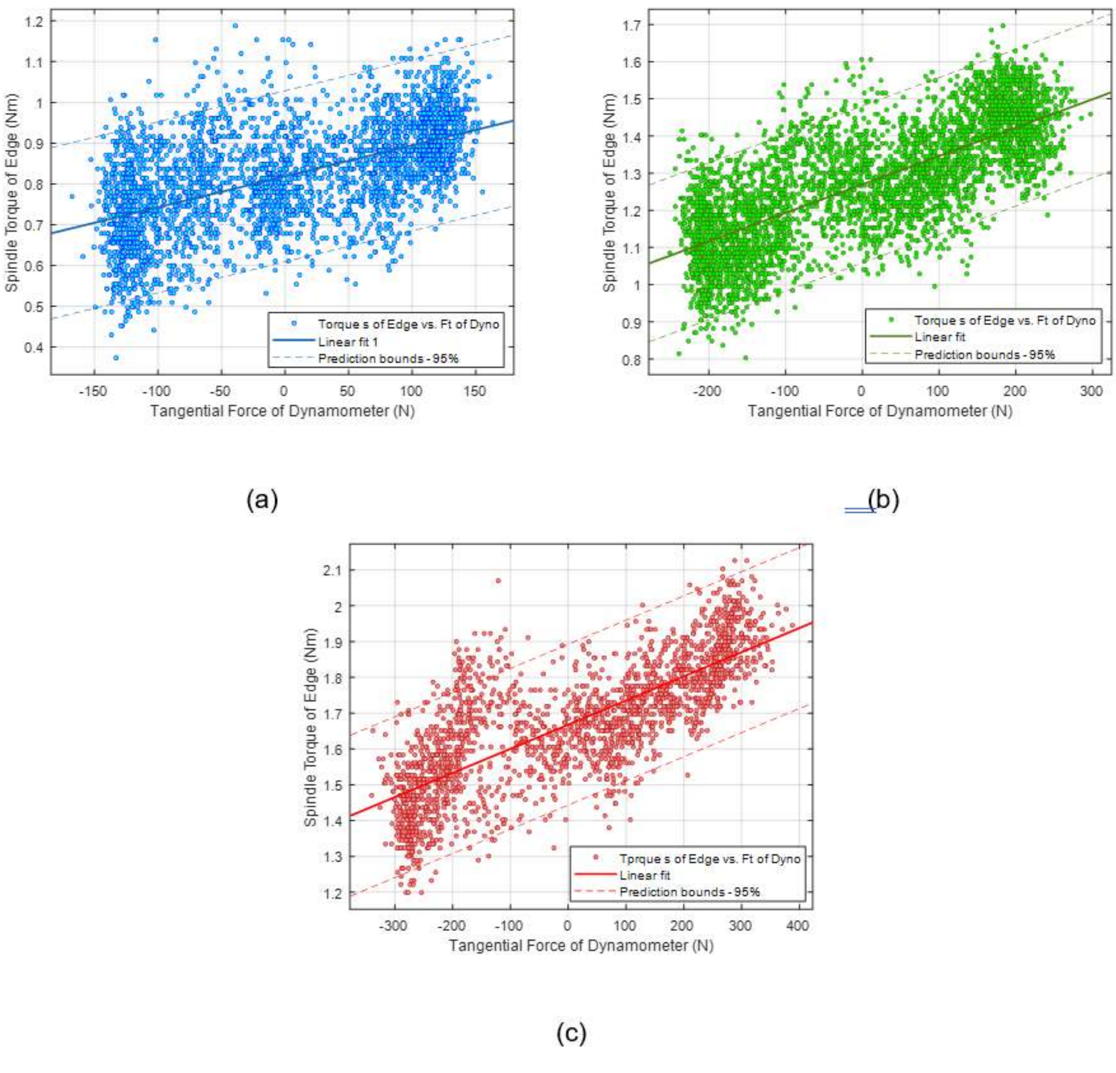

Figure 4.20: Correlation results of the spindle torque data via edge device vs. tangential force collected by dynamometer at a cutting speed of 40 m/min and with feedrate values of (a) 27 mm/min, (b) 80 mm/min, and (c) 133 mm/min.

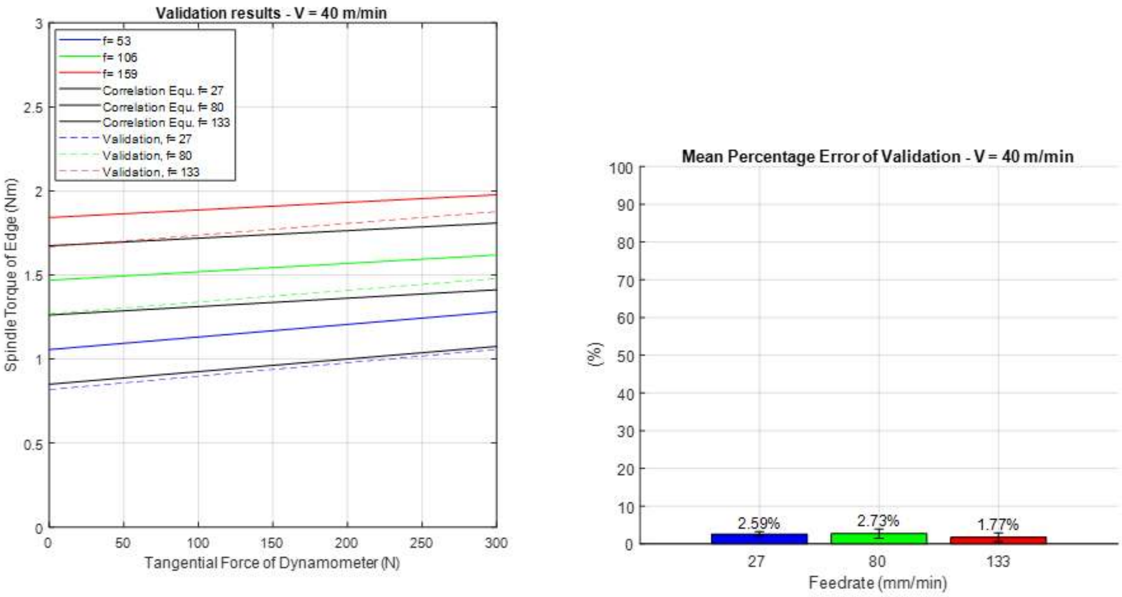

Figure 4.21: Validation of Edge device spindle torque data vs. dynamometer tangential force measurements with various feedrate values at a cutting speed of 40 m/min.

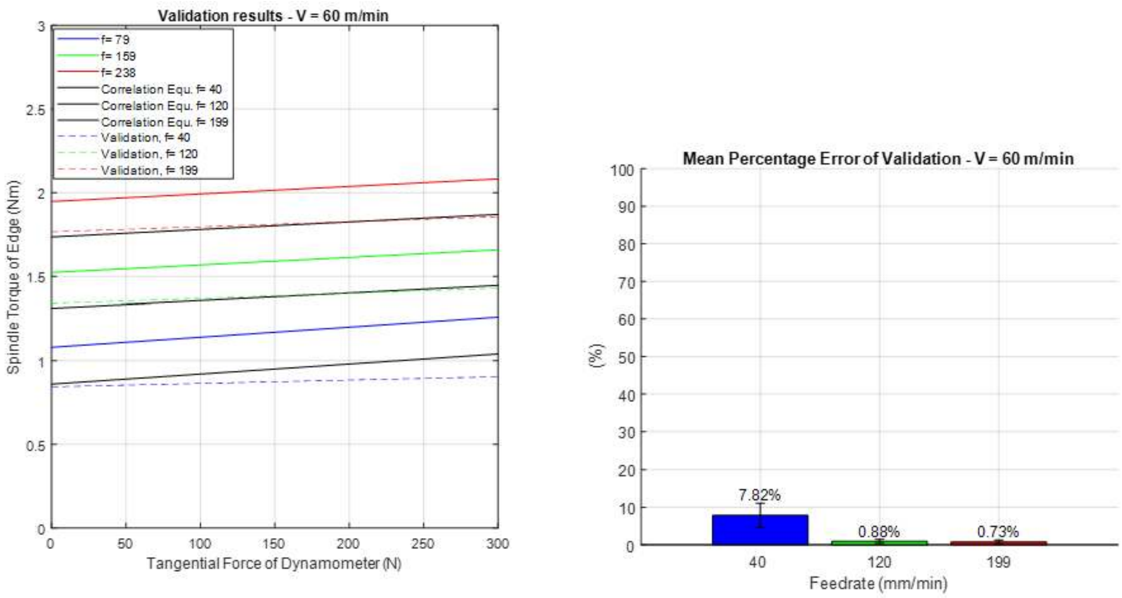

Figure 4.22: Validation of Edge device spindle torque data vs. dynamometer tangential force measurements with various feedrate values at a cutting speed of 60 m/min.

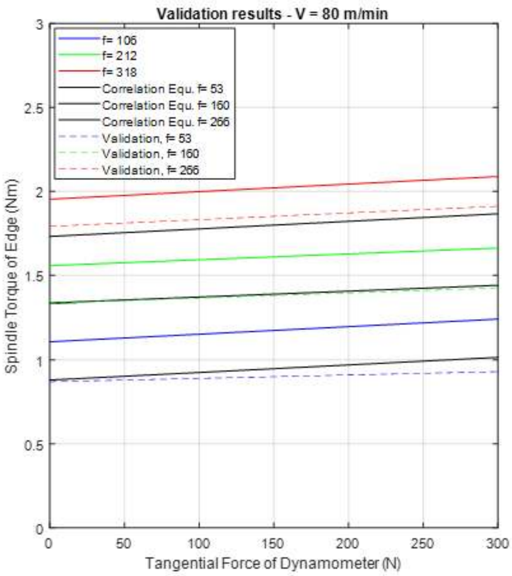

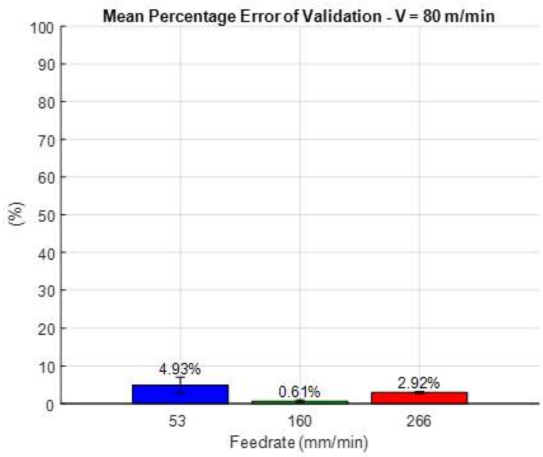

Figure 4.23: Validation of Edge device spindle torque data vs. dynamometer tangential force measurements with various feedrate values at a cutting speed of 80 m/min.

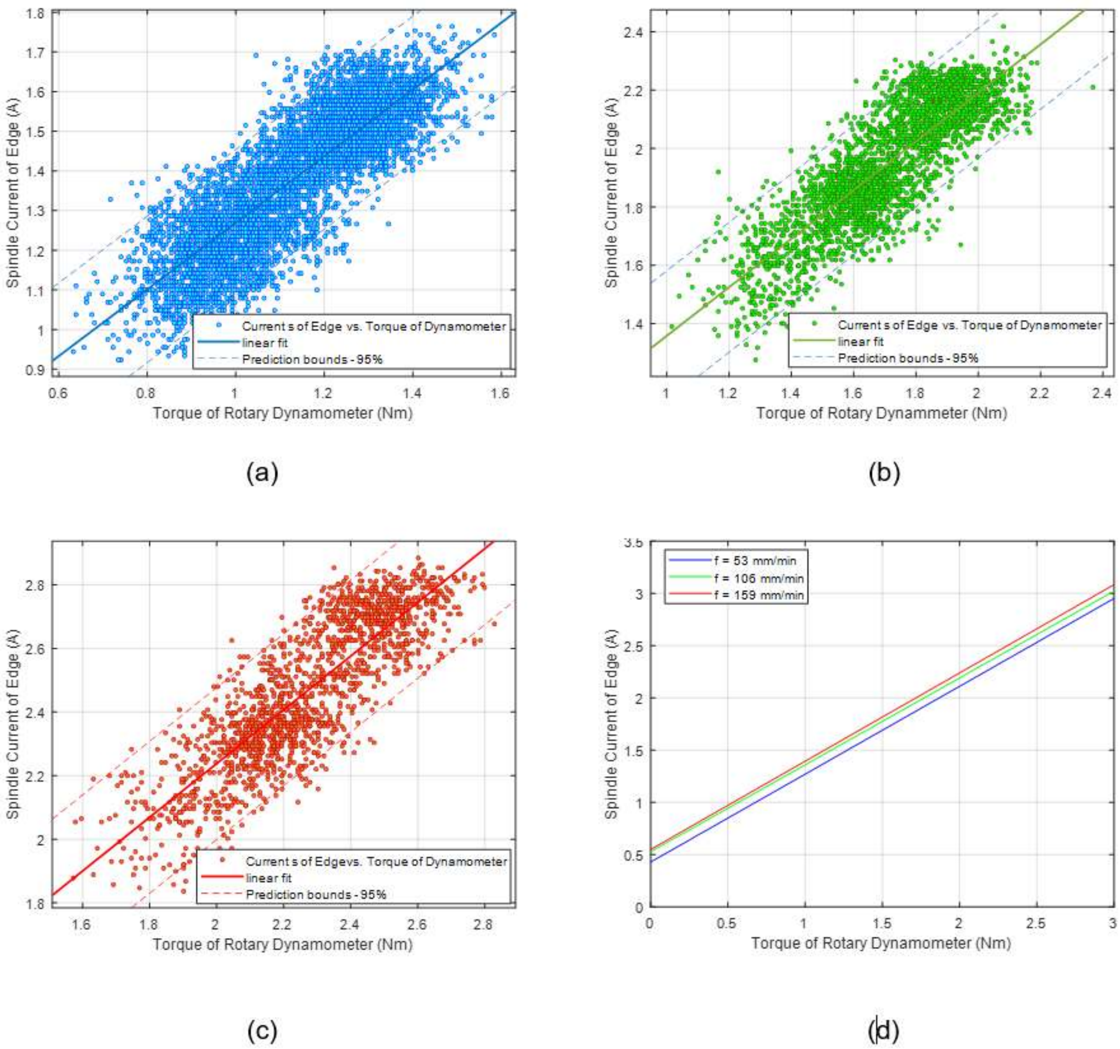

Figure 4.24: Spindle current from Edge vs. torque from dynamometer at a cutting speed of 40 m/min with feedrate values of (a) 53 (mm/min), (b) 106 (mm/min), (c) 159 (mm/min), and (d) all values for Trial 1.

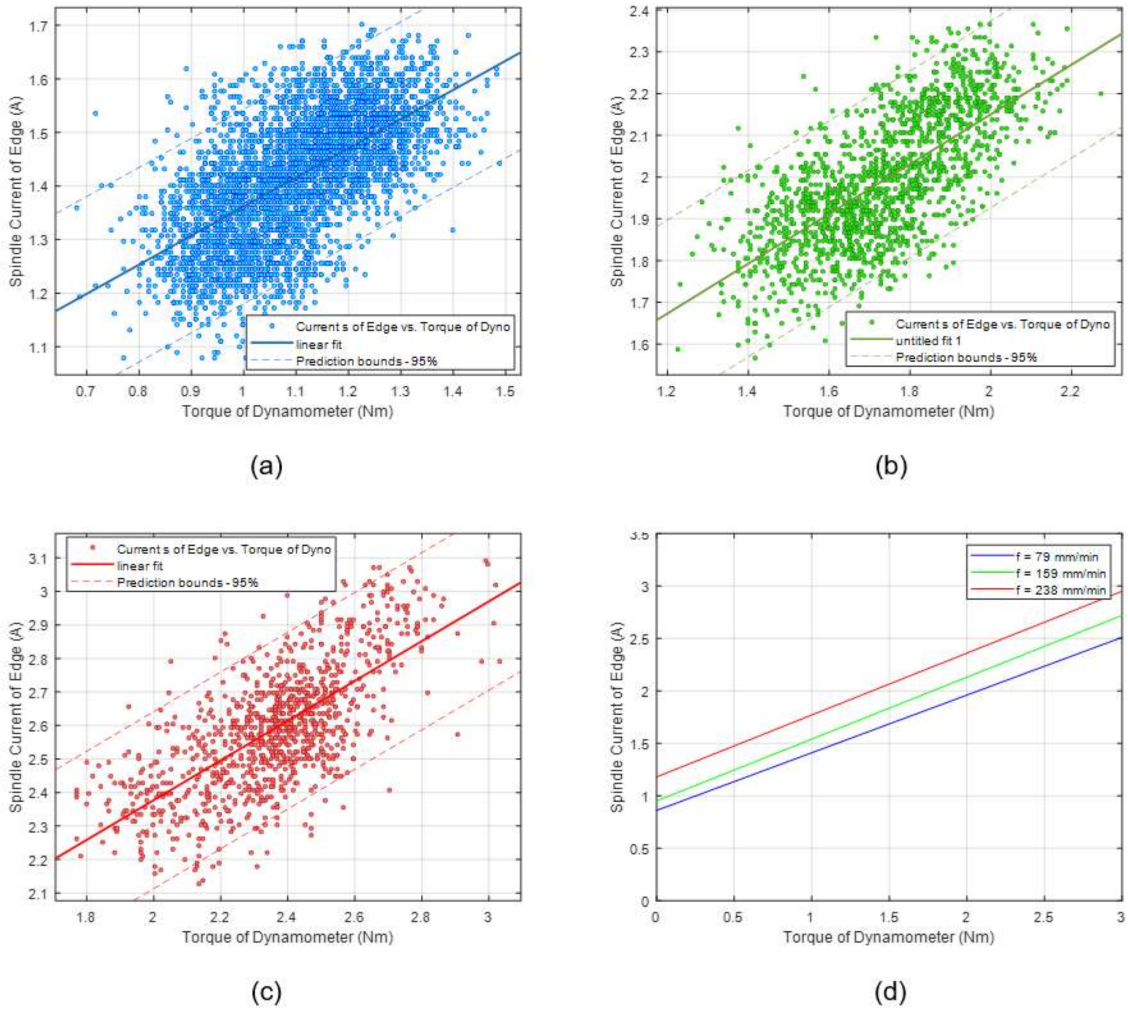

Figure 4.25: Spindle current from Edge vs. torque from dynamometer at a cutting speed of 60 m/min with feedrate values of (a) 79 (mm/min), (b) 159 (mm/min), (c) 238 (mm/min), and (d) all values for Trial 1.

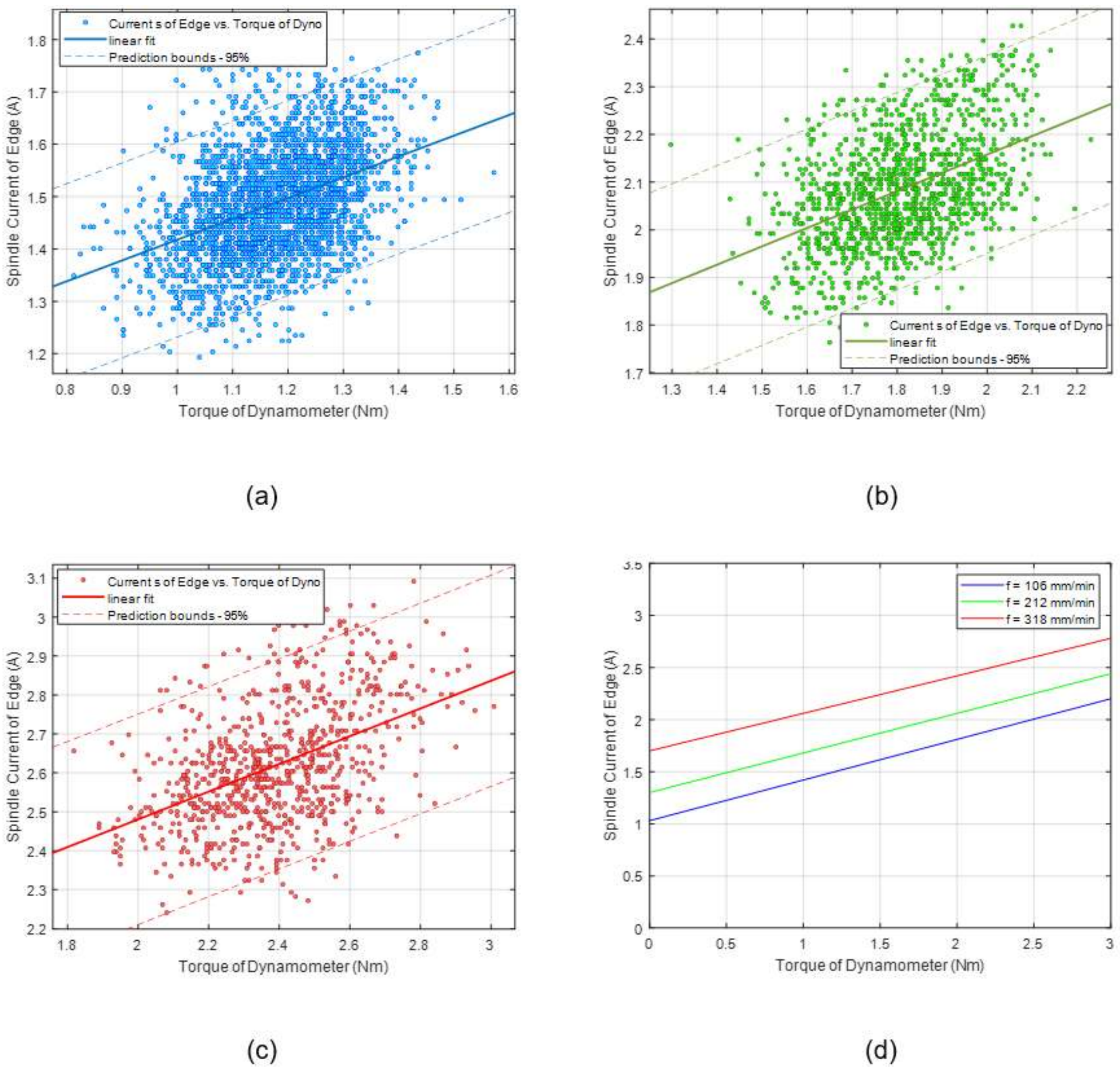

Figure 4.26: Spindle current from Edge vs. torque from dynamometer at a cutting speed of 80 m/min with feedrate values of (a) 106 (mm/min), (b) 212 (mm/min), (c) 318 (mm/min), and (d) all values for Trial 1.

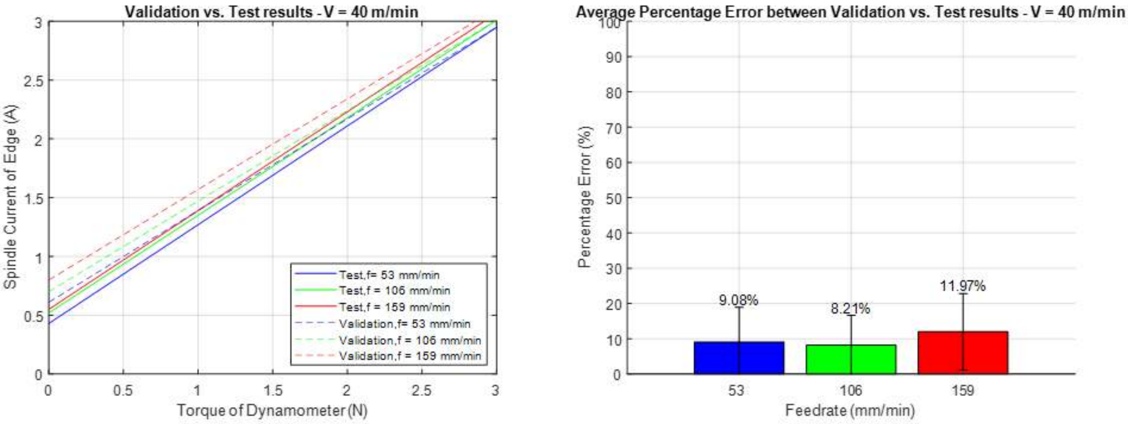

Figure 4.27: Validation of repeatability of edge device spindle current vs. dynamometer torque measurements at the cutting speed of V= 40 m/min.

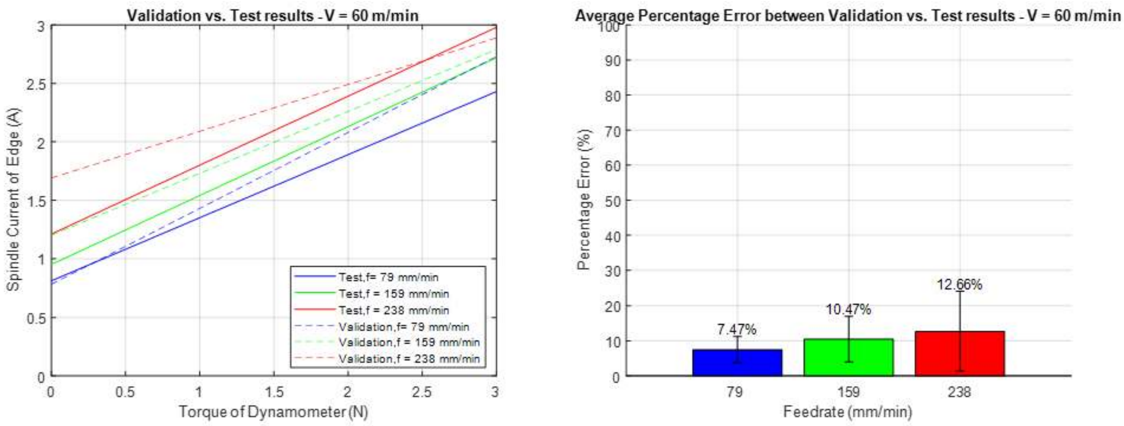

Figure 4.28: Validation of repeatability of edge device spindle current vs. dynamometer torque measurements at the cutting speed of 60 m/min.

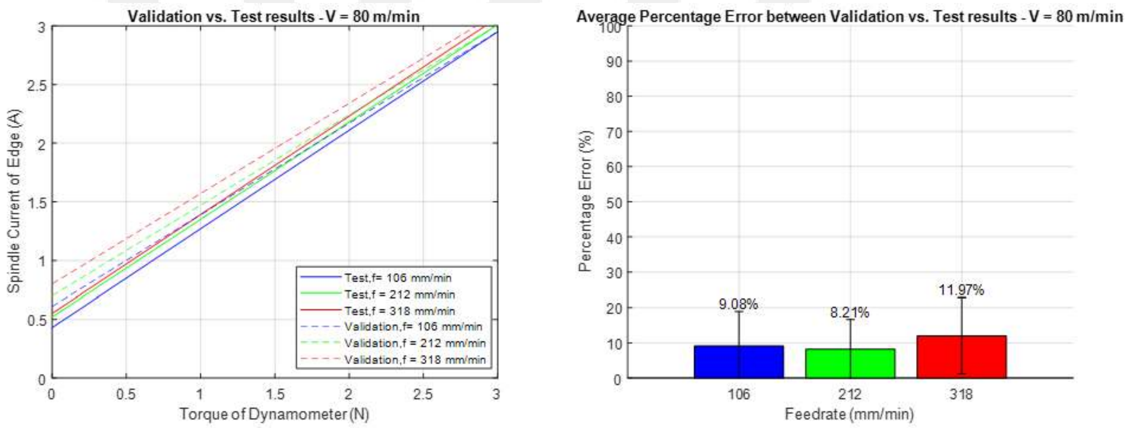

Figure 4.29: Validation of repeatability of edge device spindle current vs. dynamometer torque measurements at the cutting speed of 80 m/min.

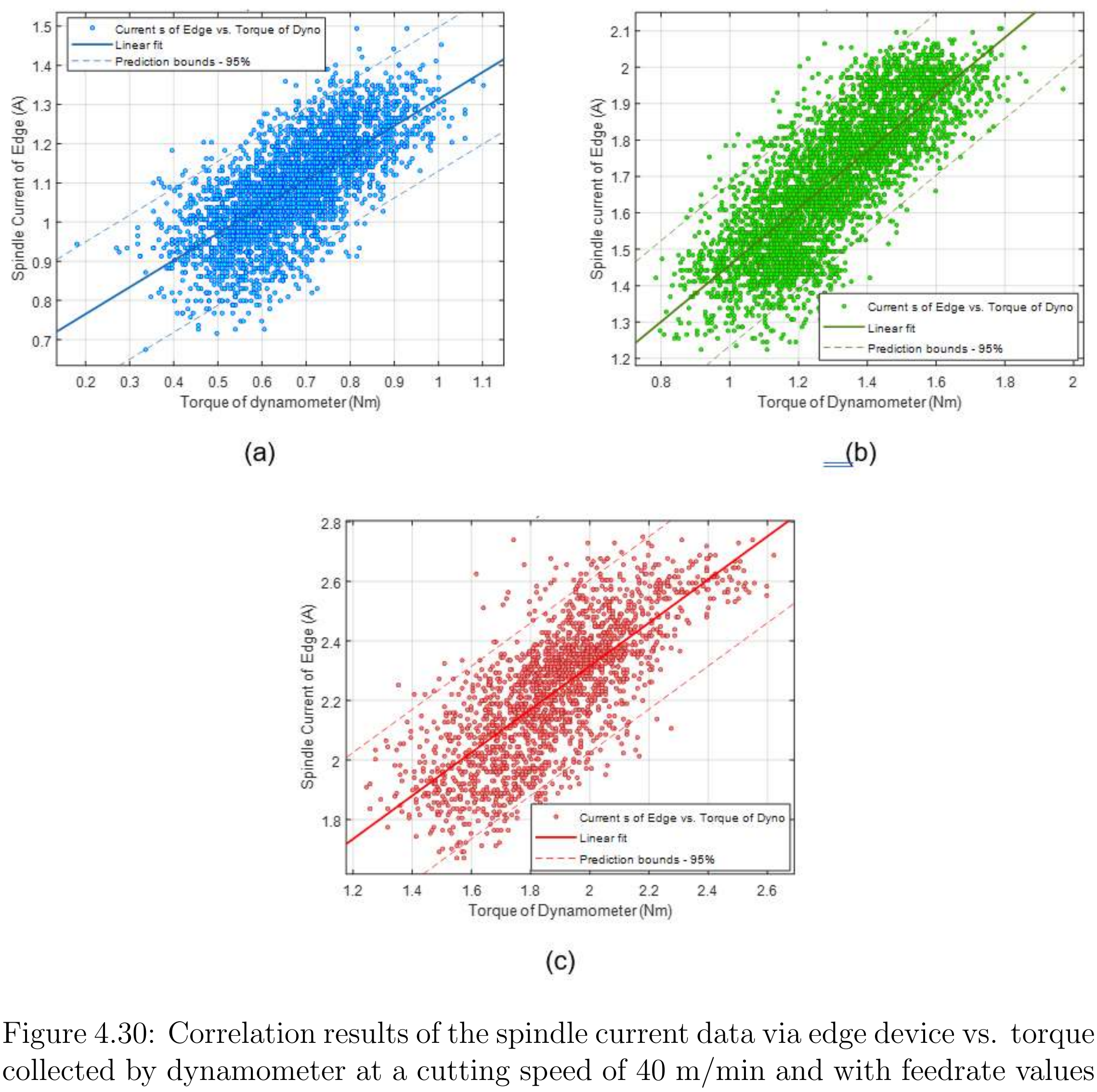

Figure 4.30: Correlation results of the spindle current data via edge device vs. torque collected by dynamometer at a cutting speed of 40 m/min and with feedrate values of (a) 27 mm/min, (b) 80 mm/min, and (c) 133 mm/min.

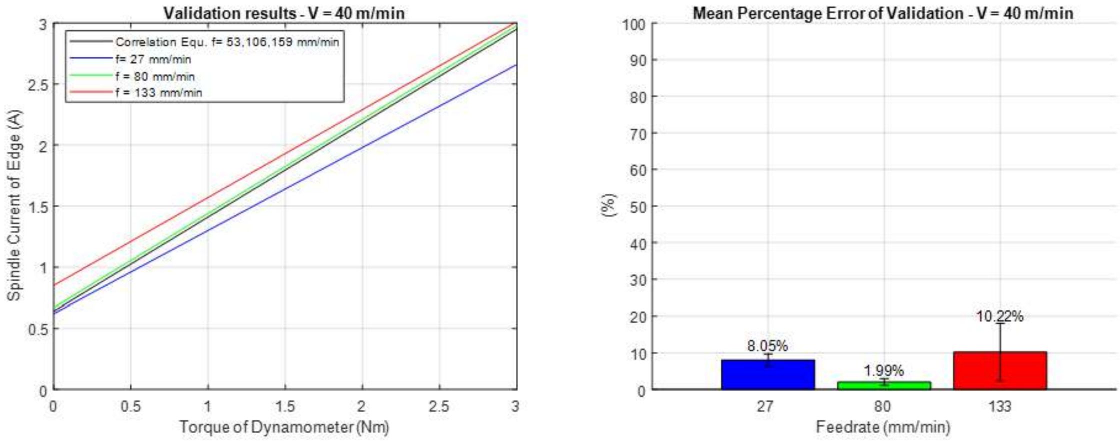

Figure 4.31: Validation of Edge device spindle current data vs. dynamometer torque measurements with various feedrate values at a cutting speed of 40 m/min.

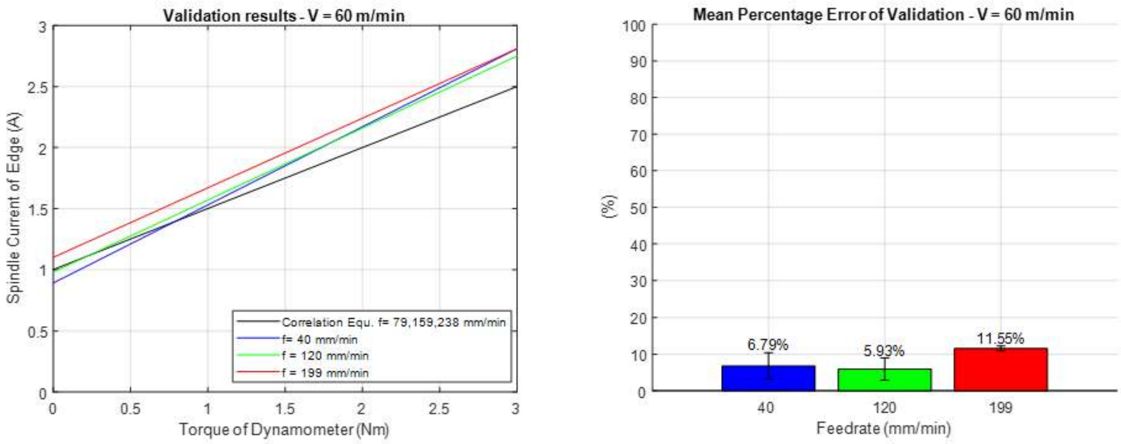

Figure 4.32: Validation of Edge device spindle current data vs. dynamometer torque measurements with various feedrate values at a cutting speed of 60 m/min.

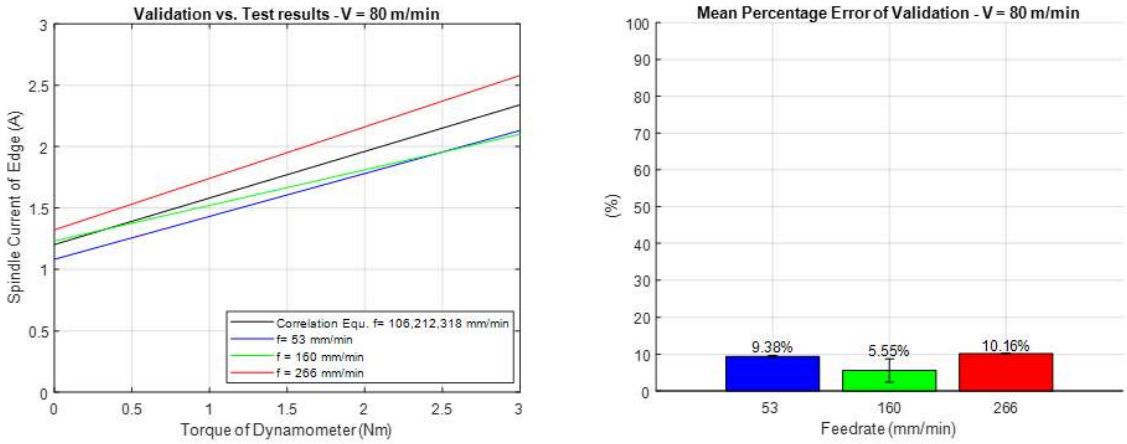

Figure 4.33: Validation of Edge device spindle current data vs. dynamometer torque measurements with various feedrate values at a cutting speed of 80 m/min.

Chapter 5

TOOL CHIPPING DETECTION USING AN INDUSTRIAL EDGE DEVICE

5.1 Overview

Milling of difficult-to-machine materials such as titanium alloys is prone to tool failures, such as cutting-edge chipping and breakage. Timely and reliable detection of cutting-edge chipping is still a challenge for researchers, as it could help to prevent early tool breakage and control the milling quality. In this study, the milling data of fresh and chipped tools were collected via a rotary-type dynamometer and a high-frequency (500 Hz) industrial Edge device. The tool chipping and wear measurement was conducted using a stereomicroscope after each experiment. After processing and analyzing the signals of the milling data in the time and frequency domains, it was observed that there are significant differences between the FFT (Fast Fourier Transform) results of the spindle current and torque signals from the Edge device during the milling process without tool chipping and after the occurrence of tool chipping. Consequently, using the industrial Edge device could be a promising approach for tool condition monitoring, particularly chipping detection during machining, and minimizing the costs of utilizing expensive multi-sensors in smart manufacturing systems.

5.2 Experimental method

In this study, several milling experiments were carried out using a Spinner U1530 five-axis CNC machining center with a Siemens SINUMERIK 840D sl controller. The milling cutting forces and torque data were collected using the Kistler 9123C rotary dynamometer mounted on the spindle of the CNC machine. The workpiece material was a titanium alloy (Ti-Al6-V4) block with dimensions of 300x200x25 mm. A 4-fluted AlCrN-coated flat-end milling tool with a diameter of 12 mm was used for the milling operation. The measured signals from the rotary dynamometer were amplified using a Kistler Type 5223 charge amplifier. They are converted to digital signals using a NI USB-6259 data acquisition system by National Instruments. Moreover, the current and torque data of the spindle motor were collected over a Siemens SINUMERIK 840D sl controller, using the industrial Edge device for machine tools of type SIMATIC IPC227E by an Internet of Things (IoT) Edge Application of Siemens. The sampling frequency of the industrial Edge device equals 500 Hz. The chipping measurements of the cutting edges were performed after experiments using a Leica S9 I Stereomicroscope. The experimental setup is shown in Figure 5.1.

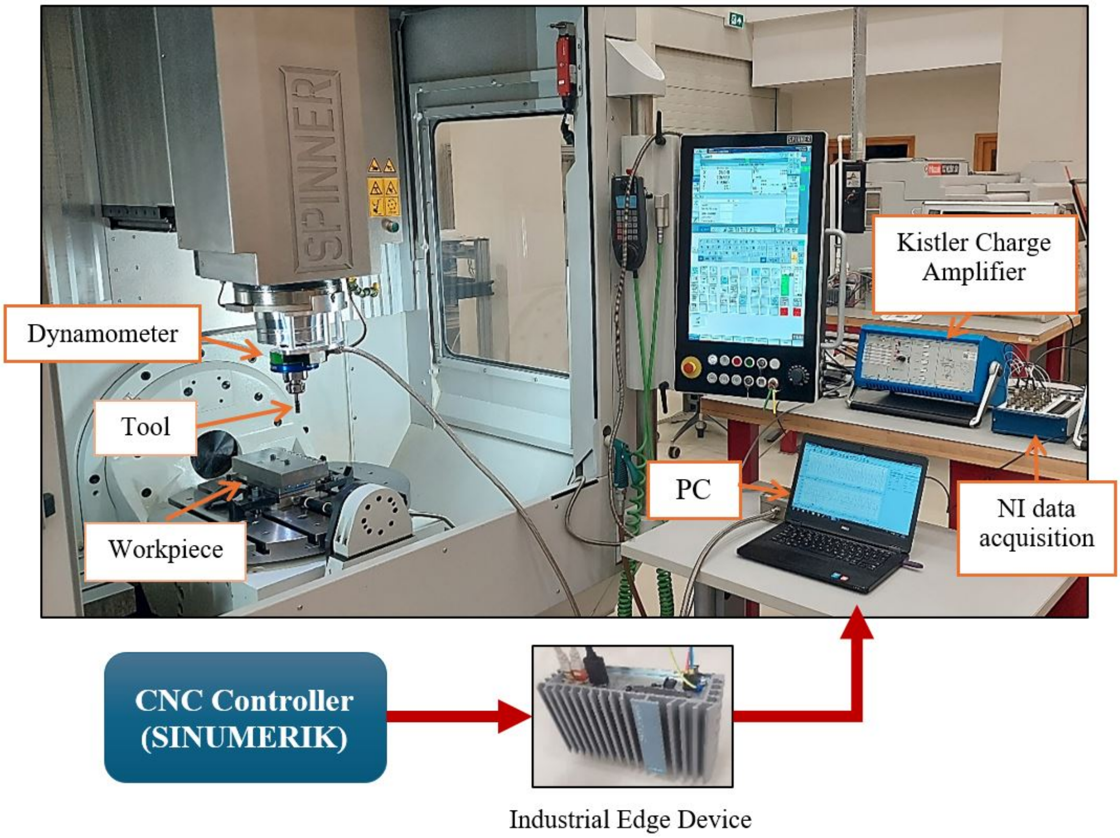

Figure 5.1: The experimental setup for collecting the milling data via the dynamometer and industrial Edge device.

Table 5.1: The design of the experiment for slot milling.

Experiment No.	1	2	3	4	5	6
Feedrate (mm/min)	127	254	127	254	127	254
Feed per tooth (micron)	30	60	30	60	30	60
Tool Status	Fresh/Chipped					

Several half-immersion down-milling tests were performed under varying feed rates and axial depths of cut, using a constant spindle speed of 1060 rpm and a cutting speed of 40 m/min. As summarized in Table 5.1, experiments were conducted with both a fresh tool and the same tool after deliberately introducing a chip on one of its cutting edges. First, milling data were collected under various cutting conditions using the fresh tool. Then, a chip was intentionally created on one cutting edge of the same tool, and additional tests were carried out under similar conditions.

After each test, the tool's cutting edges were inspected using a stereomicroscope to confirm that no unintended wear or additional chipping had occurred. The tool chipping measurement using the stereomicroscope is shown in Figure 5.2.

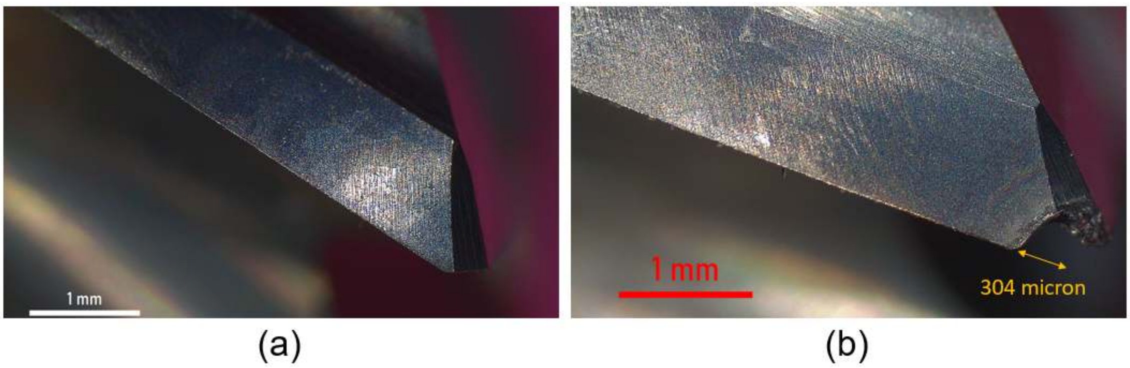

Figure 5.2: The stereomicroscope measurement results of (a) the fresh tool and (b) the chipped tool.

5.3 Results and Discussion

The cutting data were collected using the rotary dynamometer; simultaneously, the current and torque of the spindle motor data were collected using the industrial Edge device during the milling process. Before analyzing the milling data from both devices, the data were pre-processed to ensure that all cutting data corresponded to the same steady-state cutting interval during the slot milling tests. The collected milling torque raw data using the dynamometer are shown in Figure 5.3, and the spindle torque and current raw data via the industrial Edge device in the time domain are shown in Figure 5.4.

According to the milling results obtained from both the dynamometer and the industrial Edge device in the time domain, tool chipping alters the distribution of chip thickness among the cutting edges and leads to increased cutting torque on certain edges. The chipped cutting edge played a lesser role during the cutting process than before, which has led to the next cutting edge to compensate cutting. Depending on the severity of the chipping, these effects may not be easily identifiable through time-domain analysis alone. Therefore, applying Fast Fourier Transform (FFT) and analyzing the signals in the frequency domain provides a more effective approach for revealing the dominant frequencies of the cutting process.

In an ideal cutting scenario—free from runout, wear, chatter, and noise—the dominant frequency is expected to appear at the tooth passing frequency. However, tool breakage typically results in increased magnitudes at the spindle frequency and decreased magnitudes at the tooth passing frequency [90]. To investigate the effects of chipping, the FFT results of the cutting torque signals collected by the dynamometer at various feed rates and axial depths of cut for both the fresh and chipped tools are presented in Figure 5.5.

A significant increase in the magnitude of the torque signal's FFT at the spindle frequency was observed. Similarly, the FFT results of the spindle torque and current signals obtained from the Edge device are presented in Figure 6.1 and Figure 5.7 respectively. These results are consistent with those from the dynamometer, confirming that tool chipping leads to an increased magnitude at the spindle frequency in the Edge device data as well. These findings further demonstrate the effectiveness of frequency-domain analysis for detecting tool chipping during the milling process using the industrial Edge device.

5.4 Summary

In this study, tool chipping detection was investigated during the milling of a titanium alloy workpiece using an industrial Edge device as part of a smart manufacturing approach. Milling process data were collected using both a rotary dynamometer and the industrial Edge device, enabling a comparative evaluation of sensor-based and sensorless monitoring strategies. After each milling test, the cutting tool was examined under a stereomicroscope to verify the presence and extent of chipping on the cutting edges.

The analysis revealed that tool chipping causes observable disturbances in the torque signals obtained from both the dynamometer and the Edge device in the time domain. However, these changes may not always be prominent or easily distinguishable. In contrast, the frequency-domain analysis using Fast Fourier Transform (FFT) proved to be more effective. The FFT results showed a consistent and significant increase in the magnitude at the spindle frequency in both the cutting torque signals from the dynamometer and the spindle torque and current signals captured by the Edge device.

These findings demonstrate the potential of frequency-domain signal analysis for accurately identifying tool chipping during machining. Moreover, the use of an industrial Edge device for this purpose provides a cost-effective and scalable solution for online tool condition monitoring. This approach could help reduce reliance on expensive multi-sensor setups and enhance process reliability in modern smart manufacturing systems.

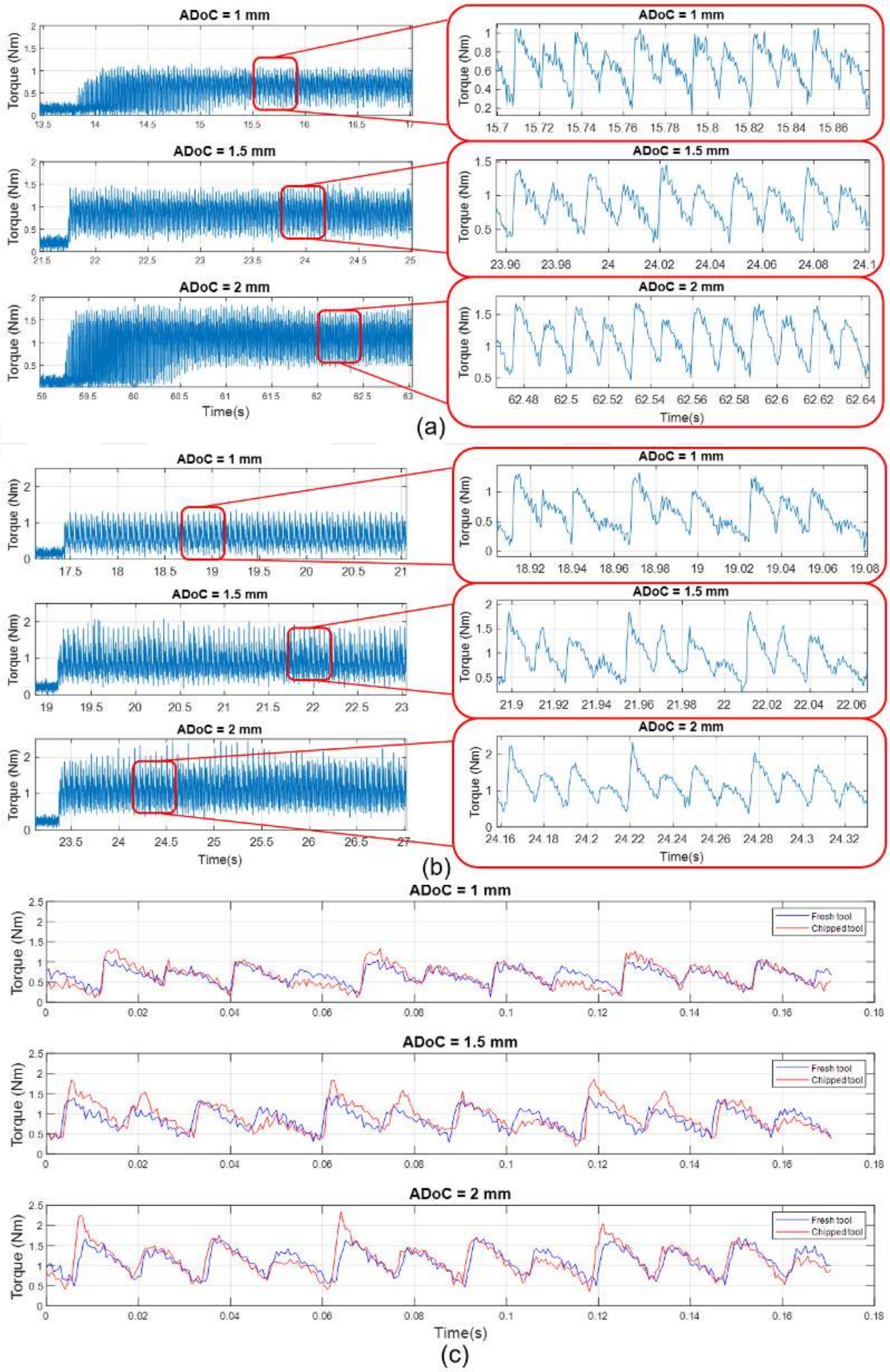

Figure 5.3: The milling torque raw data from the dynamometer at a feed per tooth of 60 micron, (a) fresh tool, (b) chipped tool, (c) comparison between fresh and chipped tool in the time domain.

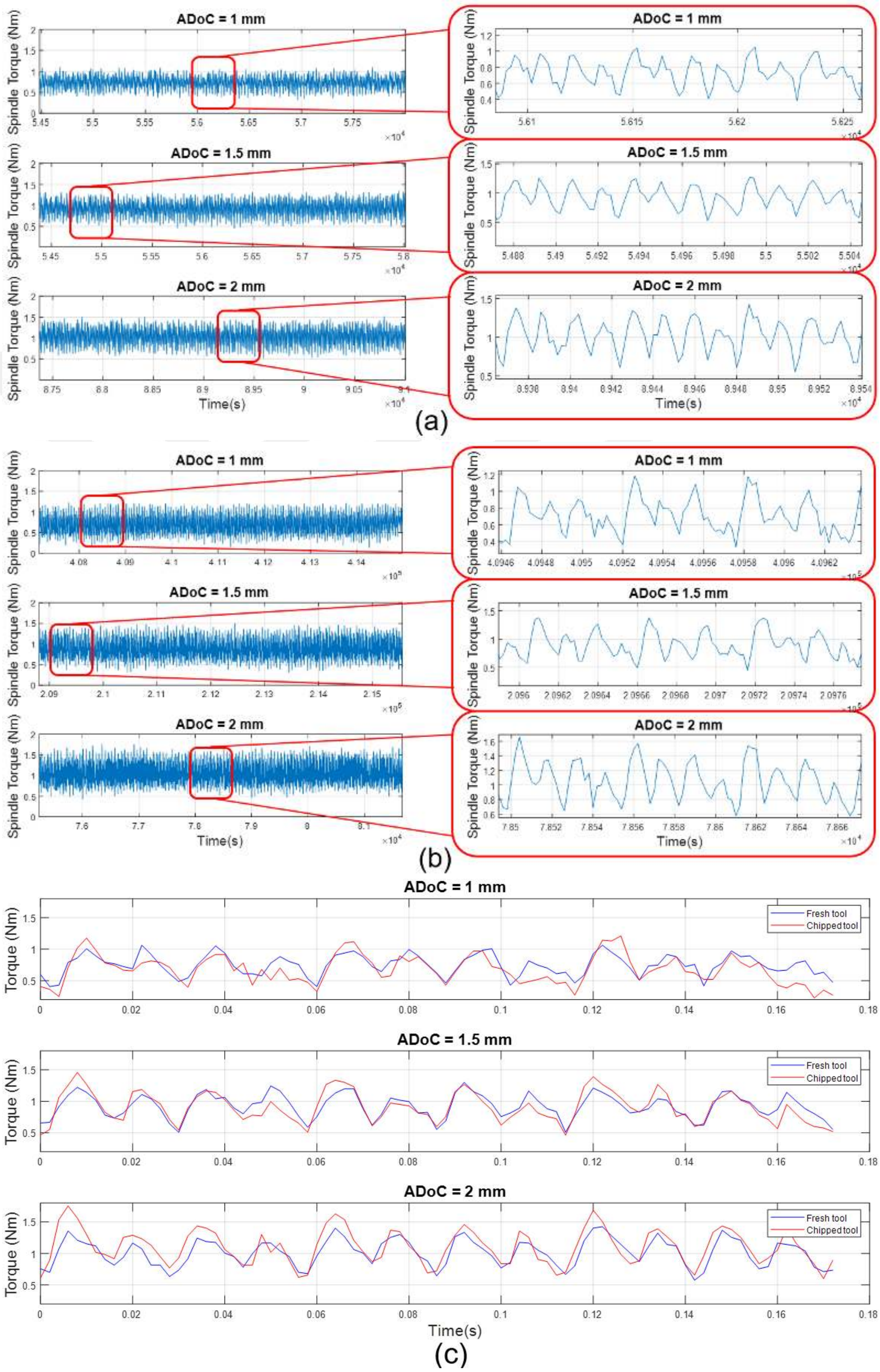
ADoC = 1 mm
ADoC = 1.5 mm
ADoC = 2 mm
Spindle Torque (Nm)
Time(s)
(a)
ADoC = 1 mm
ADoC = 1.5 mm
ADoC = 2 mm
Spindle Torque (Nm)
Time(s)
(b)
ADoC = 1 mm
ADoC = 1.5 mm
ADoC = 2 mm
Torque (Nm)
Fresh tool
Chipped tool
Time(s)
(c)

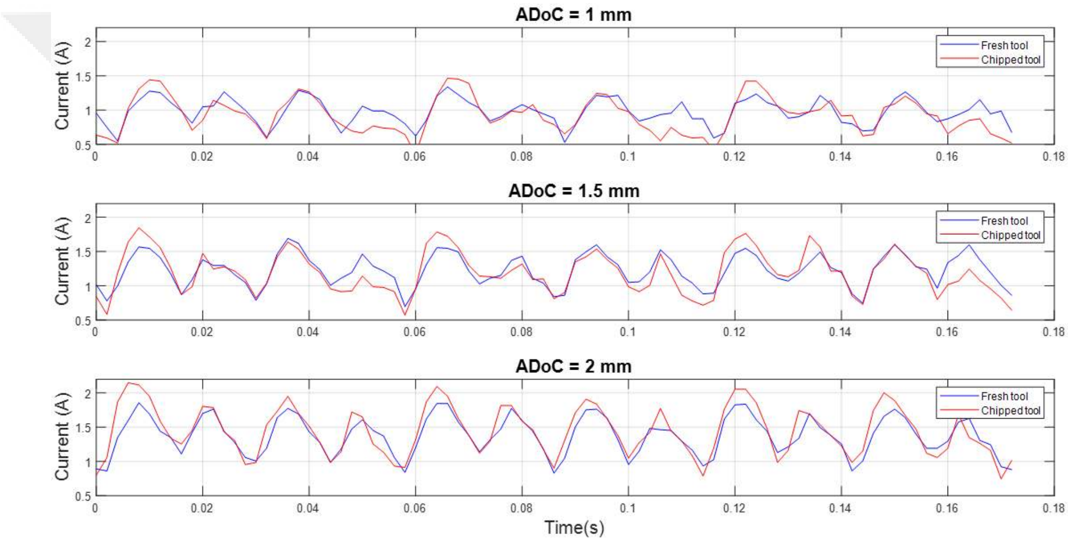

(d)

Figure 5.4: The spindle torque raw data from the Edge device at a feed per tooth of 60 micron, (a) fresh tool, (b) chipped tool, (c) spindle torque data comparison between fresh and chipped tool, (d) spindle current data comparison between fresh and chipped tool in the time domain.

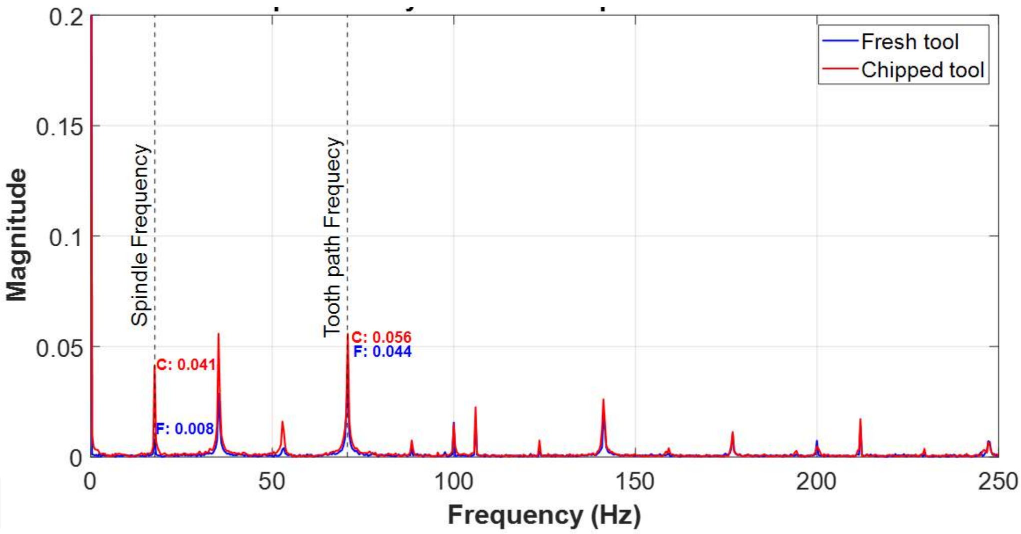
Fresh tool
Chipped tool
Spindle Frequency
Tooth path Frequecy
C: 0.041
F: 0.008
C: 0.056
F: 0.044
Magnitude
Frequency (Hz)

(a)

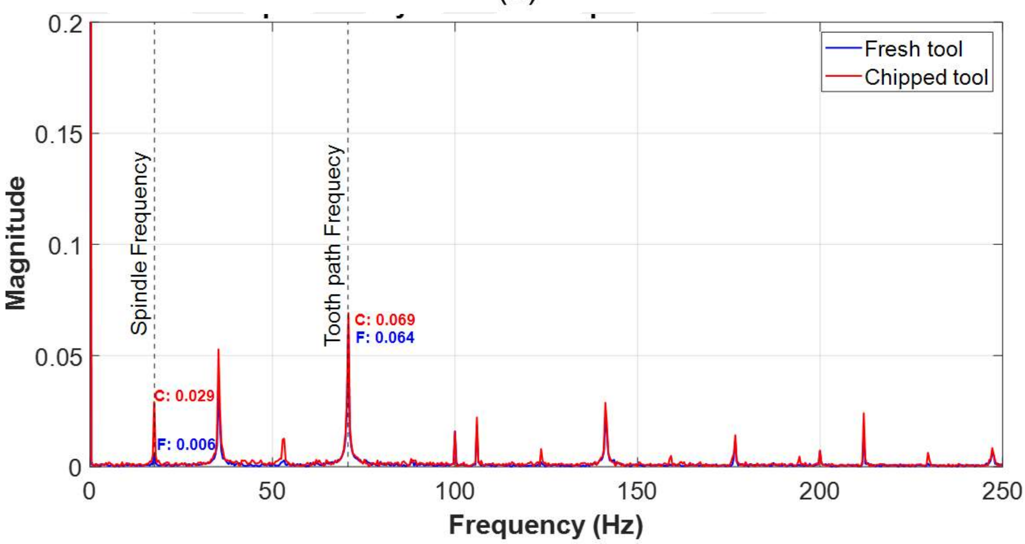
Fresh tool
Chipped tool
Spindle Frequency
Tooth path Frequecy
C: 0.029
F: 0.006
C: 0.069
F: 0.064
Magnitude
Frequency (Hz)

(b)

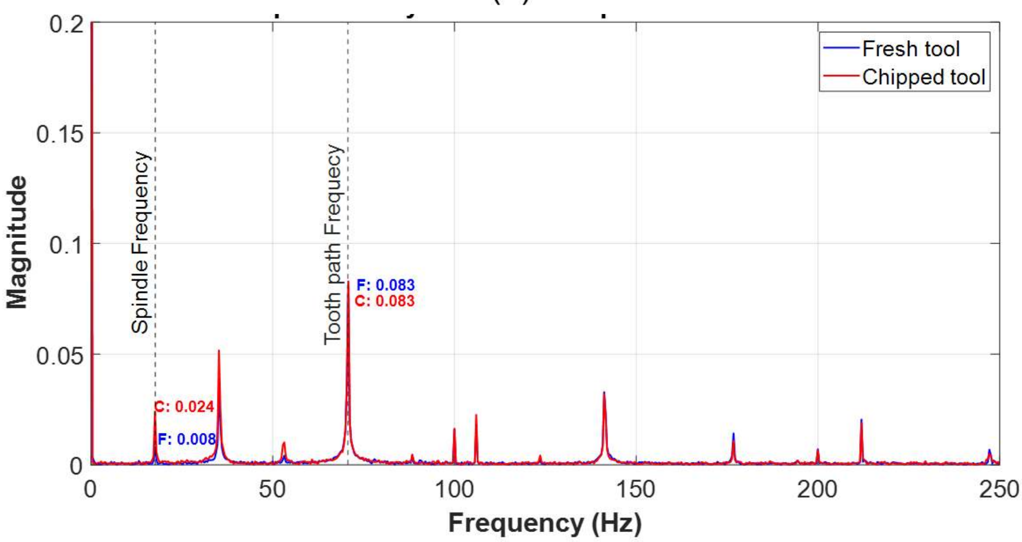
Fresh tool
Chipped tool
Spindle Frequency
Tooth path Frequecy
C: 0.024
F: 0.008
F: 0.083
C: 0.083
Magnitude
Frequency (Hz)

(c)

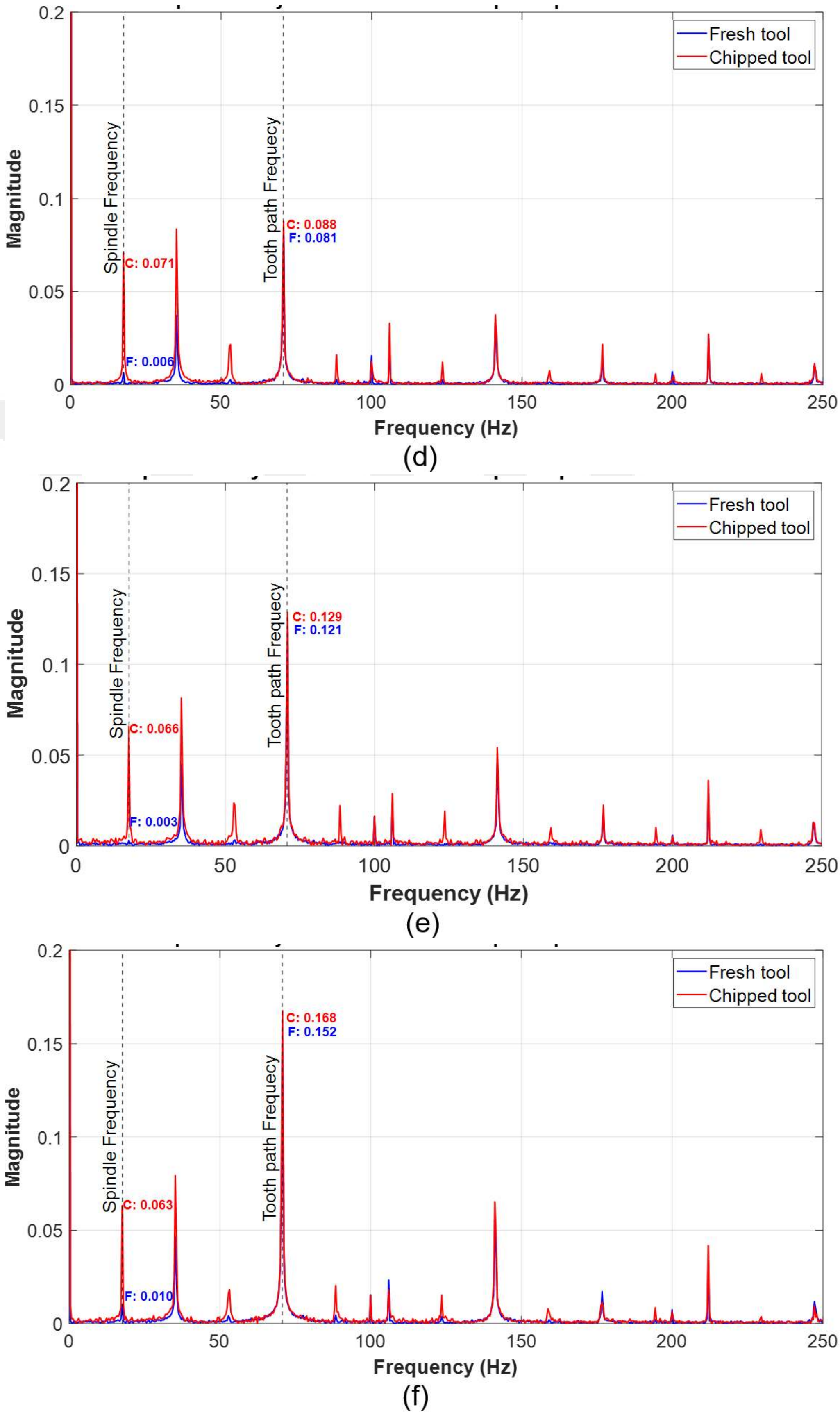

Figure 5.5: The FFT results of the torque data from the dynamometer, (a) fpt= 30 micron and ADoC= 1 mm, (b) fpt= 30 micron and ADoC= 1.5 mm, (c) fpt= 30 micron and ADoC= 2 mm, (d) fpt= 60 micron and ADoC= 1 mm, (e) fpt= 60 micron and ADoC= 1.5 mm, (f) fpt= 60 micron and ADoC= 2 mm.

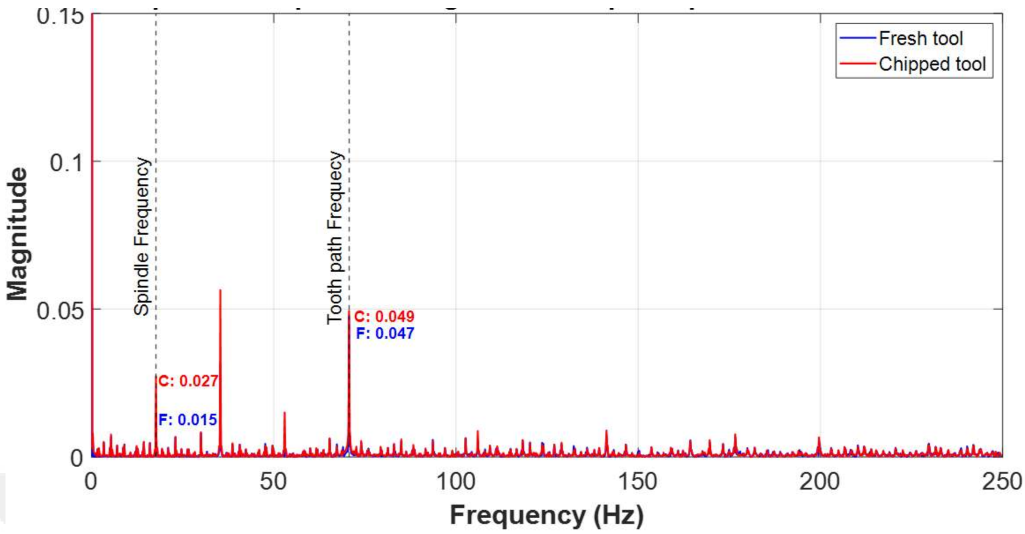
Fresh tool
Chipped tool
Spindle Frequency
Tooth path Frequecy
C: 0.049
F: 0.047
C: 0.027
F: 0.015
Magnitude
Frequency (Hz)
0.15
0.1
0.05
0
0
50
100
150
200
250

(a)

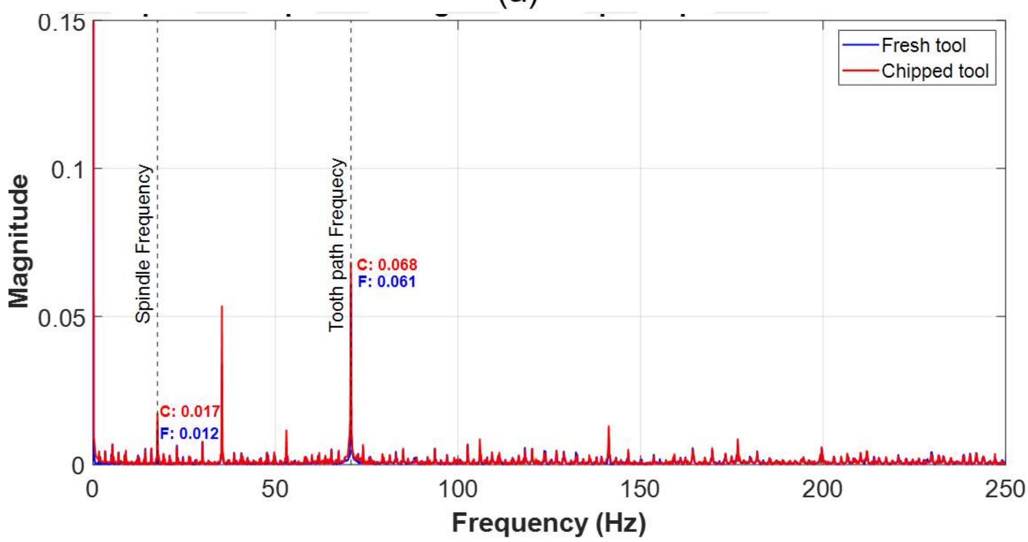
Fresh tool
Chipped tool
Spindle Frequency
Tooth path Frequecy
C: 0.068
F: 0.061
C: 0.017
F: 0.012
Magnitude
Frequency (Hz)
0.15
0.1
0.05
0
0
50
100
150
200
250

(b)

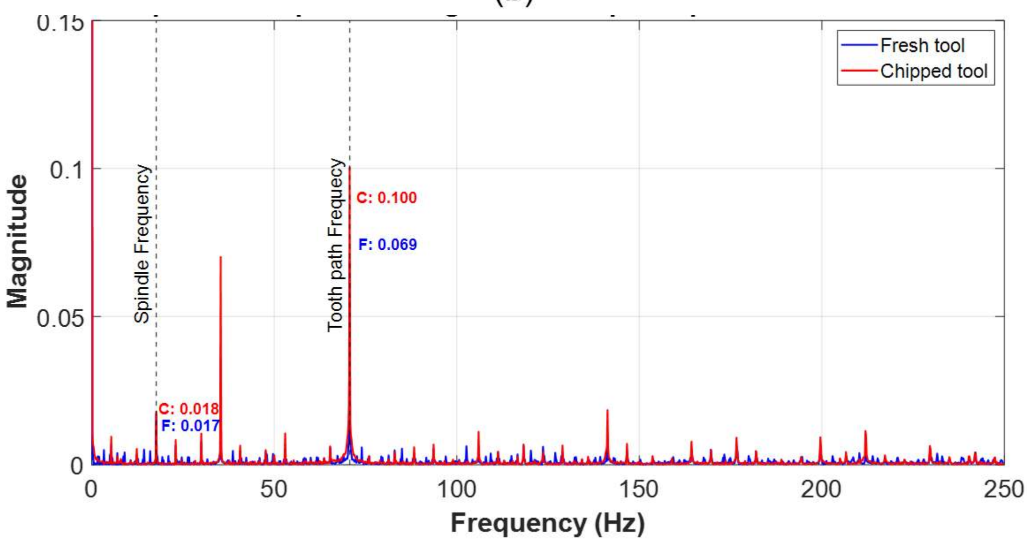
Fresh tool
Chipped tool
Spindle Frequency
Tooth path Frequecy
C: 0.100
F: 0.069
C: 0.018
F: 0.017
Magnitude
Frequency (Hz)
0.15
0.1
0.05
0
0
50
100
150
200
250

(c)

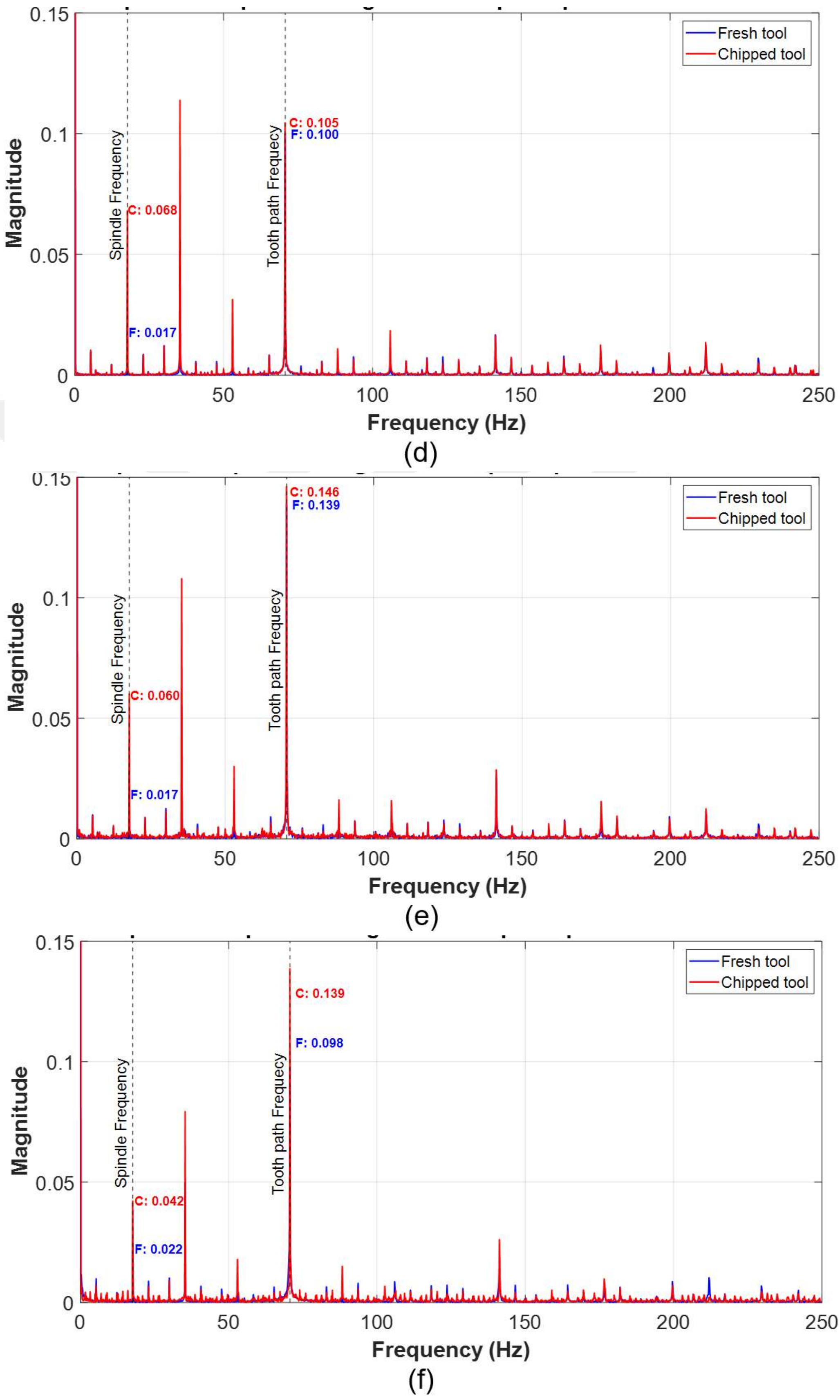

Figure 5.6: The FFT results of the spindle torque data from the Edge device, (a) fpt= 30 micron and ADoC= 1 mm, (b) fpt= 30 micron and ADoC= 1.5 mm, (c) fpt= 30 micron and ADoC= 2 mm, (d) fpt= 60 micron and ADoC= 1 mm,, (e) fpt= 60 micron and ADoC= 1.5 mm, (f) fpt= 60 micron and ADoC= 2 mm.

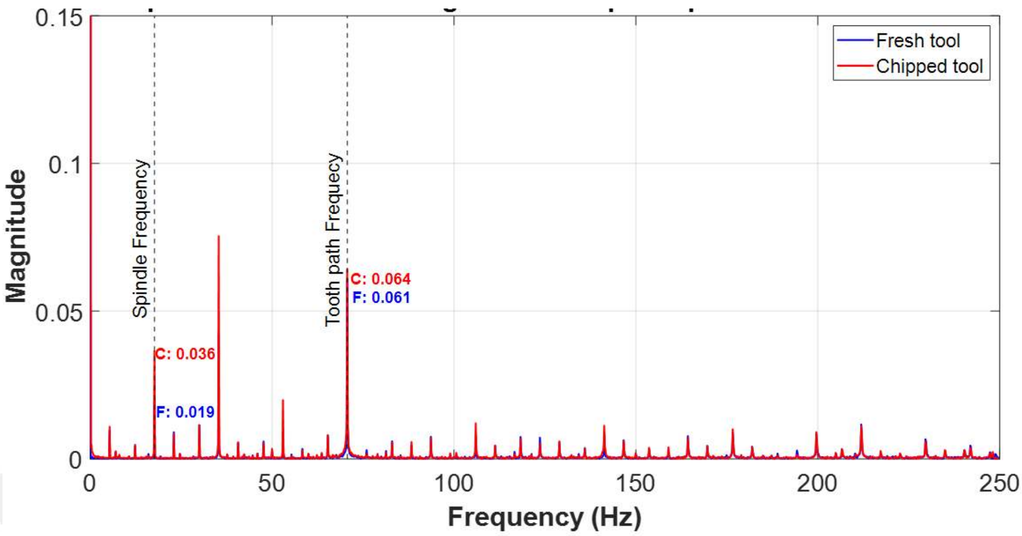
Fresh tool
Chipped tool
Magnitude
Frequency (Hz)
Spindle Frequency
Tooth path Frequecy
C: 0.064
F: 0.061
C: 0.036
F: 0.019
0.15
0.1
0.05
0
0
50
100
150
200
250

(a)

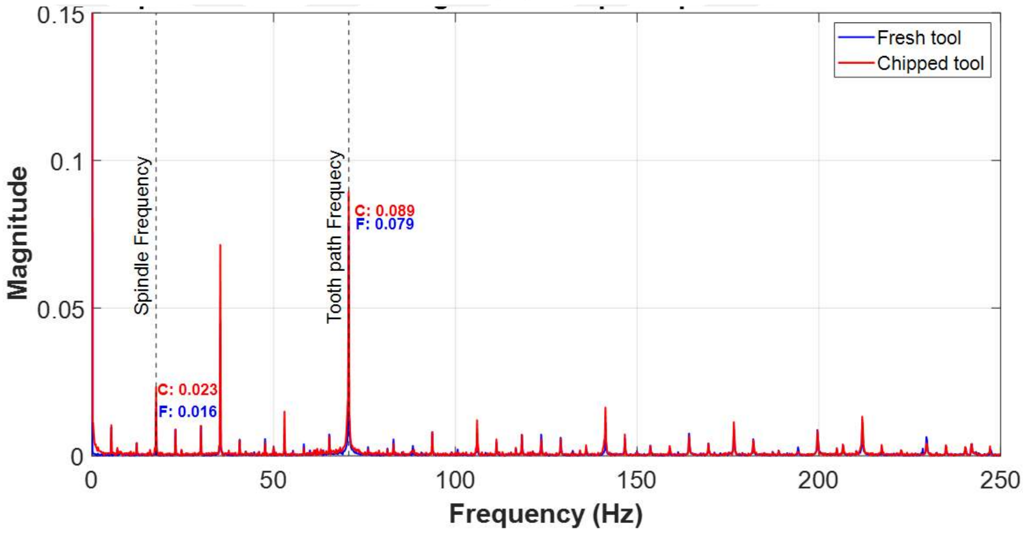
Fresh tool
Chipped tool
Magnitude
Frequency (Hz)
Spindle Frequency
Tooth path Frequecy
C: 0.089
F: 0.079
C: 0.023
F: 0.016
0.15
0.1
0.05
0
0
50
100
150
200
250

(b)

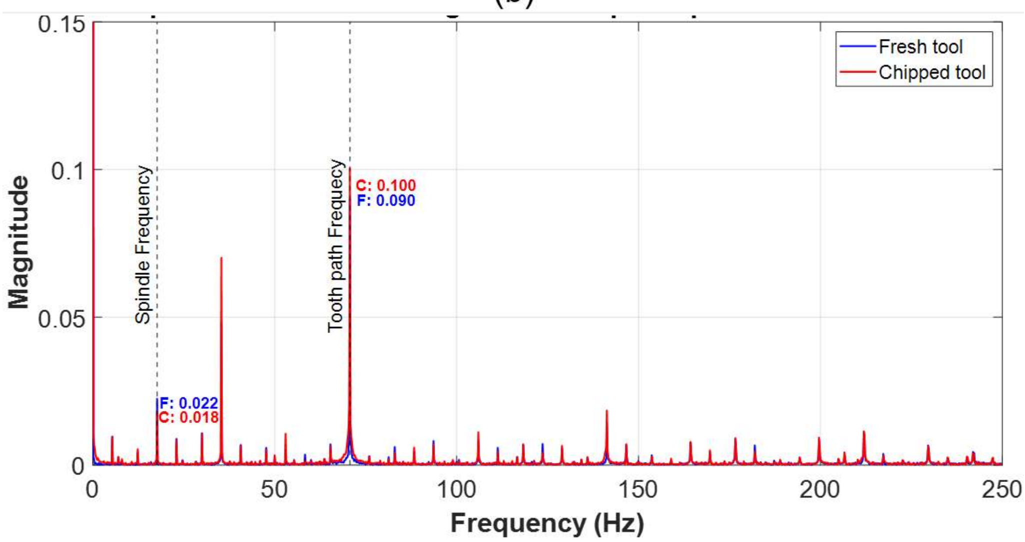
Fresh tool
Chipped tool
Magnitude
Frequency (Hz)
Spindle Frequency
Tooth path Frequecy
C: 0.100
F: 0.090
F: 0.022
C: 0.018
0.15
0.1
0.05
0
0
50
100
150
200
250

(c)

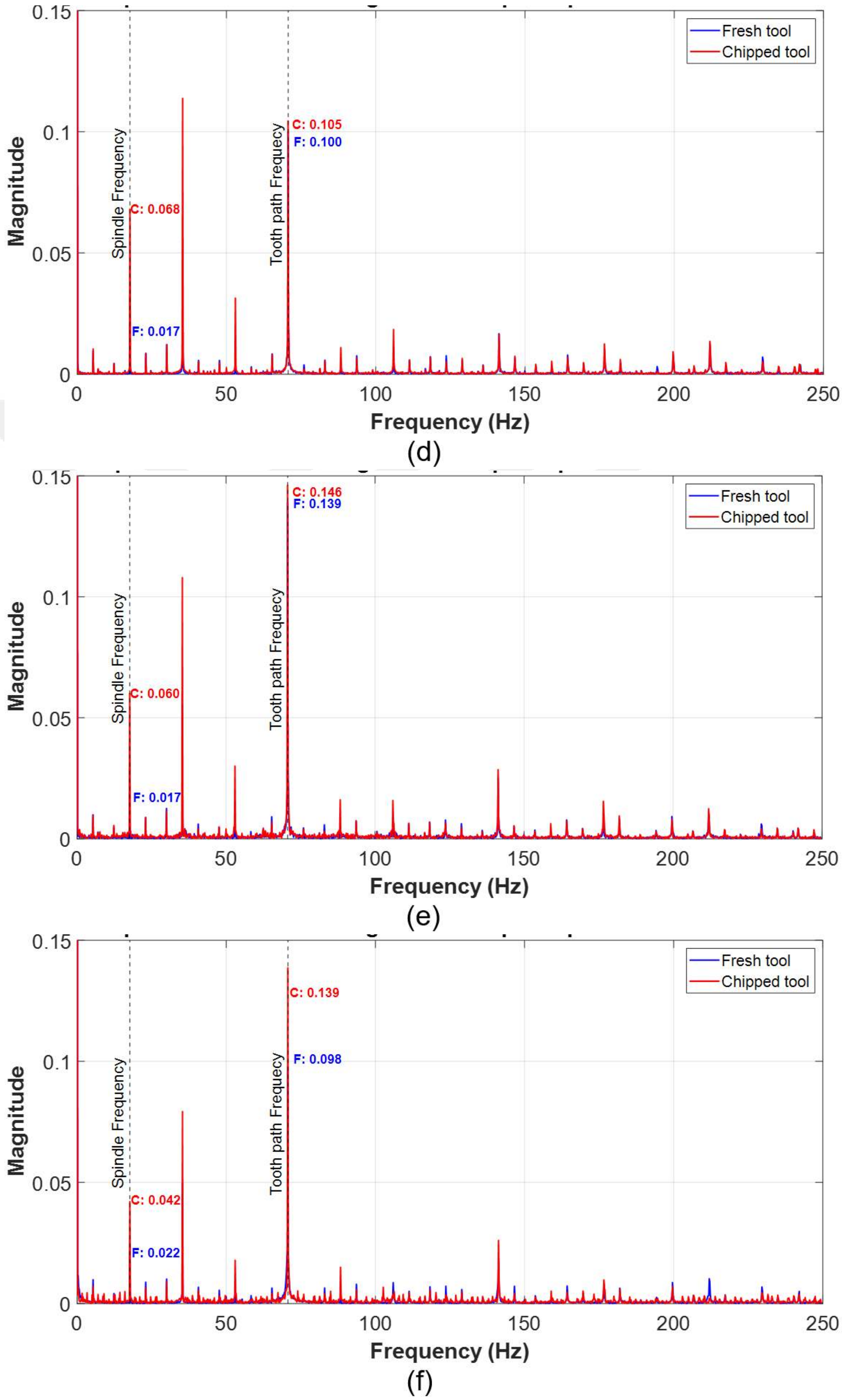

Figure 5.7: The FFT results of the spindle current data from the Edge device, (a) fpt= 30 micron and ADoC= 1 mm, (b) fpt= 30 micron and ADoC= 1.5 mm, (c) fpt= 30 micron and ADoC= 2 mm, (d) fpt= 60 micron and ADoC= 1 mm, (e) fpt= 60 micron and ADoC= 1.5 mm, (f) fpt= 60 micron and ADoC= 2 mm.

Chapter 6

RUNOUT DETECTION USING INDUSTRIAL EDGE DEVICE

6.1 Overview

Runout in CNC machine tools significantly impacts machining accuracy, surface quality, and tool life. This study presents a novel sensorless method for real-time monitoring of in-process runout during milling operations. The proposed approach utilizes an industrial edge device to analyze spindle current and torque milling data, which show a strong correlation with reference measurements from a dynamometer. By applying frequency-domain analysis to these signals, the system enables real-time, non-intrusive detection of runout. Milling experiments conducted on Ti-6Al-4V alloy validate the effectiveness of this technique, highlighting its potential as a cost-efficient solution for enhancing machining precision and process reliability in smart manufacturing environments.

6.2 Runout identification

Runout estimation was conducted using two analytical models. One of these models, based on the cutting force formulation by Liang et al. [79], represents runout as an explicit algebraic function derived from the Fourier series coefficients of the cutting forces at the spindle frequency ω_s (Hz). This method decomposes the cutting forces into nominal and runout-induced components, applying Fourier analysis to distinguish their spectral characteristics. Nominal forces are mainly concentrated at the tooth passing frequency and its harmonics, whereas runout generates additional frequency components positioned one spindle frequency above and below these harmonics. The tool runout magnitude (ρ_f) is calculated using Equation 6.1.

$$\rho_f = \left| \frac{A_{xo}(Nk+1)}{\sin\left(\frac{\pi}{2}\right)\frac{N}{2\pi}CWD(Nk)(1+p)K_t\left[P_{1o}(Nk+1)+K_rP_{2o}(Nk+1)\right]} \right| \tag{6.1}$$

Here, k denotes the normalized frequency relative to the spindle frequency, and N denotes the number of cutting edges (flutes) of the tool. The term CWD refers to the Fourier transform of chip width density, which indicates the width of the chip generated by a single flute during one unit of angular cutter rotation. K_t and K_r are specific tangential and radial cutting constants. The coefficients A_{xo}, P_{1o}, and P_{2o} are the offset-related Fourier series coefficients at $\omega_s = Nk+1$, and the constant p is cutting force power constant [79]. Cutting forces corresponding to the spindle frequency ($k = 0$) are favored because they exhibit stronger offset signals. Due to the small runout components at higher frequencies and measurement noise, the most accurate results are obtained at $k = 0$, i.e., at the spindle frequency in Equation 6.2.

$$\rho_f = \left| \frac{A_{xo}[1]}{\sin\left(\frac{\pi}{N}\right)\frac{N}{2\pi}a_p(1+p)K_t\left[P_{1o}(1)+K_rP_{2o}(1)\right]} \right|, \quad \text{for } N > 2 \tag{6.2}$$

where the axial depth of cut a_p is substituted for $CWD(0)$. In Liang's model [79], the total cutting force with runout is expressed as the sum of the nominal cutting force and additional components induced by runout. The runout-induced forces are represented as the convolution of local runout cutting forces with the cutter chip width density function, modulated by chip thickness variation from runout. Applying the convolution theorem, their frequency domain counterparts are derived as products of the respective convolution terms. According to this model, the total cutting force is modeled as the angular convolution of three components: the tooth-sequence function, the chip width density function, and the elementary cutting function. The tooth sequence function accounts for flute spacing and engagement order determined by the flute number. The chip width density function specifies chip width distribution per unit cutter angular rotation along the flute, within the axial depth of cut, dependent on axial depth of cut, helix angle, and tool diameter, as shown in Figure 6.1 and Equation 6.3. The elementary cutting function characterizes localized chip formation, governed by chip thickness variation and radial cutting geometry. The chip-width density function applies uniformly to all cutter flutes. As the tool rotates, each flute contributes to the total cutting force via the same function, shifted by the angular spacing of the flutes. Thus, the chip width density function can be interpreted as the impulse response of a linear shift-invariant process, referred to as the chip width generating process.

$$cwd(\phi) = \begin{cases} \dfrac{R}{\tan\alpha}, & 0 \le \phi \le \beta_a \\ 0, & \text{otherwise} \end{cases} \qquad \beta_a = \frac{a_p \tan\alpha}{R} \tag{6.3}$$

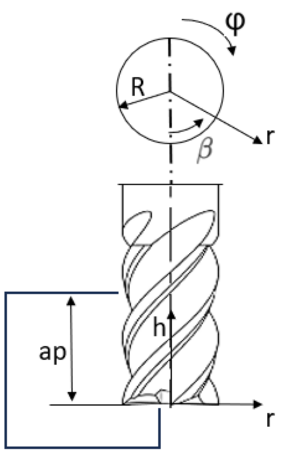

Figure 6.1: schematic relationship between axial depth of cut and chip width density function. β, r, and h represent angular, radius, and axial position variables for the cutting point in the cutter cylindrical coordinate system.

where R is the tool radius, α is the helix angle, and β_a is the angular range of axial engagement. The Fourier transform of the chip width density function is obtained as Equation 6.4.

$$CWD(\omega) = \frac{2R}{\tan\alpha} \cdot \frac{\sin\left(\frac{\omega\beta_a}{2}\right)}{\omega} e^{-j\omega\frac{\beta_a}{2}} \tag{6.4}$$

On the other hand, the runout magnitudes were also evaluated using the analytical approach proposed by Lee et al. [82], which relies on torque signal analysis in the frequency domain. The tool runout magnitude (ρ_t) was calculated as Equation 6.5:

$$\rho_t = \frac{2(\pi)^2\omega_s^2\,|T(\omega_s)|}{K_t N a_p \tan(\alpha)\sin\left(\frac{\theta_{ex}-\theta_{st}}{2}\right)\sin\left(\frac{\pi}{N}\right)} \tag{6.5}$$

where α is the helix angle of the tool, θ_{ex} and θ_{st} are exit and entry angles of tool engagement in the workpiece, ω_s spindle frequency, $T(\omega_s)$ is the rotational component of the torque at the spindle frequency, and a_p is the axial depth of cut [82].

6.3 Experimental method

6.3.1 Experimental process and data acquisition

Milling experiments were carried out on a titanium alloy (Ti6Al4V) block using a 5-axis CNC machine equipped with a Siemens SINUMERIK 840D SL controller. A flat end mill with a 12 mm diameter, five flutes, AlCrN coating, 82 mm total length, 32° helix angle, and a 0.3 mm corner radius was used as the cutting tool. This tool was installed on a Kistler 9123C rotary-type dynamometer fixed on the spindle to capture cutting forces throughout the milling operations. Concurrent data acquisition included force and torque signals from the dynamometer and spindle current and torque readings from the industrial edge device. The dynamometer outputs were conditioned using a Kistler Type 5223 charge amplifier and digitized via a National Instruments NI USB-6259 DAQ system. Meanwhile, spindle-related signals were obtained through a Simatic IPC227E industrial Edge device, specifically designed for machine tools, operating at a maximum sampling frequency of 500 Hz, and integrated via a Siemens IoT Edge Application for efficient data handling. The complete experimental configuration is depicted in Figure 6.2.

6.3.2 Runout experiment design

To explore the detection of cutter runout using cutting data from both a rotary dynamometer and an industrial edge device, a series of milling experiments were

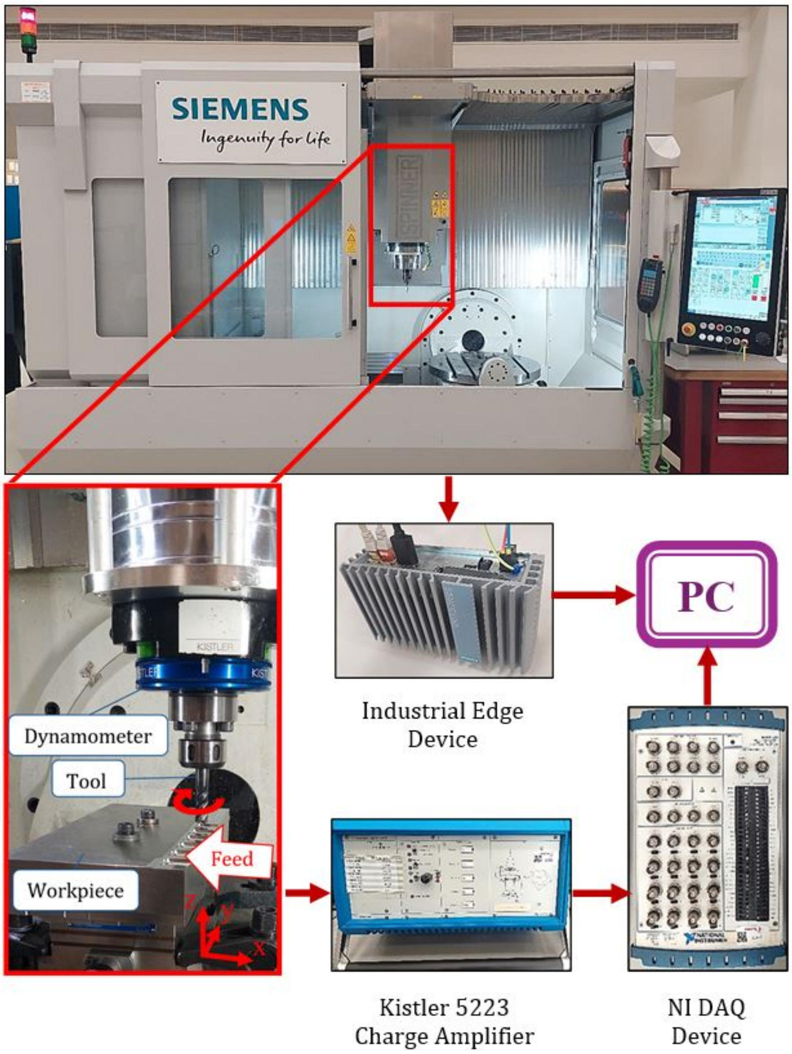

Figure 6.2: Experimental setup for runout detection using the Edge device.

carried out with deliberately varied runout conditions. These runout variations were introduced by placing a thin metal spacer between the tool and the collet to generate controlled eccentricity. The resulting static runout was accurately measured using a Mitutoyo dial gauge [91]. Side-down milling tests were carried out under controlled conditions with a constant spindle speed of 1060 rpm, a cutting speed of 40 m/min, a feed rate of 159 mm/min, and a radial depth of cut of 1 mm. The experimental design for the runout tests is summarized in Table 6.1. The directions of the tool feed force (Fx) and cross-feed force (Fy) are illustrated with red arrows in Figure 6.2.

Table 6.1: The design of the experiment for slot milling.

Exp. No.	**ADoC a_p (mm)**	**R_s (micron)**
1	1	42
2	2	42
3	3	42
4	1	130
5	2	130
6	3	130

6.4 Correlation between cutting torque and spindle current

Spindle torque and current signals obtained from the industrial edge device were employed for identifying tool runout. The relationship between the cutting torque measured by the dynamometer and the spindle torque recorded by the edge device was analyzed across multiple milling tests. The results revealed strong linear correlations, indicating that the cutting torque measured by the dynamometer can be reliably estimated using data acquired from the Edge device.

During the milling operations carried out at a cutting speed of 40 m/min, a feedrate of 159 mm/min, and an axial depth of cut of 3 mm, the raw spindle torque and current data from the industrial Edge device, along with torque readings from the dynamometer, were simultaneously recorded, as shown in Figure 6.3.

The linear relationships between the dynamometer's raw torque data and the spindle torque and current signals obtained from the industrial edge device are expressed in Equations 4.1 and 4.7.

6.4.1 Results and discussion

Figure 6.4 presents the collected feed-direction cutting forces, torque data from the dynamometer, and the spindle torque and current signals from the industrial edge device, obtained for different axial depths of cut and varying tool runout conditions

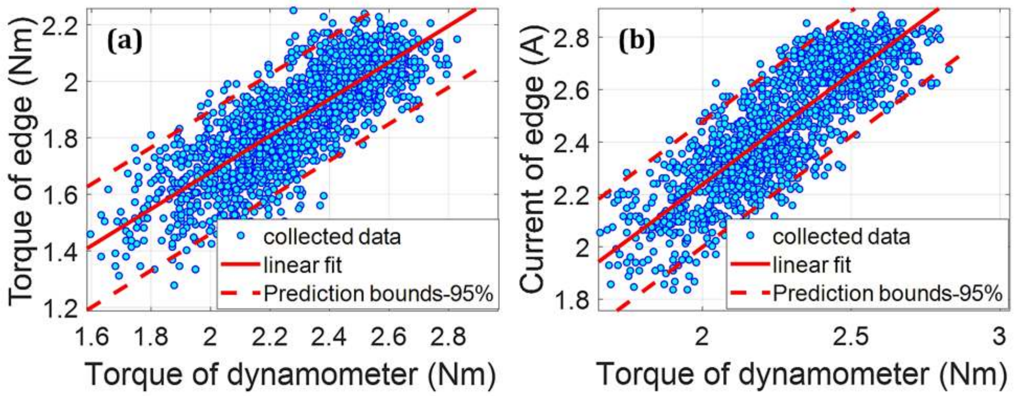

Figure 6.3: spindle torque and current raw data from the Edge device vs. torque measurements from the dynamometer.

over three tool rotations. The non-zero baseline observed in the edge device's spindle torque and current signals arises from inherent frictional losses in the spindle bearings and the characteristics of motor control.

Tool runout causes irregular engagement between one or more flutes of the cutter and the workpiece during the cutting process, leading to periodic variations in cutting forces. These variations appear as distinct frequency components in the frequency-domain analysis, as outlined in the corresponding equations. Figure 6.5 presents the FFT results of torque data of the dynamometer, as well as spindle torque and current signals of the edge device, under various axial depths of cut (a_p) and tool runout conditions.

Runout magnitudes were determined from the datasets of both the Edge device and the dynamometer by analyzing the FFT coefficients corresponding to the spindle frequency, as described in Equation 4.7. Figure 6.6 displays the runout estimation results based on cutting force, torque, and current measurements collected from both the dynamometer and the industrial Edge device.

The results reveal strong correlations between the tool runout values measured via cutting forces and torque from the dynamometer and those estimated using spindle torque and current signals from the Edge device. Moreover, the observed trend in runout magnitudes with increasing axial depth of cut (a_p), under constant radial depth of cut conditions, is consistent with the results reported in [82]. The detectability of tool runout depends on the ratio between the runout-induced chip thickness variation and the feed per tooth. As the feed per tooth increases, the relative contribution of runout to the total chip thickness diminishes, thereby reducing the sensitivity of force signals to runout effects. Conversely, larger runout amplitudes produce stronger force modulations, enhancing detectability. Increasing the feed per tooth elevates the baseline cutting force, which suppresses the relative prominence of runout-related harmonics in the frequency spectrum. These relationships are further influenced by dynamic factors such as chatter, variations in cutting coefficients, and measurement noise. In the present study, considering this ratio and the data acquisition characteristics of the edge device, the minimum detectable static runout was determined to be approximately 42 μm as shown in Table 6.1. Future work will focus on improving the detection of smaller runout amplitudes through AI-based signal enhancement, advanced noise filtering, and next-generation edge devices with higher sampling frequencies.

6.5 Summary

This study introduces an innovative sensorless method for identifying tool runout during machining, utilizing an industrial Edge device and removing the dependence on traditional, high-cost sensors. Detecting runout during operation is essential, as it directly impacts machining precision, tool longevity, and overall process stability. Nonetheless, the high cost of sensing technologies like dynamometers, lasers, or accelerometers often discourages their use in industrial environments. The proposed Edge-based solution addresses this challenge by enabling runout monitoring without additional hardware.

A series of milling experiments was performed on aerospace-grade Ti6Al4V workpieces, with controlled induction of various runout levels at different axial depths of cut. Cutting forces and torque were recorded simultaneously using a rotary dynamometer, while spindle torque and current data were collected via the industrial Edge device. Strong linear correlations were observed between the torque and current signals from the Edge device and the corresponding dynamometer measurements. Runout magnitudes were then estimated by analyzing the Fourier transform coefficients of the torque and current signals under varying cutting conditions.

The results revealed high consistency between runout measurements derived from both the dynamometer and Edge device datasets, confirming the effectiveness of the proposed sensorless approach for real-time runout detection. This methodology demonstrates significant potential for enhancing machining precision and process monitoring in smart manufacturing environments while reducing dependency on traditional sensors.

Looking ahead, this approach could be integrated with AI models for adaptive control, real-time feedback, and predictive maintenance across diverse materials and machining conditions. Such integration would strengthen the robustness and scalability of the method, advancing the development of intelligent, autonomous manufacturing systems.

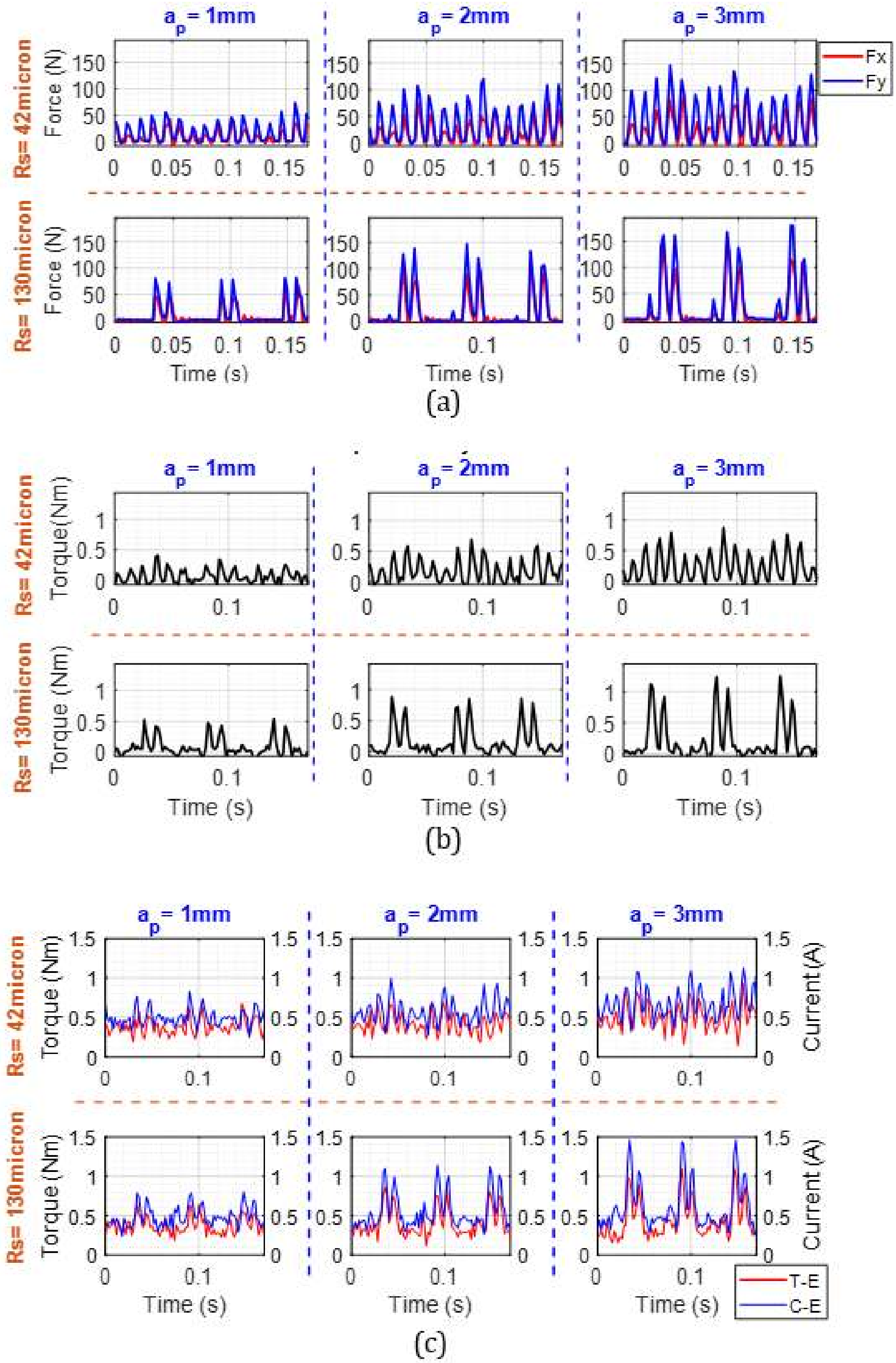

Figure 6.4: The data acquired from both measurement systems, including (a) cutting forces, (b) cutting torque by dynamometer, and (c) spindle torque and current captured by the Edge device, across various axial depths of cut (ap) and runout (Rs) values.

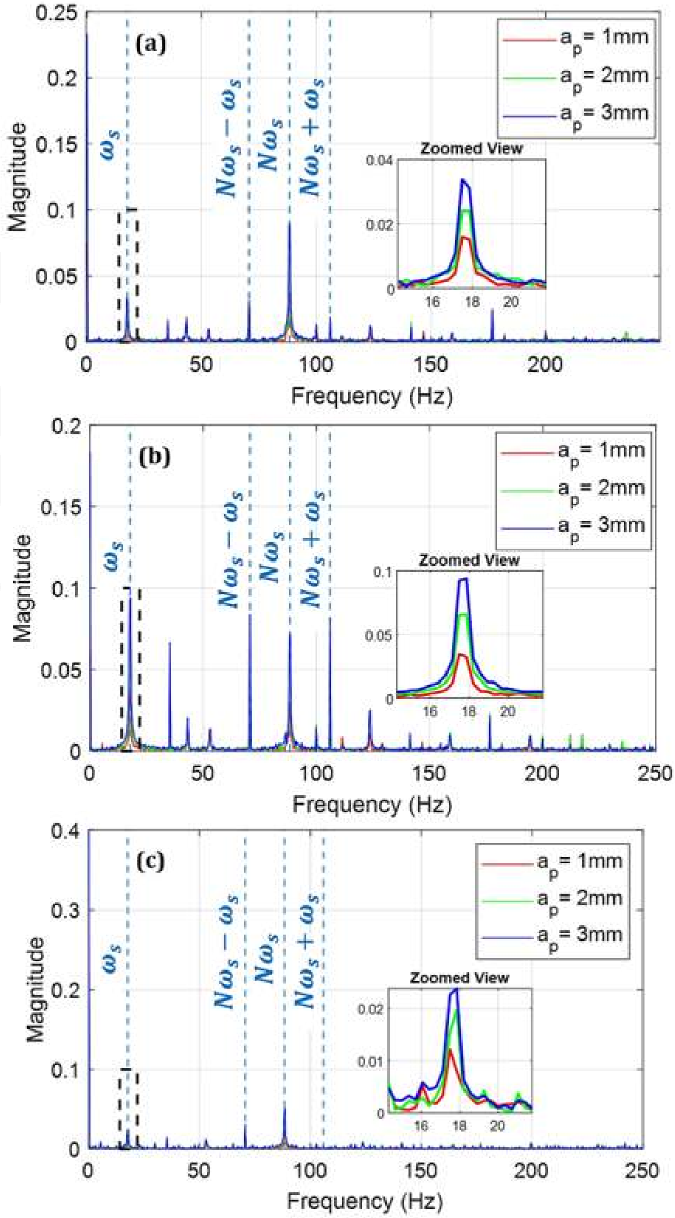
(a)
(b)
(c)
ω_s
$N\omega_s - \omega_s$
$N\omega_s$
$N\omega_s + \omega_s$
a_p = 1mm
a_p = 2mm
a_p = 3mm
Zoomed View
Magnitude
Frequency (Hz)

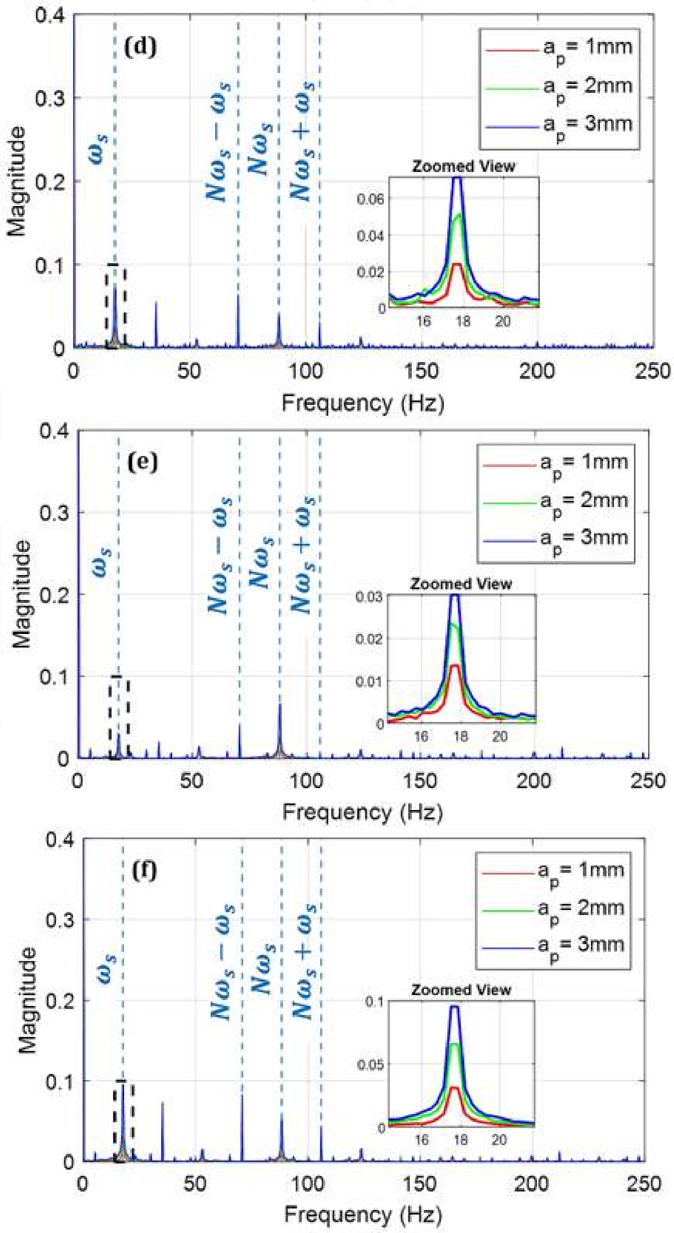

Figure 6.5: FFT plots of torque and current signals for varying axial depths of cut (ap), including: (a) dynamometer torque at Rs = 42 µm, (b) dynamometer torque at Rs = 130 µm, (c) Edge device spindle torque at Rs = 42 µm, (d) Edge device spindle torque at Rs = 130 µm, (e) Edge device spindle current at Rs = 42 µm, and (f) Edge device spindle current at Rs = 130 µm.

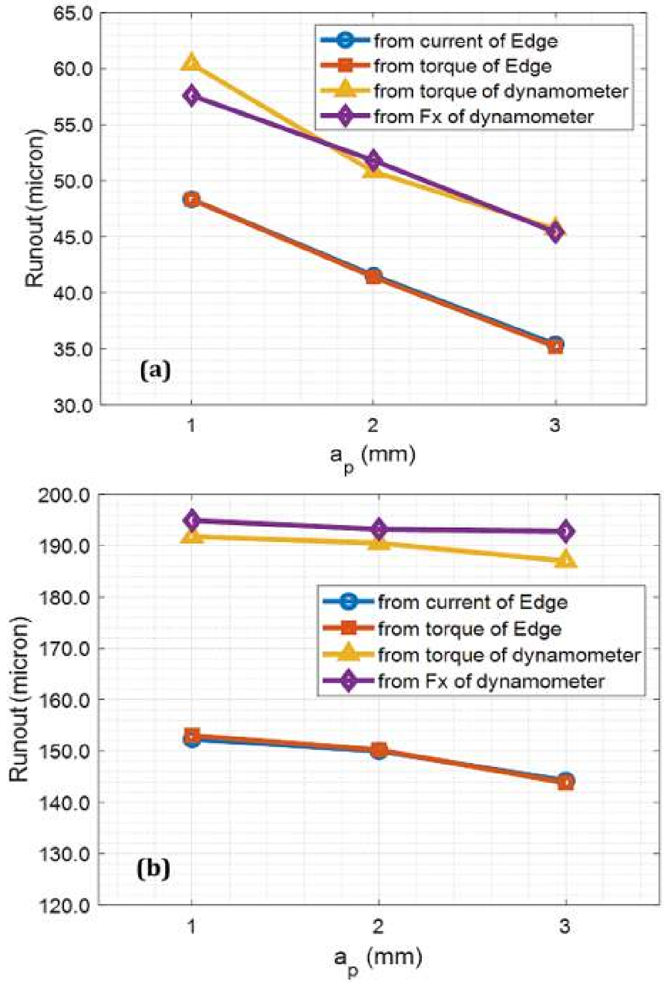

Figure 6.6: Runout results based on cutting force and torque measurements from the dynamometer, as well as spindle torque and current data from the Edge device, across various axial depths of cut (a_p) and runout values (R_s).

Chapter 7

CONCLUSION

The research presented in this thesis has introduced the significant potential of utilizing the industrial Edge in smart manufacturing during the machining processes. By leveraging real-time data acquisition, AI-driven analytics, and sensorless process monitoring, this study has provided cost-effective and efficient solutions to some challenges in machining, including tool flank wear prediction, sensorless cutting force and torque measurement, tool chipping detection, and tool runout monitoring.

The first contribution of this research was the development of an AI-assisted digital shadow for drilling tool flank wear prediction. The integration of high-frequency data acquisition, feature engineering, and deep learning models (Bi-LSTM and Bi-GRU) enabled accurate wear estimation, significantly reducing reliance on costly multi-sensor systems and unnecessary tool replacements.

The second contribution introduced a sensorless method for real-time measurement of cutting forces and torque. This approach successfully utilized spindle current and torque signals from an industrial Edge device, achieving high correlation with dynamometer measurements while reducing experimental complexity and costs. The findings validated the feasibility of using industrial Edge computing as an alternative to conventional dynamometers in smart machining environments.

The third contribution focused on tool chipping detection using Edge-based high-frequency spindle current and torque analysis in the time and frequency domains. FFT-based spectral analysis revealed dominant frequency variations of cutting signals before and after chipping events, confirming the effectiveness of industrial Edge computing for real-time tool condition monitoring. This approach can provide an early warning system, preventing tool failures and improving machining efficiency.

Finally, a sensorless in-process runout detection method was developed, showing the potential of industrial Edge devices for real-time monitoring and process optimization. The experimental validation demonstrated a significant correlation between spindle current and torque signals and runout characteristics from Edge device, enabling frequency-domain analysis for machining enhancement.

7.1 Future work

While this thesis demonstrates significant contributions to the field of smart manufacturing integrated with industrial Edge device, there remain opportunities for further investigation and enhancement as follow:

- Integrating industrial Edge computing devices into digital twin models can further improve real-time predictive capabilities and enable more adaptive process control strategies.

- The proposed methods can be extended to other manufacturing operations, such as turning, grinding, and additive manufacturing.

- Future studies can explore new advanced machine learning methods, such as transformer-based deep learning models, to improve prediction accuracy and computational efficiency.

- Collaborations with industry can help validate and standardize the proposed methodologies for integration into modern smart factories.

In conclusion, this thesis contributes to the evolution of smart manufacturing by introducing cost-effective, real-time, and sensorless solutions for machining process monitoring and optimization using the industrial Edge device. this research paves the way for next-generation intelligent manufacturing systems that are more autonomous, adaptive, and efficient. The findings of this study not only enhance machining precision and productivity but also reduce operational costs, making them highly valuable for industries striving to achieve the full potential of Industry 4.0 and beyond.

BIBLIOGRAPHY

[1] P. Gu, C. Zhu, Y. Yu, D. Liu, Z. Tao, and Y. Wu, "Evaluation and prediction of drilling wear based on machine vision," *The International Journal of Advanced Manufacturing Technology*, vol. 114, pp. 2055–2074, 2021.

[2] S. Kurada and C. Bradley, "A review of machine vision sensors for tool condition monitoring," *Computers in industry*, vol. 34, no. 1, pp. 55–72, 1997.

[3] X. Luan, S. Zhang, J. Chen, and G. Li, "Energy modelling and energy saving strategy analysis of a machine tool during non-cutting status," *International journal of production research*, vol. 57, no. 14, pp. 4451–4467, 2019.

[4] H.-S. Yoon, J.-Y. Lee, M.-S. Kim, and S.-H. Ahn, "Empirical power-consumption model for material removal in three-axis milling," *Journal of Cleaner Production*, vol. 78, pp. 54–62, 2014.

[5] C. Wang, Z. Bao, P. Zhang, W. Ming, and M. Chen, "Tool wear evaluation under minimum quantity lubrication by clustering energy of acoustic emission burst signals," *Measurement*, vol. 138, pp. 256–265, 2019.

[6] Z. Liu, Y. Guo, M. Sealy, and Z. Liu, "Energy consumption and process sustainability of hard milling with tool wear progression," *Journal of Materials Processing Technology*, vol. 229, pp. 305–312, 2016.

[7] A. Iqbal, K. A. Al-Ghamdi, and G. Hussain, "Effects of tool life criterion on sustainability of milling," *Journal of Cleaner Production*, vol. 139, pp. 1105–1117, 2016.

[8] L. Liu, X. Zhang, X. Wan, S. Zhou, and Z. Gao, "Digital twin-driven surface

roughness prediction and process parameter adaptive optimization," *Advanced Engineering Informatics*, vol. 51, p. 101470, 2022.

[9] Y. Yang, Y. Guo, Z. Huang, N. Chen, L. Li, Y. Jiang, and N. He, "Research on the milling tool wear and life prediction by establishing an integrated predictive model," *Measurement*, vol. 145, pp. 178–189, 2019.

[10] W. Kritzinger, M. Karner, G. Traar, J. Henjes, and W. Sihn, "Digital twin in manufacturing: A categorical literature review and classification," *Ifac-PapersOnline*, vol. 51, no. 11, pp. 1016–1022, 2018.

[11] A. Ladj, Z. Wang, O. Meski, F. Belkadi, M. Ritou, and C. Da Cunha, "A knowledge-based digital shadow for machining industry in a digital twin perspective," *Journal of Manufacturing Systems*, vol. 58, pp. 168–179, 2021.

[12] Y. Lu, C. Liu, I. Kevin, K. Wang, H. Huang, and X. Xu, "Digital twin-driven smart manufacturing: Connotation, reference model, applications and research issues," *Robotics and computer-integrated manufacturing*, vol. 61, p. 101837, 2020.

[13] M. Zhang, F. Tao, and A. Nee, "Digital twin enhanced dynamic job-shop scheduling," *Journal of Manufacturing Systems*, vol. 58, pp. 146–156, 2021.

[14] H. Jiang, S. Qin, J. Fu, J. Zhang, and G. Ding, "How to model and implement connections between physical and virtual models for digital twin application," *Journal of Manufacturing Systems*, vol. 58, pp. 36–51, 2021.

[15] F. Tao and M. Zhang, "Digital twin shop-floor: a new shop-floor paradigm towards smart manufacturing," *IEEE access*, vol. 5, pp. 20 418–20 427, 2017.

[16] F. Tao, J. Cheng, Q. Qi, M. Zhang, H. Zhang, and F. Sui, "Digital twin-driven product design, manufacturing and service with big data," *The International Journal of Advanced Manufacturing Technology*, vol. 94, pp. 3563–3576, 2018.

[17] A. Rossi, M. Moretti, and N. Senin, "Neural networks and narxs to replicate extrusion simulation in digital twins for fused filament fabrication," *Journal of Manufacturing Processes*, vol. 84, pp. 64–76, 2022.

[18] Z. Zhang, L. Malashkhia, Y. Zhang, E. Shevtshenko, and Y. Wang, "Design of gaussian process based model predictive control for seam tracking in a laser welding digital twin environment," *Journal of Manufacturing Processes*, vol. 80, pp. 816–828, 2022.

[19] R. Ward, C. Sun, J. Dominguez-Caballero, S. Ojo, S. Ayvar-Soberanis, D. Curtis, and E. Ozturk, "Machining digital twin using real-time model-based simulations and lookahead function for closed loop machining control," *The International Journal of Advanced Manufacturing Technology*, vol. 117, no. 11, pp. 3615–3629, 2021.

[20] A. Phua, P. S. Cook, C. H. Davies, and G. W. Delaney, "Smart recoating: A digital twin framework for optimisation and control of powder spreading in metal additive manufacturing," *Journal of Manufacturing Processes*, vol. 99, pp. 382–391, 2023.

[21] G. Chen, J. Zhu, Y. Zhao, Y. Hao, C. Yang, and Q. Shi, "Digital twin modeling for temperature field during friction stir welding," *Journal of Manufacturing Processes*, vol. 64, pp. 898–906, 2021.

[22] A. Siddhpura and R. Paurobally, "A review of flank wear prediction methods for tool condition monitoring in a turning process," *The International Journal of Advanced Manufacturing Technology*, vol. 65, pp. 371–393, 2013.

[23] G. Martínez-Arellano, G. Terrazas, and S. Ratchev, "Tool wear classification using time series imaging and deep learning," *The International Journal of Advanced Manufacturing Technology*, vol. 104, pp. 3647–3662, 2019.

[24] T. Bergs, C. Holst, P. Gupta, and T. Augspurger, "Digital image processing with deep learning for automated cutting tool wear detection," *Procedia Manufacturing*, vol. 48, pp. 947–958, 2020.

[25] E. Kaya and B. Akyüz, "Effects of cutting parameters on machinability characteristics of ni-based superalloys: a review," *Open Engineering*, vol. 7, no. 1, pp. 330–342, 2017.

[26] C. Drouillet, J. Karandikar, C. Nath, A.-C. Journeaux, M. El Mansori, and T. Kurfess, "Tool life predictions in milling using spindle power with the neural network technique," *Journal of Manufacturing Processes*, vol. 22, pp. 161–168, 2016.

[27] C. Wang, W. Ming, and M. Chen, "Milling tool's flank wear prediction by temperature dependent wear mechanism determination when machining inconel 182 overlays," *Tribology International*, vol. 104, pp. 140–156, 2016.

[28] S. Pal, P. S. Heyns, B. H. Freyer, N. J. Theron, and S. K. Pal, "Tool wear monitoring and selection of optimum cutting conditions with progressive tool wear effect and input uncertainties," *Journal of Intelligent Manufacturing*, vol. 22, pp. 491–504, 2011.

[29] M. Uekita and Y. Takaya, "Tool condition monitoring technique for deep-hole drilling of large components based on chatter identification in time–frequency domain," *Measurement*, vol. 103, pp. 199–207, 2017.

[30] S. N. B. Jaini, D.-W. Lee, S.-J. Lee, M.-R. Kim, and G.-H. Son, "Indirect tool monitoring in drilling based on gap sensor signal and multilayer perceptron feed forward neural network," *Journal of Intelligent Manufacturing*, vol. 32, pp. 1605–1619, 2021.

[31] Z. Li, X. Liu, A. Incecik, M. K. Gupta, G. M. Królczyk, and P. Gardoni,

"A novel ensemble deep learning model for cutting tool wear monitoring using audio sensors," *Journal of Manufacturing Processes*, vol. 79, pp. 233–249, 2022.

[32] C. Liu and L. Zhu, "A two-stage approach for predicting the remaining useful life of tools using bidirectional long short-term memory," *Measurement*, vol. 164, p. 108029, 2020.

[33] X. Xu, J. Wang, B. Zhong, W. Ming, and M. Chen, "Deep learning-based tool wear prediction and its application for machining process using multi-scale feature fusion and channel attention mechanism," *Measurement*, vol. 177, p. 109254, 2021.

[34] K. Gao, X. Xu, and S. Jiao, "Measurement and prediction of wear volume of the tool in nonlinear degradation process based on multi-sensor information fusion," *Engineering Failure Analysis*, vol. 136, p. 106164, 2022.

[35] K. Javed, R. Gouriveau, X. Li, and N. Zerhouni, "Tool wear monitoring and prognostics challenges: a comparison of connectionist methods toward an adaptive ensemble model," *Journal of Intelligent Manufacturing*, vol. 29, pp. 1873–1890, 2018.

[36] B. Yan, L. Zhu, and Y. Dun, "Tool wear monitoring of tc4 titanium alloy milling process based on multi-channel signal and time-dependent properties by using deep learning," *Journal of Manufacturing Systems*, vol. 61, pp. 495–508, 2021.

[37] M. Marani, M. Zeinali, V. Songmene, and C. K. Mechefske, "Tool wear prediction in high-speed turning of a steel alloy using long short-term memory modelling," *Measurement*, vol. 177, p. 109329, 2021.

[38] D. Kong, Y. Chen, N. Li, C. Duan, L. Lu, and D. Chen, "Relevance vector machine for tool wear prediction," *Mechanical Systems and Signal Processing*, vol. 127, pp. 573–594, 2019.

[39] J. Wang, J. Yan, C. Li, R. X. Gao, and R. Zhao, "Deep heterogeneous gru model for predictive analytics in smart manufacturing: Application to tool wear prediction," *Computers in Industry*, vol. 111, pp. 1–14, 2019.

[40] M. Cheng, L. Jiao, P. Yan, S. Li, and Q. T. W. X. Dai, Z., "Prediction and evaluation of surface roughness with hybrid kernel extreme learning machine and monitored tool wear," *Journal of Manufacturing Processes*, vol. 84, pp. 1541–1556, 2022.

[41] T. Mohanraj, J. Yerchuru, H. Krishnan, R. N. Aravind, and R. Yameni, "Development of tool condition monitoring system in end milling process using wavelet features and hoelder's exponent with machine learning algorithms," *Measurement*, vol. 173, p. 108671, 2021.

[42] W. Hou, H. Guo, L. Luo, and M. Jin, "Tool wear prediction based on domain adversarial adaptation and channel attention multiscale convolutional long short-term memory network," *Journal of Manufacturing Processes*, vol. 84, pp. 1339–1361, 2022.

[43] X. Liu, B. Zhang, X. Li, S. Liu, C. Yue, and S. Y. Liang, "An approach for tool wear prediction using customized densenet and gru integrated model based on multi-sensor feature fusion," *Journal of Intelligent Manufacturing*, vol. 34(2), pp. 885–902, 2023.

[44] K. Ehmann, S. G. Kapoor, R. E. DeVor, and I. Lazoglu, "Machining process modeling: a review," *Journal of Manufacturing Science and Engineering, Transactions of the ASME*, vol. 119, no. 4B, pp. 655–663, 1997.

[45] S. Jayaram, S. Kapoor, and R. DeVor, "Estimation of the specific cutting pressures for mechanistic cutting force models," *International Journal of Machine Tools and Manufacture*, vol. 41, no. 2, pp. 265–281, 2001.

[46] A. Azeem, H.-Y. Feng, and L. Wang, "Simplified and efficient calibration of a mechanistic cutting force model for ball-end milling," *International Journal of Machine Tools and Manufacture*, vol. 44, no. 2-3, pp. 291–298, 2004.

[47] E. Budak, Y. Altintas, and E. Armarego, "Prediction of milling force coefficients from orthogonal cutting data," 1996.

[48] F. Klocke, S. Gierlings, O. Adams, T. Auerbach, S. Kamps, D. Veselovac, M. Eckstein, A. Kirchheim, M. Blattner, R. Thiel *et al.*, "New concepts of force measurement systems for specific machining processes in aeronautic industry," *Procedia Cirp*, vol. 1, pp. 552–557, 2012.

[49] R. Teti, D. Mourtzis, D. D'Addona, and A. Caggiano, "Process monitoring of machining," *CIRP Annals*, vol. 71, no. 2, pp. 529–552, 2022.

[50] M. Gomez and T. Schmitz, "Low-cost, constrained-motion dynamometer for milling force measurement," *Manufacturing Letters*, vol. 25, pp. 34–39, 2020.

[51] H. Boujnah, N. Irino, Y. Imabeppu, K. Kawai, and M. Mori, "Spindle-integrated, sensor-based measurement system for cutting forces," *CIRP Annals*, vol. 71, no. 1, pp. 337–340, 2022.

[52] S. Rezvani, C.-J. Kim, S. S. Park, and J. Lee, "Simultaneous clamping and cutting force measurements with built-in sensors," *Sensors*, vol. 20, no. 13, p. 3736, 2020.

[53] H.-C. Möhring, K. Litwinski, and O. Gümmer, "Process monitoring with sensory machine tool components," *CIRP annals*, vol. 59, no. 1, pp. 383–386, 2010.

[54] M. Rizal, J. A. Ghani, M. Z. Nuawi, and C. H. C. Haron, "An embedded multi-sensor system on the rotating dynamometer for real-time condition monitoring in milling," *The International Journal of Advanced Manufacturing Technology*, vol. 95, pp. 811–823, 2018.

[55] R. Teti, K. Jemielniak, G. O'Donnell, and D. Dornfeld, "Advanced monitoring of machining operations," *CIRP annals*, vol. 59, no. 2, pp. 717–739, 2010.

[56] H. Mostaghimi, C. I. Park, G. Kang, S. S. Park, and D. Y. Lee, "Reconstruction of cutting forces through fusion of accelerometer and spindle current signals," *Journal of manufacturing processes*, vol. 68, pp. 990–1003, 2021.

[57] Y. Yamada, S. Yamato, and Y. Kakinuma, "Mode decoupled and sensorless cutting force monitoring based on multi-encoder," *The International Journal of Advanced Manufacturing Technology*, vol. 92, pp. 4081–4093, 2017.

[58] Y.-H. Jeong and D.-W. Cho, "Estimating cutting force from rotating and stationary feed motor currents on a milling machine," *International Journal of Machine Tools and Manufacture*, vol. 42, no. 14, pp. 1559–1566, 2002.

[59] A. Albrecht, S. S. Park, Y. Altintas, and G. Pritschow, "High frequency bandwidth cutting force measurement in milling using capacitance displacement sensors," *International Journal of Machine Tools and Manufacture*, vol. 45, no. 9, pp. 993–1008, 2005.

[60] F. Bleicher, C. M. Ramsauer, R. Oswald, N. Leder, and P. Schoerghofer, "Method for determining edge chipping in milling based on tool holder vibration measurements," *CIRP Annals*, vol. 69, no. 1, pp. 101–104, 2020.

[61] H.-S. Yoon, J.-Y. Lee, M.-S. Kim, E. Kim, Y.-J. Shin, S.-Y. Kim, S. Min, and S.-H. Ahn, "Power consumption assessment of machine tool feed drive units," *International Journal of Precision Engineering and Manufacturing-Green Technology*, vol. 7, pp. 455–464, 2020.

[62] J. Huang, D. T. Pham, C. Ji, and Z. Zhou, "Smart cutting tool integrated with optical fiber sensors for cutting force measurement in turning," *IEEE Transactions on Instrumentation and Measurement*, vol. 69, no. 4, pp. 1720–1727, 2019.

[63] O. Subasi, S. G. Yazgi, and I. Lazoglu, "A novel triaxial optoelectronic based dynamometer for machining processes," *Sensors and Actuators A: Physical*, vol. 279, pp. 168–177, 2018.

[64] M. K. Gupta, M. E. Korkmaz, H. Yılmaz, Ş. Şirin, N. S. Ross, M. Jamil, G. M. Królczyk, and V. S. Sharma, "Real-time monitoring and measurement of energy characteristics in sustainable machining of titanium alloys," *Measurement*, vol. 224, p. 113937, 2024.

[65] G. W. Vogl, D. A. Regli, and G. M. Corson, "Real-time estimation of cutting forces via physics-inspired data-driven model," *CIRP Annals*, vol. 71, no. 1, pp. 317–320, 2022.

[66] M. Postel, D. Aslan, K. Wegener, and Y. Altintas, "Monitoring of vibrations and cutting forces with spindle mounted vibration sensors," *Cirp Annals*, vol. 68, no. 1, pp. 413–416, 2019.

[67] M. L. P. A. Rivero, L.N., "Tool wear detection in dry high-speed milling based upon the analysis of machine internal signals," *Mechatronics*, vol. 18, no. 10, pp. 627–633, 2008.

[68] I. Aldekoa, Ander, L. Sastoque-Pinilla, S. Sendino-Mouliet, U. Lopez-Novoa, and L. N. López, "Early detection of tool wear in electromechanical broaching machines by monitoring main stroke servomotors," *Mechanical Systems and Signal Processing*, vol. 204, pp. 0888–3270, 2023.

[69] G. W. Vogl, D. A. Regli, and G. M. Corson, "Tool wear intelligent monitoring techniques in cutting: a review," *J Mech Sci Technol*, vol. 37, p. 289–303, 2023.

[70] U. L.-N. I. B. N. L. d. L. Endika Tapia, Leonardo Sastoque-Pinilla, "Assessing industrial communication protocols to bridge the gap between machine tools and software monitoring," *Sensors*, vol. 23, p. 5694, 2023.

[71] Y. Altintas, *Manufacturing automation: metal cutting mechanics, machine tool vibrations, and CNC design.* Cambridge university press, 2012.

[72] X. Luan, S. Zhang, J. Li, G. Mendis, F. Zhao, and J. W. Sutherland, "Trade-off analysis of tool wear, machining quality and energy efficiency of alloy cast iron milling process," *Procedia Manufacturing*, vol. 26, pp. 383–393, 2018.

[73] W. Lee, M. Ratnam, and Z. Ahmad, "In-process detection of chipping in ceramic cutting tools during turning of difficult-to-cut material using vision-based approach," *The International Journal of Advanced Manufacturing Technology*, vol. 85, pp. 1275–1290, 2016.

[74] J. Qu, C. Yue, J. Zhou, W. Xia, X. Liu, and S. Y. Liang, "On-machine detection of face milling cutter damage based on machine vision," *The International Journal of Advanced Manufacturing Technology*, pp. 1–15, 2024.

[75] G.-S. Kang, S.-G. Kim, G.-D. Yang, K.-H. Park, and D. Y. Lee, "Tool chipping detection using peak period of spindle vibration during end-milling of inconel 718," *International Journal of Precision Engineering and Manufacturing*, vol. 20, pp. 1851–1859, 2019.

[76] M. Chehrehzad, G. Kecibas, C. Besirova, U. Uresin, M. Irican, and I. Lazoglu, "Tool wear prediction through ai-assisted digital shadow using industrial edge device," *Journal of Manufacturing Processes*, vol. 113, pp. 117–130, 2024.

[77] Z. Jiang, F. Wang, W. Mou, S. Zhu, R. Fu, and Z. Yu, "Method for edge chipping monitoring based on vibration polar coordinate image feature analysis," *The International Journal of Advanced Manufacturing Technology*, vol. 130, no. 11, pp. 5137–5146, 2024.

[78] W. A. Kline and R. E. DeVor, "The effect of runout on cutting geometry and forces in end milling," *International Journal of Machine Tool Design and Research*, vol. 23, no. 2-3, pp. 123–140, 1983.

[79] S. Y. Liang and J. J. Wang, "Milling force convolution modeling for identification of cutter axis offset," *International Journal of Machine Tools and Manufacture*, vol. 34, no. 8, pp. 1177–1190, 1994.

[80] K. A. Hekman and S. Y. Liang, "In-process monitoring of end milling cutter runout," *Mechatronics*, vol. 7, no. 1, pp. 1–10, 1997.

[81] J.-J. Wang and C. Zheng, "Identification of cutter offset in end milling without a prior knowledge of cutting coefficients," *International Journal of Machine Tools and Manufacture*, vol. 43, no. 7, pp. 687–697, 2003.

[82] K. Lee, T. Hayasaka, and E. Shamoto, "Novel real-time monitoring method of depths of cut and runout for milling process utilizing fft analysis of cutting torque," *Precision Engineering*, vol. 81, pp. 36–49, 2023.

[83] C. Brecher, H.-M. Eckel, T. Motschke, M. Fey, and A. Epple, "Estimation of the virtual workpiece quality by the use of a spindle-integrated process force measurement," *CIRP Annals*, vol. 68, no. 1, pp. 381–384, 2019.

[84] D. Bilgili, G. Kecibas, C. Besirova, M. R. Chehrehzad, G. Burun, T. Pehlivan, U. Uresin, E. Emekli, and I. Lazoglu, "Tool flank wear prediction using high-frequency machine data from industrial edge device," *Procedia CIRP*, vol. 118, pp. 483–488, 2023.

[85] H. Sun, J. Zhang, R. Mo, and X. Zhang, "In-process tool condition forecasting based on a deep learning method," *Robotics and Computer-Integrated Manufacturing*, vol. 64, p. 101924, 2020.

[86] M. Wang, J. Zhou, J. Gao, Z. Li, and E. Li, "Milling tool wear prediction method based on deep learning under variable working conditions," *IEEE Access*, vol. 8, pp. 140 726–140 735, 2020.

[87] R. Zhao, R. Yan, J. Wang, and K. Mao, "Learning to monitor machine health with convolutional bi-directional lstm networks," *Sensors*, vol. 17, no. 2, p. 273, 2017.

[88] Y. Bengio, "On the properties of neural machinetranslation: Encoder-decoder approaches," *arXiv preprint arXiv:1409.1259*, 2014.

[89] M. Chehrehzad, M. Irican, and I. Lazoglu, "Sensorless monitoring of cutting forces and torques in machining using industrial edge device," *Journal of Manufacturing Processes*, vol. 150, pp. 981–1003, 2025.

[90] X. Li, X. Liu, C. Yue, S. Y. Liang, and L. Wang, "Systematic review on tool breakage monitoring techniques in machining operations," *International Journal of Machine Tools and Manufacture*, vol. 176, p. 103882, 2022.

[91] M. Chehrehzad and I. Lazoglu, "Sensorless in-process runout monitoring in milling via an industrial edge device," *CIRP Annals*, vol. 74, no. 1, pp. 99–102, 2025.